HHS Public Access

Author manuscript

Nat Med. Author manuscript; available in PMC 2022 March 01.

Published in final edited form as:

Nat Med. 2021 September ; 27(9): 1646–1654. doi:10.1038/s41591-021-01388-5.

Inherited PD-1 deficiency underlies tuberculosis and autoimmunity in a child

A full list of authors and affiliations appears at the end of the article.

Abstract

The pathophysiology of adverse events following PD-1 blockade, including tuberculosis (TB)[1] and autoimmunity[2], remains poorly characterized. We studied a patient with inherited PD-1 deficiency and TB who died of pulmonary autoimmunity. The patient's leukocytes did not express PD-1 or respond to PD-1-mediated suppression. The patient's lymphocytes produced only small amounts of interferon (IFN)-γ upon mycobacterial stimuli, similar to patients with inborn errors of IFN-γ production who are vulnerable to TB[3–6]. This phenotype resulted from a combined depletion of Vδ2^{+} γδ T, MAIT, and CD56^{bright} NK lymphocytes and dysfunction of other T lymphocyte

@:correspondence to Masato Ogishi (mogishi@rockefeller.edu), Stéphanie Boisson-Dupuis (stbo603@rockefeller.edu) and Jean-Laurent Casanova (casanova@rockefeller.edu).

#:equal contributions

Author Contributions Statement

M.O., S.B-D., and J-L.C. designed the study. M.O., R.Y., D.L., M.B., T.K., F.A.A., M.R., O.M.D., M.C., C.G., S.J.P, A.N.S, J.R., W-T.L, S.D., G.R., C.S.M., Y.N., T.Y., K.C., S.C.W., J-F.,E., F.Rozenberg, G.A., M.S.G., D.B., N.M., L.D.N., S.G.T., T.H., and P.G. performed experiments. M.O. and P.Z. analyzed the single-cell and bulk RNA sequencing data. P.Z., F.Rapaport, G.K., and L.A. assisted the analysis of genetic data. M.D.H., M.K.C., M.A., P.W., and J.D.W. collected data on patients treated with anti-PD-1 monoclonal antibody. C.A., I.T., D.C., F.O.H., F.D., A.I., V.K.R., L.K., V.B., and J.B. collected clinical data and biological materials of patients. S.D. assisted experiments and the writing of the case report. M.O., S.B-D., and J-L.C. interpreted the data and wrote the manuscript with the help of all co-authors. All authors reviewed the manuscript and approved its submission. S.V., R.P.L., B.B., L.A., D.B., N.M., L.D.N., S.G.T., T.H., and P.G. are co-second-to-last authors contributing equally. S.B-D. and J-L.C. are co-last authors who jointly supervised the study.

Data Availability Statement

Minor allele frequencies of *PDCD1* variants in the general population were retrieved from gnomAD r2.1.1 (https://gnomad.broadinstitute.org/). Public scRNASeq datasets were downloaded from the 10X Genomics website (https://support.10xgenomics.com/single-cell-gene-expression/datasets). For gene-set enrichment analysis (GSEA), gene sets were obtained from MSigDB Collections (http://www.gsea-msigdb.org/gsea/msigdb/index.jsp). For the construction of VirScan phage library, the complete proteome of most human-tropic viruses plus peptides derived from various microbial antigens and allergens annotated in the Immune Epitope Database (IEDB, www.iedb.org) were utilized.

Raw single-cell RNA sequencing (scRNASeq) data (for Fig. 4i and j and Extended Data Fig. 6) and RNA sequencing (RNASeq) data of sorted double-negative T cells and monocytes (for Fig. 4e–g and Extended Data Fig. 9f) can be found at the NCBI Sequence Read Archive (accession number: PRJNA723618). Processed data and relevant codes can be found on Mendeley Data for scRNASeq (http://dx.doi.org/10.17632/nb26v3mx3x.2) and RNASeq (http://dx.doi.org/10.17632/nkhbn88v7g.2), respectively. All other raw and processed data are available upon request from the corresponding authors under a Data Transfer Agreement.

Code Availability

Custom codes for the analysis of single-cell RNA sequencing data and RNA sequencing data are available on Mendeley Data for scRNASeq (http://dx.doi.org/10.17632/nb26v3mx3x.2) and RNASeq (http://dx.doi.org/10.17632/nkhbn88v7g.2), respectively. All other custom codes are available upon request from the corresponding authors.

Competing Interests Statement

M.S.G. has received consulting fees from Takeda, serves on the Scientific Advisory Board (SAB) of Vedanta Biosciences and receives consulting fees and equity, and serves on the SAB of the Pandemic Response Lab (PRL) of New York City. J.D.W. is a consultant for: Adaptive Biotech; Amgen; Apricity; Ascentage Pharma; Arsenal IO; Astellas; AstraZeneca; Bayer; Beigene; Boehringer Ingelheim; Bristol Myers Squibb; Celgene; Chugai; Daiichi Sankyo, Dragonfly; Eli Lilly; Elucida; F Star; Georgiamune; Idera; Imvaq; Kyowa Hakko Kirin; Linneaus; Maverick Therapeutics; Merck; Neon Therapeutics; Polynoma; Psioxus; Recepta; Takara Bio; Trieza; Truvax; Trishula; Sellas; Serametrix; Surface Oncology; Syndax; Syntalogic, Werewolf Therapeutics. J.D.W. receives research support grants from: Bristol Myers Squibb; Sephora. J.D.W. has equity in: Tizona Pharmaceuticals; Adaptive Biotechnologies; Imvaq; Beigene; Linneaus, Apricity, Arsenal IO; Georgiamune. All other authors declare no competing interests.

subsets. Moreover, the patient displayed hepatosplenomegaly and an expansion of total, activated, and RORγT^{+} CD4^{-}CD8^{-} double-negative αβ T cells, similar to patients with *STAT3* gain-of-function mutations who display lymphoproliferative autoimmunity[7–10]. This phenotype resulted from excessive amounts of STAT3-activating cytokines IL-6 and IL-23 produced by activated T lymphocytes and monocytes, and the STAT3-dependent expression of RORγT by activated T lymphocytes. Our work highlights the indispensable role of human PD-1 in governing both antimycobacterial immunity and self-tolerance, while identifying potentially actionable molecular targets for the diagnostic and therapeutic management of TB and autoimmunity in patients on PD-1 blockade.

Introduction

About 25% of the global population is estimated to be infected with *Mycobacterium tuberculosis* (Mtb)[11], but only 5–10% of infected individuals develop tuberculosis (TB) in their lifetime[12]. Human genetics is a strong determinant of TB following infection with Mtb[6]. Two rare monogenic inborn errors of immunity (IEIs) have been reported to underlie TB in multiple kindreds: autosomal recessive (AR) complete interleukin-12 receptor β1 (IL-12Rβ1)[3] and tyrosine kinase 2 (TYK2)[4] deficiencies. Both disorders underlie TB by impeding IFN-γ production by T and NK lymphocytes in response to IL-12 and IL-23[3,4]. We also recently described a common monogenic IEI, homozygosity for TYK2 P1104A, which selectively disrupts cellular responses to IL-23[5] and underlies about 1% of TB cases in humans of European descent[13]. The single P1104A allele originated in the ancestors of West Europeans about 30,000 years ago, and its frequency has drastically decreased in Europe over the last 2,000 years due to the negative selection imposed by TB[14]. Autoimmunity is another significant public health burden. Monogenic forms of autoimmunity have provided insight into genes governing self-tolerance in humans, including central T cell tolerance (*e.g.,* mutations in *AIRE*), regulatory T cells (Tregs) (*e.g., FOXP3*, *CTLA4*, and *LRBA*), and the deletion of self-reactive CD4^{-}CD8^{-} double-negative (DN) αβ T cells (*e.g., FAS*). Only two IEIs to date have been shown to underlie both mycobacterial disease and autoimmunity, albeit with incomplete penetrance: heterozygosity for gain-of-function (GOF) variants of *STAT1*[15] and *STAT3*[9,10,16]. The pathogenesis of mycobacterial diseases in patients with these conditions remains unexplained. Here, we studied a patient who suffered from life-threatening abdominal TB and died of pulmonary autoimmunity. The patient's older sibling also died of unexplained pneumonitis. We hypothesized that a single genetic lesion was responsible for the two unusually severe immunopathological phenotypes.

Results

A patient with severe tuberculosis and autoimmunity

We studied a patient born to consanguineous Turkish parents (Fig. 1a, see Methods for more details). He was diagnosed with type 1 diabetes (T1D), hypothyroidism, and juvenile idiopathic arthritis (JIA) at the age of three years. At the age of 10 years, he was hospitalized for large multifocal intraperitoneal abscesses (Fig. 1b). Aspiration and biopsy revealed granuloma and caseous necrosis with acid-fast bacilli (AFB) subsequently identified as

Mtb by species-specific PCR (Fig. 1c and Extended Data Fig. 1a). Chest X-ray (CXR) showed no pulmonary lesions. The patient tested positive in both the tuberculin skin test (TST) and interferon-gamma release assay (IGRA). The patient was therefore diagnosed with abdominal TB. The routine immunological workup was unremarkable (Supplementary Table 1). The patient had never experienced unusually severe infections despite exposure to common pathogens, as shown by conventional serological testing and VirScan (Extended Data Fig. 1b and Supplementary Table 2), or any adverse reaction after vaccination with several live attenuated vaccines [*i.e.*, BCG, oral polio, and measles, mumps, and rubella (MMR)]. Despite hepatotoxicity, antimycobacterial therapy led to complete remission in eight months (Extended Data Fig. 1c), as demonstrated by a computed tomography (CT) scan. However, two months later, the patient developed dyspnea, which progressed to respiratory failure (Fig. 1d and Extended Data Fig. 1d). Bronchoscopy revealed no AFB, and neither abdominal nor pulmonary TB was diagnosed while the patient was on ventilation in the intensive care unit. Clinical autoantibody (autoAb) tests were negative (Supplementary Table 3), but proteome-wide serum autoreactivity profiling identified two autoAbs against the alpha 3 chain of type IV collagen, an autoantigen underlying Goodpasture's syndrome[17], and several autoAbs associated with autoimmune thyroiditis and T1D, but not anti-IFN-γ autoAbs (Fig. 1e). T cell receptor (TCR) repertoire sequencing did not show any clonal expansion in circulating T cells (Extended Data Fig. 1e–g). Despite aggressive immunosuppressive therapy, the patient eventually died of alveolar hemorrhage at the age of 11 years, only three months after the onset of respiratory illness.

A homozygous frameshift variant of PDCD1

Both the patient's six-year-old brother and his parents are healthy, with no history of autoimmunity or TB (negative CXR and IGRA tests). By contrast, the older brother of the patient, with a history of T1D and JIA, for whom no genetic material was available for testing, had died of unexplained pneumonitis at the age of three years. Whole-exome sequencing (WES) identified three candidate variants homozygous in the patient but not in his healthy brother or parents (*i.e.*, AR inheritance with complete penetrance) (Extended Data Fig. 2a and Supplementary Table 4). A homozygous frameshift variant (c.105dupC) of *PDCD1* was the only candidate variant predicted to be loss-of-function (pLOF) due to the formation of a premature termination codon (T36Hfs*70), which was confirmed by Sanger sequencing (Fig. 1f and Extended Data Fig. 2b). We did not find any pLOF *PDCD1* variants, including c.105dupC, in the homozygous state in gnomAD (https://gnomad.broadinstitute.org/), 1000 Genomes, Bravo, or our in-house database including data for more than 8,000 patients with infectious diseases. The variant has a combined annotation-dependent depletion (CADD) score[18] of 25.7, well above the mutation significance cutoff (MSC)[19] of 3.3 (Fig. 1g and Extended Data Fig. 2c). Consistent with AR inheritance, *PDCD1* is not under strong negative selection, as demonstrated by CoNeS, a sequence-based metric for assessing gene-level selection[20], similar to other genes underlying AR IEIs (Fig. 1h). *PDCD1* encodes the immune checkpoint receptor PD-1[21]. Interestingly, PD-1-deficient mice and cancer patients on PD-1 blockade are prone to not only autoimmunity, including fatal autoimmune pneumonitis[22–24], but also severe TB[1,25,26]. These observations strongly suggested that the patient and his deceased sibling

were homozygous for a rare LOF *PDCD1* mutation and that, by inference, AR complete PD-1 deficiency is a rare genetic etiology of both TB and autoimmunity.

Autosomal recessive complete PD-1 deficiency

We examined whether the patient's *PDCD1* mutation results in complete PD-1 deficiency. To this end, we first studied the patient's *PDCD1* allele in HEK293T cells overexpressing the cDNA corresponding to the patient's allele. Immunoblotting did not show expression of full-length or truncated PD-1, excluding a re-initiation of translation (Fig. 2a). Flow cytometric analysis did not show surface PD-1 expression or binding of recombinant PD-L1/2 (Fig. 2b and c). In contrast, the wild-type *PDCD1* and four common alleles found in the homozygous state in public databases were normally expressed and bound with recombinant PD-L1/2 (Extended Data Fig. 2d and e). Moreover, HuT78 T cells (cutaneous T cell lymphoma) stably expressing wild-type, but not mutant (T36Hfs*70) PD-1 were sensitive to the inhibition of blinatumomab (anti-CD3-CD19 bispecific engager)-induced IFN-γ and TNF production by PD-L1/2 expressed on cocultured Raji B cells (Burkitt lymphoma) (Extended Data Fig. 2f). We then studied the patient's cells. Flow cytometry showed no endogenous surface PD-1 expression on the patient's Epstein-Barr virus-immortalized B (EBV-B) cells, peripheral blood mononuclear cells (PBMCs), and phytohemagglutinin (PHA)-activated T cell blasts (Fig. 2d–f), despite detectable levels of *PDCD1* mRNA in these cells (Extended Data Fig. 2g). Moreover, flow cytometric analysis showed that the patient's *Herpesvirus saimiri*-immortalized T (HVS-T) cells were insensitive to the inhibition of blinatumomab-induced IFN-γ production by PD-L1/2 expressed on cocultured Raji B cells (Fig. 2g). Lentiviral transduction with wild-type, but not mutant (T36Hfs*70) PD-1 rescued the phenotype (Fig. 2h). Furthermore, the patient's HVS-T cells and $CD3^+CD4^-CD8^-$ double-negative (DN) PHA blasts were insensitive to anti-PD-1 monoclonal antibody-mediated inhibition of CD107a surface translocation and PD-L1/2-mediated inhibition of ERK1/2 phosphorylation, respectively, as determined by flow cytometry (Extended Data Fig. 2h and i). Collectively, these data suggest that the *PDCD1* c.105dupC allele is indeed LOF, and the patient had AR complete PD-1 deficiency.

Impaired IFN-γ production by PD-1-deficient lymphocytes

We hypothesized that the patient suffered from TB due to insufficient IFN-γ production. To test this hypothesis, we examined the responses of the patient's leukocytes to mycobacteria *in vitro*. We first studied whole-blood samples from the patient (obtained after complete remission of TB or during immunosuppressive treatment for pulmonary autoimmunity). Upon stimulation with BCG plus IL-12, IFN-γ secretion by the patient's leukocytes was impaired to levels similar to those observed in patients with IL-12Rβ1 deficiency (Fig. 3a and Extended Data Fig. 3a). Following stimulation with BCG plus IFN-γ, the secretion of TNF, but not of IL-12p40, was also impaired (Extended Data Fig. 3b and c). We next studied PBMCs from the patient (obtained after complete remission of TB). Cells were stimulated with BCG and then incubated with a secretion inhibitor to evaluate both secreted and intracellular cytokines (see Methods for more details). IFN-γ secretion by the patient's PBMCs was, again, severely impaired, resembling the levels observed in the IL-12Rβ1-deficient patient tested, whereas such impairment was not observed for other proinflammatory cytokines (*e.g.,* IL-18) (Fig. 3b and Extended Data Fig. 3d). Moreover,

flow cytometry revealed defective IFN-γ production across all lymphocyte subsets studied, including Vδ2$^+$ γδ T, mucosal-associated invariant T (MAIT), and NK cells (Fig. 3c–e and Extended Data Fig. 3e). Furthermore, the patient's PBMCs and PHA blasts stimulated with anti-CD3/CD28 antibody-conjugated beads secreted less IFN-γ and TNF than cells from healthy controls, whereas the patient's immortalized HVS-T cells produced IFN-γ normally upon stimulation with anti-CD3/CD28 antibody-conjugated beads (Fig. 3f, g, and Extended Data Fig. 3f). Finally, splenocytes from PD-1-deficient mice produced less IFN-γ than cells from their wild-type age-matched controls after prolonged activation with anti-CD3/CD28 antibody-conjugated beads *ex vivo* (Extended Data Fig. 4). Thus, impaired IFN-γ production, possibly with impaired TNF production, underlies susceptibility to TB in the patient with PD-1 deficiency.

Depletion and dysfunction of T and NK lymphocyte subsets

We next investigated the cellular and molecular basis of the impaired IFN-γ production by studying PBMCs from the patient (obtained one month after the initiation of TB treatment) and his healthy brother and parents by mass cytometry (cytometry by time-of-flight, CyTOF) and flow cytometry (Extended Data Fig. 5). Monocyte and dendritic cell subsets were unaffected. Among T and NK lymphocyte subsets, the patient had significantly lower-than-normal numbers of Vδ2$^+$ γδ T cells and MAIT cells, both of which efficiently produce IFN-γ and TNF[27–29], and CD56^{bright} NK cells, a subset efficiently producing IFN-γ but not TNF[30]. By contrast, T helper (T_H) cell subsets, including T_H1 and T_H1* cells, were within the range of controls; T follicular helper (T_{FH}) cells, however, were moderately expanded. Moreover, CD4$^+$, CD8$^+$, and γδ T cells displayed enhanced expression of CD38, HLA-DR, and TIGIT, attesting to chronic activation, exhaustion, and impaired IFN-γ production[31,32]. We then investigated the molecular basis of these immunophenotypes by studying PBMCs from the patient (obtained one month after the initiation of TB treatment) and his healthy brother by single-cell RNA sequencing (scRNASeq) (Extended Data Fig. 6). Interestingly, the patient's effector T cells displayed enhanced expression of several type I IFN-stimulated genes (ISGs) (*e.g., IFIT3*, *OASL*, and *HERC5*). Type I IFN signaling is enhanced in patients on PD-1 blockade[33], attenuates IFN-γ production by T and NK cells in a STAT1-dependent manner in mice[34], and exacerbates TB in mice[35]. Type I IFNs also suppress TNF production in humans and mice[36]. Collectively, the depletion and dysfunction of multiple T and NK lymphocyte subsets compromise IFN-γ and TNF production in the patient with PD-1 deficiency.

Lymphoproliferative autoimmunity in PD-1 deficiency

Lymphoproliferative autoimmunity is observed in patients with heterozygous *STAT3* GOF mutations[8–10] or various forms of inherited FAS deficiency[37], and in PD-1-deficient mice[24]. Notably, the patient presented signs of persistent lymphoproliferation, including hepatosplenomegaly, and an expansion of total (~6.5% of leukocytes) and activated (CD38$^+$HLA-DR$^+$) CD4$^-$CD8$^-$ double-negative (DN) αβ T cells (Fig. 4a and b). Likewise, by re-analyzing previously published mouse CyTOF datasets[38], we found that effector DN αβ T cells were expanded in PD-1-deficient, but not CTLA-4-deficient, mice (Extended Data Fig. 7a and b). Furthermore, we found that DN T cells showed enhanced proliferation after anti-PD-1 monotherapy in patients bearing advanced bladder cancers or melanoma

(Extended Data Fig. 7c–f; see Methods for more details of the cohort). Both observations support the causality of inherited PD-1-deficiency for lymphoproliferative phenotypes. We then investigated the pathophysiological significance of these DN αβ T cells by analyzing the PBMCs of the patient (obtained one month after TB treatment initiation) and his healthy brother. Interestingly, the patient's DN αβ T cells upregulated FAS normally but produced less cytokines (*e.g.*, TNF) upon stimulation, as measured by flow cytometry (Extended Data Fig. 8). Finally, we comparatively analyzed PBMCs from the PD-1-deficient patient (obtained two weeks before his death) with cells from a patient with a heterozygous *STAT3* GOF mutation and two patients with inherited FAS deficiency. DN αβ T cells were expanded and, notably, showed a $CD38^{+}ROR\gamma T^{+}$ phenotype in all four patients (Fig. 4c and d). RNA sequencing of sorted DN αβ T cells revealed unique transcriptional signatures common to the PD-1-deficient and STAT3 GOF patients, but not seen in FAS-deficient patients, including i) higher levels of mRNA for anti-apoptotic genes (*e.g.*, *BCL6* and *FOXP1*) and multiple type I IFN-encoding genes, and ii) lower levels of mRNA for genes involved in calcium signaling (*e.g.*, *CAPN8*, *SYT3*, and *RYR1*) (Fig. 4e–g). Sorted $CD4^{+}$ αβ T cells from the PD-1-deficient and STAT3 GOF patients, but not from FAS-deficient patients, also showed elevated mRNA expression for *BCL6*, *IFIT3*, and *OASL* as determined by RT-qPCR (Extended Data Fig. 9a). Thus, PD-1 deficiency triggers lymphoproliferative autoimmunity that apparently phenocopies that seen in patients with *STAT3* GOF.

Excessive STAT3-activating cytokines and RORγT expression

We hypothesized that the patient suffered from systemic autoimmunity due to excessive STAT3 activity. Given the absence of non-synonymous *STAT3* variants in the patient's WES data and the normal STAT3 phosphorylation in response to IL-6 in the patient's EBV-B cells (Extended Data Fig. 9b), we excluded the possibility that the patient had any *STAT3* GOF variant. Instead, we hypothesized that enhanced production of STAT3-activating cytokines caused excessive STAT3 activity *in vivo*. Indeed, the patient's PBMCs stimulated with lipopolysaccharide (LPS) overproduced IL-6 and IL-23, and the patient's PHA blasts stimulated with anti-CD3/CD28 antibody-conjugated beads overproduced IL-6 (Fig. 4h and Extended Data Fig. 9c). Consistently, we detected elevated levels of IL-6 and IL-23, as well as soluble FAS ligand, IL-10, and osteopontin (serological markers of FAS deficiency[37]), in the patient's blood (Extended Data Fig. 9d and e). Consistent with the excessive response to LPS, the patient's myeloid cells showed various signs of dysregulation, including i) a remarkably altered transcriptional profile in classical monocytes, with significant enrichment in gene sets related to cellular responses to type I IFNs, IL-6 production, and responses to IL-6; ii) aberrant baseline expression of multiple type I IFN-encoding genes and type III *IFNL1*, but not of type II *IFNG*, in sorted monocytes, iii) enhanced expression of ICOS ligand in non-classical monocytes, and iv) decreased expression of PD-L2 in multiple myeloid cell subsets (Fig. 4i, j, and Extended Data Fig. 9f and g). We then searched for STAT3-dependent cellular phenotypes. IL-6 and IL-23 synergistically induce RORγT by activating STAT3 in humans[39]. Remarkably, i) both the patient and PD-1-deficient mice had high RORγT levels in αβ T cells; ii) both the patient's PBMCs activated with anti-CD3/CD28 antibody-conjugated beads and PHA blasts expressed high levels of *RORC* mRNA; and iii) the patient's HVS-T cells displayed enhanced RORγT expression upon activation (Extended Data Fig. 10a–e). Furthermore, a pharmacological STAT3 inhibitor

reversed the activation-induced RORγT upregulation in the patient's PHA blasts (Fig. 4k), indicating that PD-1-deficient T cells are prone to activation-induced, STAT3-dependent RORγT upregulation. Finally, the patient's sorted $CD4^+$ αβ memory T cells produced large amounts of IL-17A upon activation *ex vivo*, consistent with the enhanced RORγT expression (Extended Data Fig. 10f). RORγT is indispensable for IL-17A production in humans[40]. Overall, these data suggest that IL-6 and IL-23 excessively produced by PD-1-deficient T lymphocytes and monocytes overactivate STAT3 and drive the expansion of $ROR\gamma T^+$ DN αβ T cells, thus underlying lymphoproliferative autoimmunity.

Discussion

This study is the first report, to our knowledge, of an individual with a homozygous loss-of-function (LOF) mutation in *PDCD1* and, therefore, with inherited complete PD-1 deficiency. Our study fulfills the criteria of single-patient genetic studies[41] (the patient's sibling who died of a similar pulmonary illness was not genotyped), in that i) the homozygous *PDCD1* mutation occurs only in the patient and no other healthy individuals, ii) the *PDCD1* mutation is experimentally proven to abolish the expression and function of PD-1 protein, and iii) the causality of the *PDCD1* genotype for the clinical phenotype (*i.e.*, TB and autoimmunity) is well supported by the cellular phenotypes of the patient *in vitro*, and whole-organism phenotypes of relevant models *in vivo* (*i.e.*, PD-1-deficient mice and individuals on PD-1 blockade). Our study, therefore, sheds light on the mechanisms of TB and autoimmunity in patients on PD-1 blockade (*i.e.*, acquired PD-1 deficiency).

Both cancer patients on PD-1 blockade[2] and PD-1-deficient mice[22,24] are prone to autoimmunity, including pneumonitis. In search of etiological autoAbs underlying pneumonitis, we serologically identified two autoAbs against alpha 3 type-IV collagen, an autoantigen implicated in Goodpasture's syndrome[17], although the patient did not manifest any renal dysfunction until his terminal phase. We are currently investigating autoAbs observed in this patient and multiple patients who have developed pneumonitis after PD-1 blockade. Clinical management of PD-1-blockade-induced pneumonitis would benefit from identification of such autoAbs. We show that inherited PD-1 deficiency triggers lymphoproliferative autoimmunity that phenocopies *STAT3* GOF. Interestingly, as seen in our patient, patients with *STAT3* GOF mutations typically present thyroiditis, diabetes, and interstitial lung disease, with at least two cases of fatal alveolar hemorrhage reported[42,43]. DN αβ T cells are a hallmark of lymphoproliferative autoimmunity, abnormally expanding, expressing RORγT, and infiltrating organs in multiple cases of human monogenic and non-monogenic autoimmunity, including systemic lupus erythematosus (SLE)[9,10,37,44,45]. Consistently, an intronic polymorphism in *PDCD1* is weakly associated with susceptibility to SLE[46]. We show that PD-1-deficient DN αβ T cells have activated ($CD38^+HLA\text{-}DR^+$) and $ROR\gamma T^+$ phenotypes and express type I IFNs, while producing only modest amounts of inflammatory cytokines upon stimulation. Interestingly, unlike PD-1-deficient mice, CTLA-4-deficient mice have reduced DN αβ T cells with effector and $ROR\gamma T^+$ phenotypes, suggesting that those phenotypes are unique to PD-1 deficiency. We also show that PD-1-deficient T lymphocytes and monocytes produce large amounts of IL-6 and IL-23 upon activation, whereas PD-1-deficient T lymphocytes express RORγT in an activation-induced and STAT3-dependent manner. Tocilizumab, anti-IL-6 receptor mAb, is effective in patients

with *STAT3* GOF mutations suffering from autoimmune manifestations[42] and patients on PD-1 blockade with steroid-refractory immune-related adverse events (irAEs)[47], further suggesting shared pathophysiology. Besides, Tofacitinib, a JAK1/3 inhibitor currently used for rheumatoid arthritis and ulcerative colitis, is currently investigated for colitis induced by immune checkpoint blockade (NCT04768504). Likewise, Ustekinumab, a mAb targeting the common p40 subunit of IL-12 and IL-23 currently used for psoriasis, is empirically recommended for refractory irAEs, awaiting large-scale validation[48]. In contrast, although extensively studied in various autoimmune conditions, RORγT inhibitors are not tested in the context of irAEs following PD-1 blockade to date. Our study provides a rationale for further evaluating pharmacological inhibition of IL-6, IL-23, JAK/STAT3, and RORγT in patients on PD-1 blockade suffering from severe autoimmune manifestations.

Cancer patients[1,26] and macaques[49] on PD-1 blockade and PD-1-deficient mice[25] are all vulnerable to TB. However, the underlying mechanisms remain elusive. Interestingly, cells isolated from the lungs of Mtb-infected PD-1-deficient mice show impaired proliferation[50] and IFN-γ production[25] when compared with their wild-type counterparts after stimulation with Mtb antigens *in vitro*, reflecting their dysfunctional state *in vivo*. Moreover, PD-1 blockade impairs the accumulation of Mtb-specific IFN-γ^+/TNF^+CD4^+ T cells in both the bloodstream and bronchoalveolar lavage in infected macaques[49]. Finally, a longitudinal study of one patient shows a temporal gain and subsequent loss of Mtb-specific IFN-γ^+/TNF^+CD4^+ T cells in the bloodstream within six months of initiating PD-1 blockade before the development of necrotic TB granuloma[26]. Consistent with these findings, we report a severe impairment of IFN-γ and TNF production by PD-1-deficient leukocytes in response to stimulation with mycobacteria (after the clinical remission of TB), even though the patient had been IGRA-positive at the time of TB diagnosis. IFN-γ is a lymphokine that triggers macrophage activation and bactericidal activity[51], and IFN-γ signaling is indispensable for protective anti-TB immunity in humans[52]. Hence, we infer that the patient's IFN-γ-producing lymphocytes were quantitatively and functionally insufficient for protection against TB. We attribute the observed IFN-γ insufficiency to i) the reduced numbers of cytokine-producing lymphocytes, including $V\delta2^+$ γδ T, MAIT, and $CD56^{bright}$ NK cells, and ii) the type I IFN-mediated functional impairment of other residual T lymphocyte subsets. Likewise, TNF is mostly a monokine required for protection against TB in mice[53], and TNF blockade facilitates TB reactivation in humans[54]. The patient's lymphocytes produced only small amounts of TNF, which may have also contributed to the development of TB, although we have not tested TNF production by monocytes and tissue macrophages (the primary sources of TNF). Our findings suggest that, without appropriate PD-1 signaling, activated lymphocytes may become vulnerable to exhaustion and deletion. Overall, the concurrent autoimmunity and immunodeficiency in multiple vertebrates with inherited or acquired PD-1 deficiency suggests that PD-1:PD-L1/2 interactions are evolutionarily indispensable for both self-tolerance and protective immunity.

Methods

Case report

The patient was a Turkish boy born to first-degree consanguineous parents in 2007 and was referred for genetic analysis at the age of 10.5 years for suspected abdominal TB, based on the presence of three intraperitoneal cystic lesions. The patient had no respiratory symptoms, and his chest X-ray (CXR) was unremarkable. Percutaneous drainage of the cystic lesions was performed under ultrasound guidance. Biopsies of the mesenteric lymph node and omentum were performed at the same time. Histological examination of the mesenteric lymph node, omentum, and aspiration biopsy material revealed caseating granuloma and caseous necrosis. The smear of aspiration material was positive for acid-fast bacilli (AFB). Ziehl-Neelsen staining of the biopsy material also revealed the presence of bacilli. *M. tuberculosis* complex was detected by real-time PCR. Positive results were obtained for both the tuberculin skin test (TST) (induration size: 9×9 mm) and the interferon-gamma release assay (IGRA; QuantiFERON-TB Gold Plus-in-tube test, Qiagen). *M. tuberculosis* complex resistant to pyrazinamide but susceptible to other first-line anti-TB agents was eventually identified by culture of the aspiration material (Bactec Mycobacterium Growth Indicator Tube 960, BD Biosciences), although *M. tuberculosis* complex was not identified on Lowenstein-Jensen culture. Subsequently, species-specific PCR on DNA extracted from the paraffin-embedded biopsy material from the abdominal lesions demonstrated the presence of *M. tuberculosis*, thereby excluding the possibility of *M. bovis* infection.

The patient was diagnosed with type I diabetes (T1D), hypothyroidism, and juvenile idiopathic arthritis (JIA) at the age of three years. JIA was treated with naproxen sodium and short-term corticosteroids, which led to an improvement in symptoms. The patient also had recurrent suppurative otitis media and recurrent bone fractures. He had been vaccinated with BCG at the age of two months, with no adverse events, including BCG-itis (local reaction). He also received all the usual childhood vaccines, including live oral polio vaccine and measles, mumps, and rubella (MMR) vaccine, with no vaccine-related adverse events. His older brother was diagnosed with T1D and hypothyroidism at the age of seven months and died of a respiratory disease of undocumented etiology at the age of three years. His younger brother, parents, and all other family members up to the level of the grandparents are alive. None of the patient's relatives, except for his deceased older brother, had a remarkable clinical history, including autoimmunity or TB. The patient's six-year-old brother and parents tested negative by CXR and IGRA.

Physical examination at the initial presentation revealed splenomegaly, with a palpable spleen 9 cm below the costal margin. No lymphadenopathy was noted. A cataract and anterior uveitis sequelae were found in the right eye. Warts were observed on the patient's hands and face but not at other sites. No jaundice was observed. Despite prior vaccination with BCG, no BCG scar was observed on either the shoulder or the thigh. Laboratory tests revealed mild anemia and lymphopenia but no thrombocytopenia. Bone marrow aspiration revealed hypocellular and dysplastic marrow with sea-blue histiocytes. Megakaryocytes were reduced. The levels of CD212 (IL-12Rβ1) and CD25 expression on the peripheral blood leukocytes were similar to those in healthy controls tested simultaneously. However,

the level of HLA-DR expression was elevated, suggesting immune cell activation. Serum IgG and IgA levels were high, whereas IgM and IgE levels were normal. Serological tests revealed the presence of an anti-insulin autoantibody, but no other autoantibodies, including anti-GAD, anti-IA-2, anti-TG, and anti-TPO antibodies, were detected. Both the TST and IGRA were positive, whereas other microbiological and virological examinations were unremarkable.

The patient was diagnosed with abdominal tuberculosis, and the standard quadruple anti-TB drug treatment (isoniazid, rifampicin, ethambutol, and pyrazinamide) was initiated. However, anti-TB treatment was frequently interrupted due to hepatotoxicity. During this period, the patient received intermittent transfusions of fresh frozen plasma due to prolonged prothrombin time (PT) and activated partial thromboplastin time (APTT). The patient was also given supportive treatments (N-acetyl cysteine, ursodeoxycholic acid, and vitamin K). Drug-induced hepatotoxicity was suspected, and the regimen was modified (ethambutol and streptomycin). Cycloserine and levofloxacin were subsequently added to the treatment regimen. Despite the frequent interruption of anti-TB therapy, complete remission of abdominal TB was achieved, as demonstrated by a computed tomography (CT) scan, after eight months of treatment. Follow-up CXR revealed no lesions indicative of pulmonary TB.

At the age of 11 years, the patient presented with redness and pain in his eyes. Ophthalmological examination revealed rare cells, synechiae, and punctate epitheliopathy in the anterior segment of the eyes. Herpetic keratitis or toxic keratitis was suspected. On examination, the patient was also found to have a skin rash and stomatitis. Skin biopsy was also performed, and erythema multiforme was diagnosed. Anti-TB treatment was halted, and the patient was treated with corticosteroids for five days. No other immunomodulatory agent was administered. The symptoms resolved, and anti-TB treatment was re-initiated two weeks later. However, due to hepatotoxicity, anti-TB treatment had to be interrupted intermittently.

Three months later, the patient presented with cough, dyspnea, and exercise intolerance. CXR results were unremarkable, but chest CT showed bilateral mosaic ground-glass opacities, predominantly in the lower lobes. No mediastinal or hilar lymphadenopathy or mass lesion was detected. A diagnosis of either bronchiolitis obliterans or interstitial lung disease was suspected. Abdominal CT and ultrasonography performed simultaneously showed splenomegaly, with a hypertrophic left lobe and an atrophic right lobe of the liver, with macronodular contours. The portal vein and the left branch were wide, and periportal echogenicity was augmented. Doppler sonography of the portal system yielded findings consistent with portal hypertension. No signs of a recurrence of abdominal TB were noted.

Two months after developing dyspnea, the patient presented again with severe respiratory insufficiency. CXR revealed bilateral consolidations. Bronchoscopy was performed but did not contribute to the diagnosis. Bronchoalveolar lavage was negative for AFB and *Pneumocystis jirovecii*. Fungal culture was also negative. The patient's respiratory condition deteriorated, and he was admitted to the pediatric intensive care unit, intubated, and mechanically ventilated. He was empirically treated with methylprednisolone and abatacept (10 mg/kg, total: 400 mg), assuming a clinical diagnosis of autoimmune lung disease, even

though no autoantibodies explaining the patient's lung disease were detected. Six courses of therapeutic plasma exchange were also performed empirically to remove potentially pathogenic autoantibodies. However, the patient suffered from three alveolar hemorrhages and eventually died of multiple organ failure at the age of 11 years, three months after the onset of dyspnea, and 15 months after the onset of abdominal TB.

This report does not fully comply with the CARE guideline (https://www.care-statement.org/) in that the title does not contain the words "case report." This is because the study goes beyond a simple description of the case and hold generalizable findings in common with PD-1-deficient mice and patients on PD-1 blockade. That said, we have indicated that this is a single-patient study in the title.

Human subjects

The PD-1-deficient patient and his healthy brother and parents lived and were followed up in Turkey. Healthy volunteers were recruited at The Rockefeller University. The patient and his healthy brother and parents, together with one local control, one patient with biallelic loss-of-function (LOF) mutations of *IL12RB1*, and one patient with a heterozygous *STAT3* gain-of-function (GOF) mutation were recruited at the Necker Hospital for Sick Children. Two patients with biallelic LOF mutations of *FAS* were recruited at the National Institute of Allergy and Infectious Diseases. Patients with advanced bladder cancer or melanoma on nivolumab monotherapy were recruited for a clinical trial (the registration number: NCT02553642) and followed up at either Memorial Sloan Kettering Cancer Center (MSKCC) or Lehigh Valley Hospital. The trial is still ongoing, and no clinical endpoints are reported in this manuscript. Written informed consent was obtained from all patients and healthy volunteers enrolled in this study. As the PD-1-deficient patient and his brother were minors, parental consent was obtained for studying their biological materials and reporting the findings. The study was approved by the institutional ethics committees of The Rockefeller University, Necker Hospital for Sick Children, McGill University, Sidra Medicine, MSKCC, and The Garvan Institute of Medical Research, and was performed in accordance with the requirements of these bodies. Experiments on samples from human subjects were conducted in the United States, France, Canada, Qatar, and Australia, in accordance with local regulations and with the approval of the Institutional Review Board of the corresponding institution.

Species-specific PCR for Mycobacterium tuberculosis *complex (MTBC)*

The coding regions of *pncA* and *oxyR*, and the upstream region of *narG* were amplified from four independent DNA extracts from a block of tissue from the AFB-positive patient. *M. tuberculosis* Erdman and *M. bovis* BCG genomic DNA samples were used as positive controls. A no-template control was included for each amplified region, as a negative control. PCR was performed with *Taq* polymerase (New England Biolabs). Successful amplification was confirmed by gel electrophoresis before treatment with ExoSAP-It (USB) and subsequent sequencing (Eton Bioscience). For *pncA*, we used a single set of primers for amplification and sequencing (pncAF2 5'gtcgacgtgcagaacgactt and pncAR2 5'cgttctcgtcgactccttcg). For *oxyR*, two sets of primers were used for amplification (Set 1: oAF2302 5'ccatcgtgccgtgaagtcgc and oAF2303 5'gcgatccggctgggtggt; Set 2: oAF2304 5'

cagtgccgcaagcattctcg and oAF2305 5'cccggcaagacgctggtag). The amplified regions were sequenced with the Set 1 primers. For the upstream region of *narG*, one set of primers was used for amplification and sequencing (oAF2298 5'gcctatcgcgtgcatctg and oAF2299 5' gcactcgctggacgttac). Not all the DNA samples yielded a PCR product for all of the primer sets. The results in Extended Data Fig. 1a are, therefore, expressed as the number of samples with a given nucleotide/the number of extracts yielding an amplicon.

Phage immunoprecipitation sequencing for microbial antigens (VirScan)

Serum samples were obtained from the patient, his healthy six-year-old brother, and his parents, at two time points (at initial presentation and during follow-up). Serum samples from eight healthy pediatric controls were also included in the analysis. Moreover, Privigen® (CSL Behring), a concentrated human immunoglobulin G (IgG) product derived from pooled human plasma for intravenous immunoglobulin (IVIg) therapy, was included as a positive control, and IgG-depleted serum (Molecular Innovations, Inc.; Cat: HPLASERGFA5ML) was included as a negative control.

Phage immunoprecipitation sequencing (PhIP-Seq) was performed as previously described[55,56], with a modified version of the original VirScan T7 phage library[57] (kindly provided by Stephen Elledge, Brigham and Women's Hospital, Harvard Medical School, Boston, MA, USA). This extended version of the VirScan phage library displayed the complete proteome of most human-tropic viruses plus peptides derived from various microbial antigens and allergens annotated in the Immune Epitope Database (IEDB, www.iedb.org). Briefly, 4 μg of the IgG samples and 2×10^{10} plaque-forming units (PFUs) of the T7 phage library were incubated at 4°C overnight. The antibody-phage complexes were recovered with a mixture of protein A- and G-coated magnetic Dynabeads (Invitrogen). Unbound phages were removed by washing, and the immunoprecipitated phages were lysed to extract genomic DNA by heating the phage-bead complexes at 95°C for 10 minutes, and then cooling at 4°C for 15 minutes. Phage genomic DNA encoding presented peptides was amplified by PCR, and an additional round of PCR was then performed to barcode each sample with Illumina adapters using custom indexing primers. The final PCR products were pooled in equal volumes, except for the input library samples, which were added to the pool at a volume ~ 10 times that of all the other samples. Single-end sequencing was performed for 75 cycles with the NextSeq Kit v2 and NextSeq 500 platform (Illumina) to generate approximately two million reads per sample and ~20 million reads for the input library sample. We simultaneously prepared a sample containing the phage library without immunoprecipitation (the input library sample), and several negative control samples processed in the absence of human serum or plasma (mock IP samples). The mock samples were prepared to characterize non-specific binding for the downstream statistical analysis. We performed technical duplicates for each of the human samples, the input library without immunoprecipitation, the IVIg product, the IgG-depleted serum, and a total of 52 mock IP samples.

Species-specific enrichment scores were calculated for each pathogen, as previously described[56]. Briefly, mapping and counting of the reads to the original library sequences were conducted using *Bowtie2* (v2.3.4.3) and *SAMtools* (v1.9). The read counts were

adjusted based on the library size with a zero-inflated generalized Poisson model using Python (v3.7). The computed *P* values reflect the enrichment for each peptide relative to the background level defined by the input library data. A peptide was considered significantly enriched when the $-\log_{10} P$ value (*i.e.*, the peptide enrichment score) was at least 2.3, a cutoff value defined in the original VirScan study[55], in all of the technical replicates. Species-specific scores were calculated for each sample by counting the number of significantly enriched peptides derived from a given species (pathogen) without any continuous seven-residue or longer sequence overlap. Species-specific scores were adjusted by subtracting the number of peptides from the same species enriched in the 90th percentile of the mock IP samples (*i.e.*, species-specific background scores).

Phage immunoprecipitation sequencing for human autoantigens

PhIP-Seq was performed with a T7 phage library displaying 90-aa peptides almost completely covering the human proteome, with a 45-aa overlap, as previously described[58]. Serum samples from the patient, his healthy six-year-old brother, and his parents were obtained at the initial presentation. Briefly, 4 μg of the IgG samples and 5×10^{10} PFUs of the T7 phage library were incubated. The Privigen IVIg product, IgG-depleted serum, and mock IP samples were used as negative controls. PCR and sequencing were performed, reads were mapped to the original phage library sequences, and per-peptide enrichment scores were calculated as described in the previous section. Differential enrichment in the patient's sample relative to samples from other family members and negative controls was determined with the *limma* package in R. A $\log_2$ fold-change of 1 was used as a cutoff, and autoantigens potentially relevant to the patient's autoimmune diseases were explored manually.

T cell receptor (TCR) repertoire sequencing

Genomic DNA extracted from whole-blood samples from the patient and his healthy six-year-old brother was subjected to TCR β-chain (TRB) repertoire sequencing (Adaptive Biotechnologies Seattle, WA). The rearranged TRB genomic products were amplified by multiplex PCR with 52 forward primers for the *TRBV* gene segments and 13 reverse primers for the *TRBJ* gene segments. The PCR products were sequenced on the Illumina HiSeq platform.

The raw sequences were filtered for errors and aligned with reference genome sequences. The aligned sequences were then analyzed with the ImmunoSeq set of online tools. Total reads representing productive rearrangements were extracted for subsequent analyses. The length of complementarity-determining region 3 (CDR3), the Shannon entropy index of diversity [H], and the Simpson index of clonality [1-D] were calculated with the ImmunoSeq set of online tools. The grand average of hydropathy (GRAVY) score was calculated with the *alakazam* package in R. The *TRBV*-to-*TRBJ* pairing circos plots were generated with the *circlize* package in R.

Whole-exome sequencing (WES) and variant filtering

WES was performed, and the homozygosity rate was estimated with genomic DNA from the patient, his healthy six-year-old brother, and his parents, as previously described[59]. Variant

blacklisting was performed as previously described[60]. Minor allele frequencies (MAFs) in the general population, as reported in gnomAD database v2.1.1, and precomputed combined annotation–dependent depletion (CADD) scores v1.3[18] were used for variant filtering. The mutation significance cutoff (MSC) was calculated as previously described[19].

Sanger sequencing

Genomic DNA was extracted from whole-blood samples obtained from one healthy control, the patient, his six-year-old brother, and his parents. The region of interest was amplified by PCR. The PCR products were sequenced with the BigDye Terminator Cycle Sequencing Kit (Applied Biosystems). Sequencing products were purified with Sephadex G-50 Superfine Resin (GE Healthcare). Sequences were determined with an ABI 3730 DNA Analyzer (Applied Biosystems). Sequencing spectrum data were analyzed with Geneious software v8 (https://www.geneious.com).

Primary cells

Peripheral blood mononuclear cells (PBMCs) were isolated by the Ficoll-Hypaque density gradient centrifugation (GE Healthcare) of venous blood samples obtained from healthy volunteers, the patient, his parents, and his six-year-old brother. Cells were cryopreserved and stored at −150°C until use.

Cell culture

The HEK293T cell line was purchased from the ATCC and cultured in Dulbecco's modified Eagle medium (DMEM; Gibco) supplemented with 10% fetal bovine serum (FBS; Gibco). The HuT78 T-lymphoma cell line and Raji B-lymphoma cell line were purchased from the ATCC and cultured in Roswell Park Memorial Institute (RPMI)-1640 medium with GlutaMAX (Gibco), supplemented with 10% FBS (referred to hereafter as Lymphocyte medium). *Herpesvirus saimiri*-transformed T (HVS-T) and Epstein-Barr virus-transformed B (EBV-B) cell lines were generated in-house by infecting PBMCs with HVS or EBV. EBV-B cells were cultured in Lymphocyte medium. HVS-T cells were cultured in a specially formulated HVS-T medium [100 mL Panserin 401 (Pan Biotech), 100 mL RPMI-1640, 50 mL FBS, 3 mL GlutaMAX, and 2.5 mL gentamycin]. Recombinant human interleukin 2 (rIL-2; Roche, Cat: 11147528001) was added at a final concentration of 10 ng/mL. In continuous cultures, rIL-2 was added to the culture medium every 48 or 72 hours. PBMCs were rested in Lymphocyte medium. Phytohemagglutinin (PHA) blasts were generated by culturing PBMCs in Lymphocyte medium containing 1% PHA-M (Gibco, Cat: 10576015) and 10 ng/mL rIL-2 (PeproTech, Cat: 200–02). During continuous culture, Lymphocyte medium containing rIL-2 but not PHA was added every 48 or 72 hours. After two weeks of culture, PHA blasts were restimulated with ImmunoCult Human CD3/CD28/CD2 T Cell Activator (STEMCELL Technologies, Cat: 10970, 1:80) once in 10~14 days and maintained in ImmunoCult XF T Cell Expansion Medium (STEMCELL Technologies, Cat: 10981) containing rIL-2.

Subcloning

A full-length wild-type human *PDCD1* coding sequence (CDS) was inserted into the pcDNA3.1(+) plasmid. The CDS of a protein tagged with a DYKDDDDK-tag was prepared by adding the tag sequence directly after the last coding codon by PCR with a modified primer. The patient's frameshift variant (c.105dupC) and the common homozygous non-synonymous variants found in the gnomAD database (https://gnomad.broadinstitute.org/) were constructed by site-directed mutagenesis. The entire CDS was validated by Sanger sequencing.

A full-length CDS of wild-type (WT) or mutant (M, c.105dupC) human *PDCD1* (encoding PD-1), human WT *CD274* (encoding PD-L1) or human WT *PDCD1LG2* (encoding PD-L2) was inserted into the pTRIP-CMV-Puro-2A vector (gift from Nicolas Manel; Addgene plasmid #102611)[61]. The entire CDS was validated by Sanger sequencing.

Transient transfection

HEK293T cells were dispended into a 24-well plate at a density of 1×10^5 cells/well and were incubated overnight. On the next day, cells were transfected with a mixture of the plasmid (400 ng) and Lipofectamine 2000 (Invitrogen, 0.8 μL) and incubated overnight before use for experiments.

Analysis of PD-1 expression by western blotting

Transiently transfected HEK293T cells in a 24-well plate were lysed with 500 μL RIPA buffer [50 mM Tris-HCl (pH 8.0), 150 mM NaCl, 5 mM ethylenediaminetetraacetic acid (EDTA), 1% NP-40, 1% sodium deoxycholate, and 0.1% sodium dodecyl sulfate (SDS)] supplemented with cOmplete Mini Protease Inhibitor Cocktail (Sigma). Cells were transferred to a microtube and incubated for 30 minutes at 4°C, with rotation. Cells were then centrifuged for 20 minutes at a relative centrifugal force (rcf) of 20,000 x *g* at 4°C, and the supernatant was collected. Protein yield was determined with the DC Protein Assay (BioRad), and equal amounts of total protein and SDS-polyacrylamide gel electrophoresis (PAGE) sample buffer supplemented with 10% 2-mercaptoethanol were mixed, incubated for 10 minutes at 37°C, and loaded onto a 15% polyacrylamide gel. Proteins were separated by SDS-PAGE and transferred onto a polyvinylidene difluoride (PVDF) membrane. The membrane was blocked by incubation with a blocking buffer [5% bovine serum albumin (BSA) in TBS] for one hour at room temperature. The transferred proteins were detected by immunoblotting with the following primary antibodies: anti-PD-1 antibody for the N-terminal epitope (LSBio, Clone: 12A7D7, Cat: LS-C1444488, 1:1000, 4°C overnight), anti-PD-1 antibody for the C-terminal epitope (BioRad, rabbit polyclonal, Cat: AHP1705, 1:1000, 4°C overnight), HRP-tagged anti-DYKDDDDK Tag antibody (BioLegend, Clone: L5, Cat: 637312, 1:2000, two hours at room temperature), and HRP-tagged anti-GAPDH antibody (Santa Cruz, Clone: 0411, Cat: sc-47724 HRP, 1:5000, two hours at room temperature). All primary antibodies were diluted in the blocking buffer. The membrane was washed in wash buffer (0.1% Tween 20 in TBS) and incubated with the following secondary antibodies: HRP-tagged anti-mouse IgG (GE Healthcare, Cat: NXA931, 1:15000, one hour at room temperature) and HRP-tagged anti-rabbit IgG (GE Healthcare, Cat: NA934V, 1:15000, one hour at room temperature). Detection was performed with the

SuperSignal West Femto Maximum Sensitivity Substrate (Thermo Fisher Scientific). Images were acquired with an Amersham Imager 600 (GE Healthcare).

Analysis of PD-1 expression by flow cytometry

Transiently transfected HEK293T cells were removed from the well by incubation with TryPLE Express solution (Gibco) for 5 minutes at 37°C. Cells were washed once with phosphate-buffered saline (PBS) and stained with the Live/Dead Fixable Aqua Dead Cell Stain kit [reconstituted in 50 μL dimethyl sulfoxide (DMSO); used at 1:1000 in PBS] for 20 minutes at 4°C in the dark. Cells were washed once with FACS buffer (2% FBS and 2 mM EDTA in PBS, filter-sterilized) and stained with anti-PD-1-PE (eBioscience, Clone: MIH4, Cat: 12–9969-42, 1:50, one hour at 4°C in the dark) or isotype control (eBioscience, Clone: P3.6.2.8.1, Cat: 12–4714-41) antibody. The antibodies were diluted with FACS buffer supplemented with FcR Blocking Reagent (Miltenyi Biotec, Cat: 130–059-901, 1:50) and 0.1% sodium azide. Cells were washed once with FACS buffer and acquired with a BD LSR II Flow Cytometer (BD Biosciences). Data were analyzed with FlowJo software v10 (FlowJo, LLC).

EBV-B cells were dispensed into a V-bottomed 96-well plate at a density of 1×10^6 cells/well and were stained with Live/Dead Aqua and then with anti-PD-1-PE antibody. Cells were washed once with FACS buffer and then stained with PE-conjugated anti-biotin antibody (eBioscience, Clone: eBioPE-DLF, Cat: 13–4120-82, 1:250, one hour at 4°C in the dark). Cells were washed once with FACS buffer and finally stained with streptavidin-PE (eBioscience, Cat: 12–4317-87, 1:100, two hours at 4°C in the dark). Streptavidin-PE was diluted with FACS buffer supplemented with 0.1% sodium azide. Cells were washed twice with FACS buffer and then acquired.

Freshly thawed PBMCs were dispensed into a U-bottomed 96-well plate at a density of 2×10^5 cells/well and were allowed to rest overnight. On the next day, cells were stained with Live/Dead Aqua, and then with anti-PD-1-PE or isotype control antibody, together with the following antibodies: anti-CD3-APC (BioLegend, Clone: UCHT1, Cat: 300412, 1:100), anti-CD4-APC/Cy7 (BioLegend, Clone: RPA-T4, Cat: 300518, 1:100), anti-CD8-PerCP/Cy5.5 (BioLegend, Clone: SK1, Cat: 344710, 1:100), anti-CD14-Alexa Fluor 488 (BD, Clone: M5E2, Cat: 557700, 1:100), anti-CD19-Pacific Blue (BioLegend, Clone: HIB19, Cat: 302224, 1:100), and anti-CD56-Alexa Fluor 700 (BD, Clone: B159, Cat: 557919, 1:100). Cells were washed once with FACS buffer, and were then stained with PE-conjugated anti-biotin antibody followed by streptavidin-PE, and acquired.

PHA blasts were dispensed into a V-bottomed 96-well plate at a density of 1×10^6 cells/well. Cells were stained with Live/Dead Aqua and then with anti-PD-1-PE antibody, as well as anti-CD3-APC, anti-CD4-APC/Cy7, and anti-CD8-PerCP/Cy5.5 antibodies, for one hour at 4°C in the dark. The cells were then washed, stained with PE-conjugated anti-biotin antibody followed by streptavidin-PE, and then acquired.

Analysis of PD-1:PD-L1 and PD-1:PD-L2 ligation by flow cytometry

Transiently transfected HEK293T cells were removed from the well, washed once, and stained with Live/Dead Aqua, as described above. Cells were washed once with complete

culture medium and incubated (2.5 μg/100 μL/test, one hour at 37°C) with recombinant PD-L1-Fc (PeproTech, Cat: 310–35) or PD-L2-Fc (PeproTech, Cat: 310–38). The supernatant was removed, and cells were stained with anti-human IgG Fc-biotin (BioLegend, Clone: M1310G05, Cat: 410718, 1:50, one hour at 4°C in the dark) in FACS buffer supplemented with FcR Blocking Reagent (Miltenyi Biotec, 1:50) and 0.1% sodium azide. As a negative control, anti-human IgM-biotin (BioLegend, Clone: MHM-88, Cat: 314504, 1:50) and biotin-conjugated rat IgG2a isotype control (BioLegend, Clone: RTK2758, Cat: 400504, 1:50) antibodies were also used. Cells were washed once with FACS buffer and stained with streptavidin-PE (eBioscience, Cat: 12–4317-87, 1:100, one hour at 4°C in the dark) in FACS buffer supplemented with 0.1% sodium azide. Cells were washed twice with FACS buffer and acquired with a BD LSR II Flow Cytometer (BD Biosciences).

Analysis of PDCD1 expression by reverse transcription-quantitative PCR (RT-qPCR)

EBV-B cells and PHA blasts were dispensed into a U-bottomed 96-well plate at a density of 1×10^5 cells/well. Cells were lysed and reverse-transcribed with the Cells-to-Ct kit (Thermo Fisher Scientific) in accordance with the manufacturer's instructions. The cDNA was then used for qPCR with the *Taq*Man Gene Expression Master Mix (Applied Biosystems) and the FAM-MGB *Taq*Man probes for *PDCD1* (Hs01550088_m1 and Hs00169472_m1). The VIC-TAMRA probe for *GUSB* (Applied Biosystems, Cat: 4310888E) was used as an endogenous control. Real-time PCR amplification was monitored with the 7500 Fast Real-Time PCR System (Applied Biosystems). Relative expression levels were determined by the ΔCt method.

Lentiviral transduction

HEK293T cells were dispensed into a six-well plate at a density of 8×10^5 cells/well, in 2 mL/well DMEM supplemented with 10% FBS. On the next day, cells were transfected with pCMV-VSV-G (0.2 μg), pHXB2-env (0.2 μg; NIH-AIDS Reagent Program; #1069), psPAX2 (1 μg; a gift from Didier Trono; Addgene plasmid #12260), and either pTRIP-CMV-Puro-2A or the vector encoding a protein of interest (1.6 μg) in Opti-MEM (Gibco, 300 μL) containing Lipofectamine 2000 (Invitrogen, 10 μL) and PLUS Reagent (Invitrogen, 3 μL), according to the manufacturer's protocol. After six hours of transfection, the medium was replaced with 3 mL DMEM supplemented with 10% FBS and 150 μL 20% BSA/PBS (final 1% BSA), and the cells were incubated for a further 60 hours to produce lentiviral particles. The viral supernatant was harvested and centrifuged at 500 x *g* for 10 minutes at 4°C to remove debris. Protamine sulfate (Sigma, 10 μg/mL) was added to the supernatant, which was then used immediately or stored at −80°C until use.

HuT78 cells, HVS-T cells, or Raji cells were dispensed into a U-bottomed 96-well plate at a density of 2×10^5 cells/well, in 100 μL of Lymphocyte medium (supplemented with rIL-2), HVS-T medium (supplemented with rIL-2), and Lymphocyte medium, respectively. Viral supernatant was added (100 μL per well), and the cells were spinoculated for 2 hours at 1200 x *g* at 25°C. The cells were then further incubated for 48 hours at 37°C, and the medium was then replaced. Puromycin was added 96 hours after spinoculation at a concentration of 5 μg/mL, 2 μg/mL, or 10 μg/mL for HuT78 cells, HVS-T cells, and Raji cells, respectively.

For validation of the surface expression of PD-1, PD-L1, and PD-L2, cells were stained by incubation for one hour at 4°C in the dark with anti-PD-1-PE (eBioscience, Clone: MIH4, Cat: 12–9969-42, 1:100), anti-PD-L1-Alexa Fluor 488 (eBioscience, Clone: MIH1, Cat: 53–5983-42, 1:100), and anti-PD-L2-APC (eBioscience, Clone: MIH18, Cat: 17–5888-42, 1:100), or mouse IgG1 isotype control antibodies conjugated with identical fluorochromes (eBioscience, Clone: P3.6.2.8.1). Cells were then stained by incubation for 10 minutes at 4°C in the dark with 7-AAD (Tonbo Biosciences), washed once with FACS buffer, and acquired with a BD LSR II Flow Cytometer (BD Biosciences). Cells were kept on ice during acquisition.

T:B cell coculture assay

HuT78 cells (1×10^5 cells/well) were dispensed into a U-bottomed 96-well plate and cocultured with Raji cells (5×10^5 cells/well) with or without blinatumomab (BPS Biosciences, Cat: #100441, 10 ng/mL) in 100 μL of Lymphocyte medium. Blinatumomab is an engineered protein directed against CD3 and CD19 in a bispecific fashion, which binds $CD3^+$ T cells to $CD19^+$ Raji cells. Cells were incubated with GolgiStop (BD Biosciences, Cat: 554724, 1:1600) for six hours at 37°C. Cells were then washed once with PBS, stained by incubation with Live/Dead Aqua for 15 minutes at 4°C in the dark, and then surface-stained by incubation with anti-CD3-FITC (Tonbo Biosciences, Clone: UCHT1, Cat: 35–0038, 1:200) and anti-CD19-Super Bright 645 (eBioscience, Clone: SJ25C1, Cat: 64–0198-42, 1:200) antibodies at 4°C in the dark for 30 minutes. Cells were then washed once with FACS buffer and fixed by incubation with the fix buffer from the True-Nuclear Transcription Factor Buffer Set (BioLegend, Cat: 424401) at room temperature for 45 minutes in the dark. Cells were washed once with FACS buffer, permeabilized by incubation with True-Nuclear permeabilization buffer at room temperature in the dark for five minutes, and stained, by incubation overnight at 4°C in the dark with the following panel in permeabilization buffer: FcR blocking reagent (Miltenyi Biotec, 1:50), anti-IFN-γ-PE/Dazzle 594 (BioLegend, Clone: 4S.B3, Cat: 502546, 1:100), and anti-TNF-BV711 (BioLegend, Clone: MAb11, Cat: 502940, 1:100) antibodies. On the next day, cells were washed three times with FACS buffer and acquired with a BD LSR II Flow Cytometer (BD Biosciences). The expression levels of IFN-γ and TNF in $CD3^+CD19^-$ T cells were assessed with FlowJo.

HVS-T cells (1×10^5 cells/well) were dispensed into a U-bottomed 96-well plate and cocultured with Raji cells (5×10^5 cells/well) with or without blinatumomab (BPS Biosciences, 1 ng/mL) in 100 μL of HVS-T medium. Cells were incubated for ~18 hours at 37°C. On the next day, the cell culture was spiked with anti-CD107a-Alexa Fluor 647 antibody (BioLegend, Clone: H4A3, Cat: 328612, 1:200) and GolgiStop (BD Biosciences, Cat: 554724, 1:1600) and incubated for an additional six hours at 37°C. Cells were washed once with PBS, stained by incubation with Live/Dead Aqua for 15 minutes at 4°C in the dark, and then surface-stained by incubation with anti-CD3-BV421 (BioLegend, Clone: UCHT1, Cat: 300434, 1:100), anti-CD4-redFluor 710 (Tonbo Biosciences, Clone: OKT4, Cat: 80–0048, 1:100), anti-CD8-FITC (BioLegend, Clone: RPA-T8, Cat: 301060, 1:100), and anti-CD19-Super Bright 645 (eBioscience, Clone: SJ25C1, Cat: 64–0198-42, 1:100) antibodies at 4°C in the dark for 30 minutes. Cells were washed, fixed, permeabilized,

and stained by incubation overnight at 4°C in the dark with the following panel in permeabilization buffer: FcR blocking reagent (Miltenyi Biotec, 1:50), anti-IFN-γ-PE/Dazzle 594 (BioLegend, Clone: 4S.B3, Cat: 502546, 1:100), anti-TNF-BV711 (BioLegend, Clone: MAb11, Cat: 502940, 1:100), anti-IL-6-PE/Cy7 (BioLegend, Clone: MQ2–13A5, Cat: 501120, 1:100), and anti-IL-17A-APC/Cy7 (BioLegend, Clone: BL168, Cat: 512320, 1:100) antibodies. On the next day, cells were washed three times with FACS buffer and acquired with a BD LSR II Flow Cytometer (BD Biosciences). The expression levels of CD107a, IFN-γ, TNF, IL-6, and IL-17A in $CD3^{+}CD19^{-}$ T cells were assessed with FlowJo.

Preparation of artificial antigen-presenting cells (aAPCs)

Artificial antigen-presenting cells (aAPCs) were prepared as previously described[62]. Briefly, Dynabeads M-450 Epoxy (Invitrogen, Cat: 14011, 2×10^{8} beads per reaction) were washed once with buffer 1 (0.1 M sodium phosphate buffer), and covalently conjugated with antibodies or recombinant proteins by overnight incubation at room temperature. The following antibodies and recombinant proteins were used for conjugation: Ultra-LEAF purified anti-CD3 antibody (BioLegend, Clone: OKT3, Cat: 317236, 8 μg), Ultra-LEAF purified anti-CD28 antibody (BioLegend, Clone: CD28.2, Cat: 302934, 10 μg), recombinant human IgG1 Fc protein (R&D Systems, Cat: 110-HG-100, 82 μg), PD-L1-Fc (PeproTech, Cat: 310–35, 82 μg), PD-L2-Fc (PeproTech, Cat: 310–38, 82 μg), PD-L1-Fc (R&D Systems, Cat: 156-B7, 82 μg), PD-L2-Fc (R&D Systems, Cat: 1224-PL, 82 μg), Ultra-LEAF purified mouse IgG1 isotype control (BioLegend, Clone: MOPC-21, Cat: 400165, 82 μg), mouse IgG1 anti-PD-1 antibody (GenScript, Clone: PD1.D3, Cat: A01829, 82 μg), Ultra-LEAF purified mouse IgG2b isotype control (BioLegend, Clone: MG2b-57, Cat: 401215, 82 μg), and mouse IgG2b anti-PD-1 antibody (MyBioSource, Clone: 9X21, Cat: 690864, 82 μg). On the next day, the beads were washed twice with buffer 2 (0.1% BSA/PBS supplemented with 2 mM EDTA) and were stored in buffer 2 at 4°C in the dark for subsequent experiments. Experiments with PD-L1-Fc or PD-L2-Fc purchased from two vendors (PeproTech or R&D Systems) were combined as technical replicates unless otherwise indicated.

Degranulation assay

HVS-T cells were dispensed into a U-bottomed 96-well plate at a density of 2×10^{5} cells/well, in 200 μL HVS-T medium without rIL-2. Cells were simultaneously stimulated and stained with aAPCs (6×10^{5} beads/well) and anti-CD107a-Alexa Fluor 647 (BioLegend, Clone: H4A3, Cat: 328612, 1:200) for five hours at 37°C. Cells were then transferred to the wells of a V-bottomed 96-well plate containing 7 μL of the staining mix [7-amino-actinomycin D (7-AAD, Tonbo Biosciences, Cat: 13–6993) 2 μL, anti-CD3-BV421 (BioLegend, Clone: UCHT1, Cat: 300434) 1 μL, anti-CD4-APC/Cy7 (BioLegend, Clone: RPA-T4, Cat: 300518) 2 μL, and anti-CD8-FITC (BioLegend, Clone: RPA-T8, Cat: 301060) 2 μL] and incubated for 10 minutes at 4°C in the dark. The supernatant was removed, and cells were washed once and then resuspended in cold FACS buffer and acquired with a BD LSR II Flow Cytometer (BD Biosciences). Cells were kept on ice during acquisition.

TCR signaling assay

PHA blasts were dispensed into a U-bottomed 96-well plate at a density of 2×10^{5} cells/well in 100 μL Lymphocyte medium, and were stimulated with aAPCs (6×10^{5} beads/well) for 24

hours. On the next day, cells were washed once with PBS, stained with Live/Dead Aqua for 15 minutes at 4°C in the dark, and washed once with FACS buffer. Cells were then surface-stained with anti-CD3-BV421 (BioLegend, Clone: UCHT1, Cat: 300434, 1:200), anti-CD4-redFluor 710 (Tonbo Biosciences, Clone: OKT4, Cat: 80–0048, 1:100), and anti-CD8-FITC (BioLegend, Clone: RPA-T8, Cat: 301060, 1:100) antibodies at 4°C in the dark for 30 minutes. Cells were fixed by directly adding BD Cytofix Fixation Buffer (BD Biosciences, Cat: 554655) and incubating at room temperature for 15 minutes in the dark. Cells were then washed once with FACS buffer and permeabilized by incubation with methanol at 4°C in the dark for 15 minutes. The methanol was removed, and the cells were stained with anti-phospho ERK1/2 (Thr202/Tyr204)-Alexa Fluor 647 (BioLegend, Clone: 6B8B69, Cat: 369504, 1:10) antibody, for three hours, at room temperature, in the dark. Finally, cells were washed three times with FACS buffer and acquired with a BD LSR II Flow Cytometer (BD Biosciences).

T cell activation assay

HVS-T cells or PHA blasts were dispensed in a U-bottomed 96-well plate at a density of 5×10^4 cells/well, in 100 μL/well of either HVS-T medium and Lymphocyte medium, respectively. The medium was not supplemented with rIL-2. Cells were incubated with mock Dynabeads, Dynabeads conjugated with Ultra-LEAF purified anti-CD3 antibody (BioLegend, Clone: OKT3) and Ultra-LEAF purified anti-CD28 antibody (BioLegend, Clone: CD28.2), Raji cells (2.5×10^5 cells/well), or Raji cells (2.5×10^5 cells/well) plus blinatumomab (BPS Biosciences, 0.1 ng/mL) for ~18 hours at 37°C. On the next day, the cell culture was spiked with anti-CD107a-Alexa Fluor 647 antibody (BioLegend, Clone: H4A3, Cat: 328612, 1:200) and GolgiStop (BD Biosciences, Cat: 554724, 1:1600) and incubated for an additional six hours at 37°C. The supernatants were collected and stored at −20°C for measuring cytokine concentrations, and the cells were harvested by centrifugation for flow cytometry analysis. Cells were washed once with PBS, stained with Live/Dead Aqua for 15 minutes at 4°C in the dark, and then surface-stained by incubation with anti-CD3-BV421 (BioLegend, Clone: UCHT1, Cat: 300434, 1:100), anti-CD4-redFluor 710 (Tonbo Biosciences, Clone: OKT4, Cat: 80–0048, 1:100), anti-CD8-FITC (BioLegend, Clone: RPA-T8, Cat: 301060, 1:100), and anti-CD19-Super Bright 645 (eBioscience, Clone: SJ25C1, Cat: 64–0198-42, 1:100) antibodies at 4°C in the dark for 30 minutes. Cells were then washed once with FACS buffer and fixed by incubation with the fix buffer from the True-Nuclear Transcription Factor Buffer Set (BioLegend, Cat: 424401) at room temperature for 45 minutes in the dark. Cells were washed once with FACS buffer, permeabilized by incubation with True-Nuclear permeabilization buffer at room temperature in the dark for five minutes, and then stained by incubation with permeabilization buffer at 4°C in the dark overnight, with the cytokine panel [FcR Blocking Reagent (Miltenyi Biotec, 1:50), anti-IFN-γ-PE/Dazzle 594 (BioLegend, Clone: 4S.B3, Cat: 502546, 1:100), anti-TNF-BV711 (BioLegend, Clone: MAb11, Cat: 502940, 1:100), anti-IL-6-PE/Cy7 (BioLegend, Clone: MQ2–13A5, Cat: 501120, 1:100), and anti-IL-17A-APC/Cy7 (BioLegend, Clone: BL168, Cat: 512320, 1:100) antibodies] or the RORγT staining mix [FcR blocking reagent (Miltenyi Biotec, 1:50) and anti-RORγT-PerCP/eFluor 710 (eBioscience, Clone: AFKJS-9, Cat: 46–6988-80, 3:500) antibodies]. On the next day, the cells were washed three times with FACS buffer and acquired with a BD LSR II Flow

Cytometer (BD Biosciences). $CD3^{+}CD19^{-}$ T cells were gated with FlowJo. Secreted IFN-γ levels were determined using the human IFN-γ uncoated ELISA kit (Invitrogen, Cat: 88–7316-88).

Whole-blood stimulation with BCG

Venous blood samples were drawn from one local control, the brother, the parents, and the patient. Samples were collected in heparin-containing tubes and processed as previously described[5]. Briefly, blood samples were diluted 1:2 in RPMI-1640 medium (Gibco) and supplemented with penicillin (100 U/mL) and streptomycin (Gibco, 100 μg/mL). The samples were then dispensed into a 48-well plate (1 mL/well), either left non-stimulated or stimulated with live *Mycobacterium bovis* BCG Pasteur substrain at a multiplicity of infection (MOI) of 20 BCG cells per leukocyte alone, or with BCG plus recombinant human IL-12 (R&D Systems, Cat: 219-IL, 20 ng/mL). As a positive control, cells in separate wells were stimulated with phorbol 12-myristate 13-acetate (PMA, Sigma, Cat: P8139, 40 ng/mL) and ionomycin (Sigma, Cat: I9657, 10 μM). After 48 hours of stimulation, secreted cytokine levels in the supernatants were determined with the human IFN-γ ELISA Ready-SET-Go kit (Invitrogen, Cat: 50–173-27) and the human IL-12p40 ELISA kit (Invitrogen, Cat: KAC1561).

PBMC stimulation assay with BCG

Freshly thawed PBMCs were dispensed into a U-bottomed 96-well plate at a density of 2×10^{5} cells/well, in 200 μL of Lymphocyte medium/well. Technical duplicates were prepared for the PBMCs from the PD-1 patient and the IL-12Rβ1$^{-/-}$ patient. Cells were incubated in the presence or absence of live BCG, at an MOI of 1, with or without recombinant human IL-12 (R&D Systems, 500 pg/mL) or recombinant human IL-23 (R&D Systems, Cat: 1290-IL, 10 ng/mL). After 40 hours of stimulation, GolgiPlug (BD Biosciences, Cat: 555029, 1:1000) was added to each well to inhibit cytokine secretion. After another eight hours of incubation, supernatants were collected and stored at −20°C for measuring cytokine concentration, and the cells were harvested by centrifugation for flow cytometry analysis. In brief, cells were stained with the Zombie NIR Fixable Viability Kit (BioLegend, 1:2000) at room temperature for 15 minutes, and then on ice for 30 minutes with a surface staining panel containing FcR blocking reagent (Miltenyi Biotec, 1:50), anti-CD3-Alexa Fluor 532 (eBioscience, Clone: UCHT1, Cat: 58–0038-42, 1:50), anti-γδTCR-FITC (eBioscience, Clone: B1.1, Cat: 11–9959-41, 1:50), anti-Vδ2-APC/Fire 750 (BioLegend, Clone: B6, Cat: 331419, 1:100), anti-CD56-BV605 (BioLegend, Clone: 5.1H11, Cat: 362537, 1:100), anti-CD4-BV750 (BD Biosciences, Clone: SK3, Cat: 566356, 1:800), anti-CD8a-Pacific Blue (BioLegend, Clone: SK1, Cat: 344717, 1:100), anti-Vα7.2 TCR-APC (BioLegend, Clone: 3C10, Cat: 351708, 1:100), anti-Vα24-Jα18-PE/Cy7 (BioLegend, Clone: 6B11, Cat: 342912, 1:100), anti-CD20-BV785 (BioLegend, Clone: 2H7, Cat: 302356, 1:200), and anti-PD-1-PE (eBioscience, Clone: MIH4, Cat: 12–9969-42, 1:100) antibodies. Cells were fixed by incubation with 2% paraformaldehyde (PFA)/PBS on ice for 15 minutes. Cells were then permeabilized/stained by incubation overnight at −20°C in the perm buffer from the Nuclear Transcription Factor Buffer Set (BioLegend), with an intracellular cytokine panel containing FcR blocking reagent (Miltenyi Biotec, 1:50), anti-IFN-γ-BV711 (BioLegend, Clone: 4S.B3, Cat: 502540, 1:50), anti-TNF-BV510

(BioLegend, Clone: MAb11, Cat: 502950, 1:50), and anti-IL-10-PE/Dazzle594 (BioLegend, Clone: JES3–19F1, Cat: 506812, 1:50) antibodies. As a positive control, cells in separate wells were stimulated by incubation with PMA (Sigma, 25 ng/mL) and ionomycin (Sigma, 500 nM) for eight hours without GolgiPlug (for measuring secreted cytokines) or for one hour without GolgiPlug followed by a further seven hours with GolgiPlug (for staining intracellular cytokines). Cells were acquired with an Aurora cytometer (Cytek). Data were manually gated with FlowJo and then imported into R for further analysis. The cellular composition was visualized through Uniform Manifold Approximation and Projection (UMAP) in R based on the expression levels of CD3, CD4, CD8a, CD20, Vδ2 TCR, Vα7.2 TCR, and Vα24-Jα18. Data were down-sampled to 10,000 cells per sample for visualization. Data from technical duplicates were combined before down-sampling. Secreted cytokine levels in the supernatants were determined with the LEGENDplex Human Inflammation Panel 1 13-plex kit (BioLegend, Cat: 740809). Data were analyzed in R.

PBMC stimulation assay with non-mycobacterial stimulants

Freshly thawed PBMCs were dispensed into a U-bottomed 96-well plate at a density of 2×10^5 cells/well, in 200 μL of Lymphocyte medium/well. Cells were either left unstimulated or were stimulated for 24 hours with lipopolysaccharide (LPS; Sigma, Cat: L4641, 10 ng/mL), Dynabeads Human T-Activator CD3/CD28 (Gibco, 8×10^4 beads/well), or PMA (Sigma, 25 ng/mL) plus ionomycin (Sigma, 500 nM). Supernatants were collected and stored at −20°C. The levels of secreted cytokines in the supernatants were determined with the LEGENDplex Human Inflammation Panel 1 13-plex kit (BioLegend). Data were analyzed in R.

Murine splenocyte activation assay

All mouse experiments related to this study were approved by the Institutional Review Board of Graduate School of Medicine, Kyoto University, Japan (Registration number: MedKyo21035). Spleens from PD-1-deficient mice or their wild-type age-matched controls (C57BL/6N, female, 4 months old) were briefly dissociated and suspended in ammonium chloride potassium buffer (0.15 M NH_4Cl, 1 mM $KHCO_3$, 0.1 mM Na_2.EDTA) to lyse red blood cells. The isolated splenocytes were washed and dispensed in 96-well U-bottomed plates at a density of 2×10^5 cells per well in 200 μL of RPMI-1640 medium including 10% FBS, L-glutamine, 1 mM sodium pyruvate, 1% MEMNEAA, 55 μM 2-mercaptoethanol, penicillin-streptomycin, and 20 U/mL recombinant human IL-2 (PeproTech, Cat: 200–02). Human IL-2 is effective for the culture of mouse T lymphocytes. Cells were stimulated for 48 hours with Dynabeads Mouse T-Activator CD3/CD28 (Gibco, Cat: 11456D, 8×10^4 beads/well). On days 2 and day 6, cells were restimulated with fresh beads. Half the number of cells were passaged on day 2 to prevent overgrowth. The supernatant was collected every two days and replaced with fresh medium. The levels of secreted IFN-γ were determined by ELISA. On day 8, cells were further stimulated with PMA (Sigma, Cat: P8139, 50 ng/mL) and ionomycin (Sigma, Cat: 10634, 1 μg/mL) for two hours, and then for an additional four hours in the presence of brefeldin A (eBioscience, Cat: 00–4506-51, 1:1000) and monensin (eBioscience, Cat: 00–4505-51, 1:1000). The supernatant was then collected for ELISA, and the cells were stained with the Zombie NIR Fixable Viability kit (BioLegend, Cat: 423105) for 10 minutes at 4°C, and then incubated with anti-CD16/CD32 Fc receptor blocker

(eBioscience, Cat: 16–0161-86, 1:1000), anti-γδTCR-FITC (BioLegend, Cat: 118106, Clone: GL3, 1:300), anti-CD3-BUV395 (BD Biosciences, Cat: 563565, Clone: 145–2C11, 1:500), anti-CD4-PE-cyanine 7 (Invitrogen, Cat: 25–0041-82, Clone: GK1.5, 1:500), anti-CD8-Super Bright 780 (eBioscience, Cat: 78–0081-82, Clone: 53–6.7, 1:500) antibodies for 20 minutes at 4°C. The cells were fixed with the True-Nuclear Transcription Factor Buffer set (BioLegend) and intracellularly stained by overnight incubation at 4°C with anti-IFN-γ-PE antibody (BioLegend, Cat: 505807, Clone: XMG1.2, 1:50) in Perm buffer. After staining, the volume of the sample was adjusted to 150 μL and mixed with 5 μL of CountBrigft absolute counting beads (molecular probes, Cat: C36950). Cells were acquired with a BD LSRFortessa X-20 Flow Cytometer (BD Biosciences). Data were manually gated with FlowJo.

Immunophenotyping of primary leukocytes by mass cytometry

Mass cytometry (cytometry by time-of-flight, CyTOF) was performed with two different antibody panels: a general immunophenotyping panel (CyTOF-G) and a T cell-focused panel (CyTOF-T). Freshly thawed PBMCs (1.0×10^6 cells per panel) were stained with Fc block and then with a panel of metal-conjugated antibodies obtained from Fluidigm or by customized conjugation. The CyTOF-G panel consisted of the following antibodies: anti-CD45–89Y, anti-CD57–113In, anti-CD11c-115In, anti-CD33–141Pr, anti-CD19–142Nd, anti-CD45RA-143Nd, anti-CD141–144Nd, anti-CD4–145Nd, anti-CD8–146Nd, anti-CD20–147Sm, anti-CD16–148Nd, anti-CD127–149Sm, anti-CD1c-150Nd, anti-CD123–151Eu, anti-CD66b-152Sm, anti-CD86–154Sm, anti-CD27–155Gd, anti-CCR5–156Gd, anti-CD117–158Gd, anti-CD24–159Tb, anti-CD14–160Gd, anti-CD56–161Dy, anti-γδTCR-162Dy, anti-CRTH2–163Dy, anti-CLEC12A-164Dy, anti-CCR6–165Ho, anti-CD25–166Er, anti-CCR7–167Er, anti-CD3–168Er, anti-CX3CR1–169Tm, anti-CD38–170Er, anti-CD161–171Yb, anti-CD209–172Yb, anti-CXCR3–173Yb, anti-HLA-DR-174Yb, anti-PD-1–175Lu, anti-CCR4–176Yb, and anti-CD11b-209Bi. The CyTOF-T panel consisted of the following antibodies: anti-CD57–113In, anti-CD103–141Pr, anti-CD19–142Nd, anti-CD45RA-143Nd, anti-KLRG1–144Nd, anti-CD4–145Nd, anti-CD8–146Nd, anti-CD28–147Sm, anti-CD16–148Nd, anti-CD127–149Sm, anti-CD1c-150Nd, anti-CD123–151Eu, anti-CD66b-152Sm, anti-TIGIT-153Eu, anti-ICOS-154Sm, anti-CD27–155Gd, anti-TIM-3–156Gd, anti-CCR6–158Gd, anti-CD14–160Gd, anti-CD56–161Dy, anti-γδTCR-162Dy, anti-CXCR5–163Dy, anti-CD69–164Dy, anti-4–1BB-165Ho, anti-CD25–166Er, anti-CCR7–167Er, anti-CD3–168Er, anti-OX40–169Tm, anti-CD38–170Er, anti-CD95–171Yb, anti-LAG-3–172Yb, anti-CXCR3–173Yb, anti-HLA-DR-174Yb, anti-PD-1–175Lu, and anti-CCR4–176Yb. Stained cells were washed, fixed, and permeabilized with barcode permeabilization buffer (Fluidigm) and were then barcoded with the Cell-ID 20-Plex Pd Barcoding Kit from Fluidigm. Samples were then washed, pooled into a single tube, and stored until acquisition on a Helios mass cytometer (Fluidigm). Dead cells and doublets were excluded by staining the cells with a rhodium-based dead cell exclusion intercalator (Rh103) before fixation, and cationic iridium nucleic acid intercalators (Ir191 and Ir193) after fixation. Subsets were manually gated with FlowJo and further analyzed in R. CyTOF-G data for a subset of healthy controls were generated in a previous study[63].

Analysis of innate-like T cells by flow cytometry

Freshly thawed PBMCs (1.0–1.5×10^6 cells) were stained with the Zombie NIR Fixable Viability Kit (BioLegend, 1:2000) for 15 minutes at room temperature. Cells were then stained with the following panel for 30 minutes on ice: FcR blocking reagent (Miltenyi Biotec, 1:50), anti-CD3-Alexa Fluor 532 (eBioscience, Clone: UCHT1, Cat: 58–0038-42, 1:50), anti-CD4-BV750 (BD Biosciences, Clone: SK3, Cat: 566356, 1:800), anti-CD8a-BV510 (BioLegend, 1:200), anti-CD56-BV605 (BioLegend, Clone: 5.1H11, Cat: 362537, 1:100), anti-γδTCR-FITC (eBioscience, Clone: B1.1, Cat: 11–9959-41, 1:50), anti-Vδ1-VioBlue (Miltenyi Biotec, Clone: REA173, Cat: 130–120-583, 1:50), anti-Vδ2-APC/Fire 750 (BioLegend, Clone: B6, Cat: 331419, 1:100), anti-CD161-PE (BioLegend, Clone: HP-3G10, Cat: 339938, 1:100), anti-Vα7.2-BV711 (BioLegend, Clone: 3C10, Cat: 351731, 1:100), anti-Vα24-Jα18-PE/Cy7 (BioLegend, Clone: 6B11, Cat: 342912, 1:100), and anti-Vβ11-APC (Miltenyi Biotec, Clone: REA559, Cat: 130–125-508, 1:50) antibodies. The cells were fixed by incubation with 2% PFA in PBS for 15 minutes at room temperature in the dark. Cells were acquired with an Aurora Flow Cytometer (Cytek). Data were analyzed with FlowJo.

Analysis of major leukocyte subsets by flow cytometry

Freshly thawed PBMCs (2×10^6 cells for controls and 5×10^6 cells for the patient) were stained with the Zombie NIR Fixable Viability Kit (BioLegend, 1:2000) for 15 minutes on ice. Cells were then stained with the following panel for 30 minutes on ice: FcR blocking reagent (Miltenyi Biotec, 1:50), anti-CD3-BD Horizon V450 (BD Biosciences, Clone: UCHT1, Cat: 560365, 1:450), anti-CD4-BUV563 (BD Biosciences, Clone: SK3, Cat: 612913, 1:450), anti-CD8-BUV737 (BD Biosciences, Clone: SK1, Cat: 612754, 1:150), anti-CD14-BUV395 (BD Biosciences, Clone: MφP9, Cat: 563561, 1:100), anti-CD16-PE/Dazzle 594 (BioLegend, Clone: 3G8, Cat: 302053, 1:150), anti-CD20-BV785 (BioLegend, Clone: 2H7, Cat: 302356, 1:150), anti-CD56-BV605 (BioLegend, Clone: 5.1H11, Cat: 362537, 1:50), anti-γδTCR-Alexa Fluor 647 (BioLegend, Clone: B1, Cat: 331214, 1:50), anti-Vδ1-FITC (Miltenyi Biotec, Clone: REA173, Cat: 130–118-498, 1:450), anti-Vδ2-APC/Fire 750 (BioLegend, Clone: B6, Cat: 331419, 1:1350), anti-Vα7.2-Alexa Fluor 700 (BioLegend, Clone: 3C10, Cat: 351727, 1:50), MR1-BV421 (provided by the NIH Tetramer Core Facility, 1:200), anti-Vα24-Jα18-BV480 (BD Biosciences, Clone: 6B11, Cat: 746788, 1:50), and anti-Vβ11-APC (Miltenyi Biotec, Clone: REA559, Cat: 130–125-508, 1:150) antibodies. Cells were then fixed on ice for 30 minutes and permeabilized with the True-Nuclear Transcription Factor Buffer Set (BioLegend). The cells were stained for intracellular transcription factors by incubation at 4°C in the dark overnight with the following panel: anti-Tbet-PE/Cy7 (BioLegend, Clone: 4B10, Cat: 644823, 1:1350), anti-RORγT-PE (BD Biosciences, Clone: Q21–559, Cat: 563081, 1:50), and anti-EOMES-PerCP/eFluor 710 (eBioscience, Clone: WD1928, Cat: 46–4877-41, 1:50) antibodies. Cells were acquired with an Aurora Flow Cytometer (Cytek). Data were analyzed with FlowJo.

Analysis of αβ T cell and myeloid cell subsets by flow cytometry

Freshly thawed PBMCs (2×10^6 cells for controls, 5×10^5 cells for the brother, and 1×10^6 cells for the patient) were stained by incubation with the Zombie NIR Fixable Viability

Kit (BioLegend, 1:1000 in PBS) for 15 minutes at 4°C in the dark. Cells were washed once and surface-stained by incubation for 30 minutes at 4°C in the dark with FACS buffer containing the following reagents: 0.1% sodium azide, FcR blocking reagent (Miltenyi Biotec, 1:50), anti-αβTCR-BV750 (BioLegend, Clone: IP26, Cat: 306745, 1:25), anti-CD4-BUV563 (BD Biosciences, Clone: SK3, Cat: 612912, 1:100), anti-CD8-BUV805 (BD Biosciences, Clone: SK1, Cat: 612889, 1:100), anti-CD14-Spark NIR 685 (BioLegend, Clone: 63D3, Cat: 367149, 1:100), anti-CD16-PE/Fire 640 (BioLegend, Clone: 3G8, Cat: 302067, 1:100), anti-CD19-BV650 (BD Biosciences, Clone: HIB19, Cat: 740568, 1:100), anti-CD56-BV570 (BioLegend, Clone: HCD56, Cat: 318329, 1:100), anti-CD141-BV605 (BioLegend, Clone: M80, Cat: 344117, 1:100), anti-CD1c-BUV496 (BD Biosciences, Clone: F10/21A3, Cat: 750182, 1:100), anti-CD11c-BV510 (BioLegend, Clone: 3.9, Cat: 301633, 1:100), anti-CD123-BV480 (BD Biosciences, Clone: 9F5, Cat: 566133, 1:100), anti-CD38-BV785 (BioLegend, Clone: HIT2, Cat: 303529, 1:100), anti-HLD-DR-APC/Fire 810 (BioLegend, Clone: L243, Cat: 307674, 1:100), anti-CD80-BUV661 (BD Biosciences, Clone: 2D10.4, Cat: 751731, 1:100), anti-CD86-BV421 (BioLegend, Clone: IT2.2, Cat: 305426, 1:100), anti-ICOS-PE/Cy5.5 (eBioscience, Clone: ISA-3, Cat: 35–9948-42, 1:100), anti-ICOSL-BUV737 (BD Biosciences, Clone: 2D3/B7-H2, Cat: 748934, 1:100), anti-PD-1-PE (eBioscience, Clone: MIH4, Cat: 12–9969-42, 1:100), anti-PD-L1-Alexa Fluor 488 (eBioscience, Clone: MIH1, Cat: 53–5983-42, 1:100), anti-PD-L2-APC (eBioscience, Clone: MIH18, Cat: 17–5888-42, 1:100), anti-FAS-BUV395 (BD Biosciences, Clone: DX2, Cat: 740306, 1:100), and anti-FASL-BUV615 (BD Biosciences, Clone: NOK-1, Cat: 752306, 1:100) antibodies. Cells were then fixed and permeabilized with the True-Nuclear Transcription Factor Buffer set (BioLegend) and intracellularly stained by incubation overnight at 4°C with anti-CD3-Spark Blue 550 (BioLegend, Clone: SK7, Cat: 344852, 1:100), anti-Tbet-PE/Cy5 (eBioscience, Clone: 4B10, Cat: 15–5825-82, 1:500), and anti-RORγT-PerCP/eFluor 710 (eBioscience, Clone: AFKJS-9, Cat: 46–6988-82, 1:500) antibodies in Perm buffer. Cells were then washed three times and acquired with an Aurora Flow Cytometer (Cytek). Data were analyzed with FlowJo.

For assessing cellular phenotypes after stimulation, freshly thawed PBMCs were dispensed into a U-bottomed 96-well plate at a density of 5×10^5 cells/well, in 100 μL of Lymphocyte medium/well. Cells were either left unstimulated or were stimulated with LPS (Sigma, 10 ng/mL), ImmunoCult Human CD3/CD28/CD2 T Cell Activator (STEMCELL Technologies, 1:100), or PMA (Sigma, 25 ng/mL) plus ionomycin (Sigma, 500 nM). After 18 hours of stimulation, cells were spiked with monensin (Tonbo Biosciences, Cat: TNB-4505-L001, 1:1000) and brefeldin A (Tonbo Biosciences, Cat: TNB-4506-L001, 1:1000), and incubated for a further six hours. Cells were then harvested by centrifugation for flow cytometry analysis. Adherent cells were detached by incubation with TrypLE Express Enzyme (Gibco, Cat: 12604013) for 5 minutes in the incubator. Cells were stained with Zombie NIR dye, surface-stained, and fixed and permeabilized as described above. Cells were then intracellularly stained by overnight incubation at 4°C with anti-CD3-Spark Blue 550 (BioLegend, Clone: SK7, 1:100), anti-IL-6-PE/Cy7 (BioLegend, Clone: MQ2–13A5, Cat: 501120, 1:100), anti-IL-12p35-eFluor 660 (eBioscience, Clone: SNKY35, Cat: 50–7359-42, 1:100), anti-IL-17A-APC/Cy7 (BioLegend, Clone: BL168, Cat: 512320, 1:500), anti-IL-17F-eFluor 450 (eBioscience, Clone: SHLR17, Cat: 48–7169-42, 1:100),

anti-IL-22-PerCP/Cy5.5 (BioLegend, Clone: 2G12A41, Cat: 366709, 1:100), anti-IL-23p19-Alexa Fluor 700 (R&D Systems, Clone: 727753, Cat: IC17161N, 1:100), anti-IFN-γ-PE/Dazzle 594 (BioLegend, Clone: 4S.B3, Cat: 502546, 1:500), anti-TNF-BV711 (BioLegend, Clone: MAb11, Cat: 502940, 1:500), anti-Tbet-PE/Cy5 (eBioscience, Clone: 4B10, Cat: 15–5825-82, 1:500), and anti-RORγT-PerCP/eFluor 710 (eBioscience, Clone: AFKJS-9, Cat: 46–6988-82, 1:500) antibodies in Perm buffer. Cells were then washed three times and acquired with an Aurora Flow Cytometer (Cytek). Data were analyzed with FlowJo.

Analysis of transcription factors in αβ T cells by flow cytometry

Freshly thawed PBMCs (2×10^5 cells) were stained by incubation with Live/Dead Aqua dye (1:1000 in PBS) for 20 minutes at 4°C in the dark. Cells were washed once and surface-stained by incubation for one hour at 4°C in the dark with FACS buffer containing the following reagents: 0.1% sodium azide, FcR blocking reagent (Miltenyi Biotec, 1:50), anti-αβTCR-PE/Cy7 (BioLegend, Clone: IP26, Cat: 306719, 1:100), anti-CD3-FITC (Tonbo Biosciences, Clone: UCHT1, Cat: 35–0038, 1:200), anti-CD4-APC/Cy7 (Tonbo Biosciences, Clone: RPA-T4, Cat: 25–0049, 1:100), anti-CD8-BD Horizon V450 (BD Biosciences, Clone: RPA-T8, Cat: 560347, 1:100), anti-CD25-BV711 (BioLegend, Clone: M-A251, Cat: 356137, 1:100), and anti-CD127-PE/Dazzle 594 (BioLegend, Clone: A019D5, Cat: 351336, 1:100) antibodies. Cells were then fixed and permeabilized with the FOXP3/Transcription Factor Staining Buffer Set (eBioscience, Cat: 00–5523-00). Intracellular staining was performed for three hours at room temperature in the dark, in Perm buffer containing the following reagents: FcR blocking reagent (Miltenyi Biotec, 1:50), anti-FOXP3-PE (BioLegend, Clone: 259D, Cat: 320207, 1:100), anti-HELIOS-Alexa Fluor 700 (eBioscience, Clone: 22F6, Cat: 56–9883-41, 1:100), anti-EOMES-eFluor 660 (eBioscience, Clone: WD1928, Cat: 14–4877-82, 1:100), and anti-RORγT-PerCP/eFluor 710 (eBioscience, Clone: AFKJS-9, Cat: 46–6988-80, 3:500). Cells were then washed three times and acquired with a BD LSR II Flow Cytometer (BD Biosciences). Data were analyzed with FlowJo.

Analysis of RORC expression by RT-qPCR

Freshly thawed PBMCs were dispended into a U-bottomed 96-well plate at a density of 2×10^5cells/well and were stimulated for 24 hours with Dynabeads Human T-Activator CD3/CD28 (Gibco, Cat: 111.61D, 8×10^4 beads/well). Cells were lysed and reverse-transcribed with the Cells-to-Ct kit (Thermo Fisher Scientific). Two FAM-MGB *Taq*Man probes for *RORC* (Hs01076122_m1 and Hs00172860_m1) were used to assess the expression of *RORC*. The VIC-TAMRA probe for *GUSB* (Applied Biosystems) was used as an endogenous control. Real-time qPCR was performed as described above.

PHA blasts were dispended into a U-bottomed 96-well plate at a density of 5×10^4cells/well without further stimulation. Cells were lysed and reverse-transcribed with the Cells-to-Ct kit (Thermo Fisher Scientific). A FAM-MGB *Taq*Man probe for *RORC* (Hs00172860_m1) was used to assess the expression of *RORC*. The VIC-TAMRA probe for *GUSB* (Applied Biosystems) was used as an endogenous control. Real-time qPCR was performed as described above.

Analysis of IL-17A production

$CD4^+$ αβ memory T cells were sorted from cryopreserved PBMCs and cultured for five days with T Cell Activation/Expansion beads (Miltenyi Biotec, Cat: 130–091-441), as described previously[64]. Supernatants were harvested, and the production of IL-17A was determined with cytometric bead arrays (BD Biosciences).

STAT3 phosphorylation assay

EBV-B cells were dispended into a U-bottomed 96-well plate at a density of 5×10^5cells/well and were serum-starved for two hours in RPMI-1640 medium with GlutaMAX supplemented with 1% FBS. Cells were then stained with Live/Dead Aqua for 15 minutes at 4°C, and stimulated with recombinant human IL-6 (PeproTech, Cat: 200–06, 100 ng/mL) for 30 minutes at 37°C. Cells were subsequently fixed with BD Cytofix Buffer (BD Biosciences, Cat: 554655) for 15 minutes at room temperature, permeabilized with methanol for 15 minutes at 4°C, and stained with the following antibody panel at 4°C in the dark overnight: FcR blocking reagent (Miltenyi Biotec, 1:50), anti-pSTAT3 (pY705)-Alexa Fluor 647 (BD Biosciences, Clone: 4/P-STAT3, Cat: 557815, 1:100), and anti-pSTAT1 (pY701)-PE-CF594 (BD Biosciences, Clone: 4a, Cat: 562674, 1:100) antibodies. Cells were then washed three times and acquired with a BD LSR II Flow Cytometer (BD Biosciences). Data were analyzed with FlowJo. Background levels were determined with the corresponding isotype controls.

STAT3 inhibition assay

PHA blasts were dispensed into a U-bottomed 96-well plate at a density of 2×10^5 cells/well in 100 μL of Lymphocyte medium/well. The medium was not supplemented with rIL-2. Cells were incubated with either mock Dynabeads or Dynabeads conjugated with Ultra-LEAF purified anti-CD3 antibody (BioLegend, Clone: OKT3) and Ultra-LEAF purified anti-CD28 antibody (BioLegend, Clone: CD28.2), in the presence or absence of a STAT3-specific inhibitor (Stattic, Santa Cruz Biotechnology, Cat: sc-202818, 2–200 μM) for 6 hours at 37°C. Cells were then stained with Live/Dead Aqua for 15 minutes at 4°C, and surface-stained by incubation for 30 minutes at 4°C with anti-CD3-APC (Tonbo Bioscience, Clone: UCHT1, Cat: 35–0038, 1:100), anti-CD4-redFluor 710 (Tonbo Biosciences, Clone: OKT4, Cat: 80–0048, 1:100), and anti-CD8-FITC (BioLegend, Clone: RPA-T8, Cat: 301060, 1:100) antibodies. Cells were then fixed and permeabilized with the True-Nuclear Transcription Factor Buffer Set (BioLegend, Cat: 424401), and intracellular staining was performed by incubation in the dark overnight at 4°C with permeabilization buffer containing FcR Blocking Reagent (Miltenyi Biotec, 1:50) and anti-RORγT-PerCP/eFluor 710 (eBioscience, Clone: AFKJS-9, Cat: 46–6988-80, 1:500) antibody. On the next day, the cells were washed three times with FACS buffer and acquired with a BD LSR II Flow Cytometer (BD Biosciences). Cells were gated with FlowJo.

Analysis of mouse immunophenotyping datasets

CyTOF datasets for adult PD-1-deficient and CTLA-4-deficient mice and their littermates generated in a previously published study[38] were downloaded from Flow Repository

(accessions FR-FCM-ZYFS and FR-FCM-ZYFQ, respectively). Subsets were manually gated with FlowJo and further analyzed in R.

Analysis of T cell proliferation in patients treated with PD-1 blockade immunotherapy

PBMC samples were obtained longitudinally before and after nivolumab monotherapy from patients with advanced bladder cancer or melanoma (*N*=37). Six patients were treated at the Lehigh Valley Hospital, while other patients were treated at MSKCC. All patients provided written informed consent for their PBMC samples to be used for research at the corresponding sites. All cryopreserved PBMC samples were analyzed at MSKCC. Freshly thawed PBMC samples were stained with Live/Dead Aqua and then with anti-CD4-Qdot 655 (Invitrogen, Clone: S3.5, Cat: Q10007, 1:500) and anti-CD8-Qdot 605 (Invitrogen, Clone: 3B5, Cat: Q10009, 1:250) antibodies. Cells were then fixed and permeabilized with the FOXP3/Transcription Factor Fixation/Permeabilization Concentrate and Diluent (eBioscience, Cat: 00–5521-00), and subjected to intracellular staining with anti-CD3-BV570 (BioLegend, Clone: UCHT1, Cat: 300436, 1:200) and anti-Ki-67-Alexa Fluor 700 (BD Biosciences, Clone: B56, Cat: 561277, 1:83) antibodies. Cells were acquired on a BD LSRFortessa Flow Cytometer (BD Biosciences) and analyzed with FlowJo.

Single-cell RNA sequencing (scRNASeq)

Single-cell RNA sequencing was performed on PBMCs obtained from the patient and his healthy six-year-old brother. The frozen PBMCs were rapidly thawed at 37°C and gently resuspended by serial additions of DMEM containing 10% FBS to a final volume of 14 mL. Cells were centrifuged at 300 x *g* for 5 minutes and were washed twice with 5 mL of medium to remove debris. Viability was assessed with the LIVE/DEAD Aqua viability kit (Thermo Fisher Scientific, Cat: L3224). The preparation was enriched in viable cells by resuspending 1×10^6 cells in 200 μL of 2% FBS and 1 mM calcium chloride in PBS and passing the suspension through a strainer with 40 μm pores, before removing dead cells with the EasySep Dead Cell Removal Kit (StemCell Technologies, Cat: 17899). Cells were then centrifuged at 300 x *g* for 5 minutes and resuspended at a concentration of 1×10^3 cells/μL in 0.04% BSA in PBS. The initial viability of ~50% was increased to 79% and 75% for the samples of the patient and his brother, respectively. The samples were loaded onto a 10X Genomics Chromium chip for single-cell capture. Libraries were prepared with the Chromium Single Cell 3’ Reagent Kit (v3.1). Library quality was assessed with a Bioanalyzer DNA chip. The libraries were sequenced on one lane (S4 flowcell) of an Illumina NovaSeq 6000 sequencer. Sequences were processed with Cell Ranger 3.1.0. The filtered feature-cell matrix was used for subsequent analyses. Separately, PBMCs from four healthy controls were processed and sequenced as described above (*i.e.*, historical controls), and the data were analyzed simultaneously.

Publicly available control PBMC datasets were downloaded from the 10X Genomics website (https://support.10xgenomics.com/single-cell-gene-expression/datasets). The filtered feature-cell matrix was retrieved for the following datasets: frozen PBMCs (Donors A to C) from Zheng et al.[65], 33,000 PBMCs from a healthy donor from the Chromium demonstration (v1 Chemistry, processed by Cell Ranger 1.1.0), 8,000 PBMCs from a healthy donor from the Chromium demonstration (v2 Chemistry, processed by Cell Ranger

2.1.0), 10,000 PBMCs from a healthy donor from the Chromium demonstration (v3 Chemistry, processed by Cell Ranger 3.0.0) with or without cell surface protein levels determined by TotalSeq, 5,000 PBMCs from a healthy donor from the Chromium Next GEM demonstration (v3.1 Chemistry, processed by Cell Ranger 3.0.2) with or without cell surface protein levels determined by TotalSeq, and a total of 66,000 PBMCs from an aggregate of eight Chromium connect channels and eight manual channels (v3.1 Chemistry, processed by Cell Ranger 3.1.0). These 10 datasets were used as the baseline for subsequent analyses.

The data were analyzed as follows. First, data-adaptive quality control filtering was performed based on the number of features detected and the percentage of mitochondrial genes. The library was then normalized for size, with both log-transformed and non-transformed count values retained. Genes that were not expressed in any of the datasets were discarded. Second, batch effects were corrected with the log-normalized counts by the Fast-MNN method implemented in the *Batchelor* package with default parameters[66]. The datasets obtained from the 10X Genomics website consisted of four batches [Next GEM (NG), V3, V2, and V1]. Four historical controls were considered a separate batch (HGIDCtrl) distinct from another batch containing the patient and his brother (HGIDPD1). Third, the batch-corrected log-normalized counts were dimension-reduced through UMAP, and the top 50 components were used to construct a shared nearest-neighbor graph with the *buildSNNGraph* function implemented in the *scran* package with default parameters. The graph was then divided into clusters with the Louvain algorithm implemented in the *igraph* package. The clusters were then manually inspected, merged, and reannotated, based on the expression patterns of characteristic genes. For the two TotalSeq datasets, the following cell types were defined based on surface marker expression levels: $CD14^{+}$ monocyte, $CD3^{-}CD14^{+}CD16^{-}CD19^{-}CD56^{-}$; $CD16^{+}$ monocyte, $CD3^{-}CD14^{-}CD16^{+}CD19^{-}CD56^{-}$; DC, $CD3^{-}CD14^{-}CD16^{-}CD19^{-}CD56^{-}HLA\text{-}DR^{+}$; B, $CD3^{-}CD14^{-}CD16^{-}CD19^{+}CD56^{-}$, NK, $CD3^{-}CD14^{-}CD16^{-}CD19^{-}CD56^{+}$. T cells ($CD3^{+}CD14^{-}CD16^{-}CD19^{-}CD56^{-}$) were further gated into: $CD8^{+}$ T, $CD4^{-}CD8^{+}$; DN T, $CD4^{-}CD8^{-}$; $CD4^{+}$ Treg, $CD4^{+}CD25^{+}CD127^{lo}$. Non-Treg cells were further gated into: $CD4^{+}$ naïve T, $CCR7^{+}CD45RO\text{-}CD45RA^{+}$; $CD4^{+}$ memory T, $CD45RO^{+}CD45RA^{-}$. These gated subsets were overlaid on the graph-based clusters to facilitate their annotation. Finally, the following clusters were defined: Naive CD4, Naive CD8, Memory T, Effector T, NK, Naive B, Memory B, Plasma, CD14 Mono, Int. Mono, CD16 Mono, mDC, pDC, Basophil, Platelet, and Dying. Platelets, basophils, and dying cells were excluded from subsequent analyses.

For identification of the genes from a given cluster upregulated in the patient's cells relative to those of his brother and the public controls, we performed per-cluster multigroup differential expression (DE) analysis. This analysis aimed to identify a subset of genes differentially regulated in the patient's cells relative to those of his brother and other controls. This analysis is different from conventional between-cluster DE analysis, in which genes characteristic of each cluster are defined. The Naive B, Memory B, and Plasma clusters were merged as "B," whereas the CD14 Mono, Int. Mono, and CD16 Mono clusters were merged as "Monocyte." The two TotalSeq datasets and corresponding non-TotalSeq datasets were considered technical duplicates and were therefore aggregated before DE analysis. To detect only the most robustly differentially expressed genes in the patient, we

employed a “pseudobulk” approach, in which read counts from all single cells in a given cluster were aggregated into a single metric. Pseudobulk DE methods have been shown to outperform single-cell DE methods in terms of false-discovery rate (FDR) and true-positive rate (TPR)[67]. Furthermore, we used two different pseudobulk aggregation strategies. First, raw (non-normalized) read counts were summed, mimicking the total read counts obtained in a conventional RNA sequencing experiment. Second, read counts normalized by a per-cell library size (but not log-transformed) were averaged and further normalized by the mean expression levels of multiple housekeeping genes: *C1orf43*, *CHMP2A*, *EMC7*, *GPI*, *PSMB2*, *PSMB4*, *RAEB7A*, *REEP5*, *SNRPD3*, *VCP*, and *VPS29*, as recommended by Eisenberg and Levanon[68]. This metric essentially reflects the mean gene expression levels per single cell normalized against housekeeping genes, thus mimicking conventional RT-qPCR. We then applied *DESeq2*[69] and *edgeR*[70] to the summed read counts, and *NOISeq*[71] to the normalized mean read counts. In *edgeR*, we used the likelihood ratio test (LRT) instead of the quasi-likelihood test (QLT), because QLT estimates of condition-specific dispersions from biological replicates were not appropriate for our single-patient study. In *DESeq2*, we also used LRT rather than the standard Wald test. Finally, we focused on genes upregulated in the patient relative to both his brother and the public controls, by using consensus results from all three DE testing strategies. The criteria for DE were: (i) statistical significance relative to controls, (ii) $\log_2$ fold-change > 1 relative to controls, and (iii) $\log_2$ fold-change > 1 relative to the patient’s brother. For *DESeq2* and *edgeR*, FDR-adjusted *P* values < 0.05 were considered significant. For *NOISeq*, a probability > 0.9 was considered significant, and $\log_2$ fold-change was calculated by taking the $\log_2$ of the level of expression in the patient and dividing it by the mean expression level in controls and the brother. For the genes identified as differentially expressed by all the three approaches, a heatmap was generated with the *ComplexHeatmap* package, with the $\log_2$ fold-change values compared with controls (10X and in-house controls combined) derived from housekeeping gene-normalized expression levels. All analyses were performed in R.

To delineate more subtle differences within a given cell subset, we used TooManyCells, a suite of graph-based algorithms equipped with divisive hierarchical clustering for the unbiased exploration of single-cell clades[72], with default settings based on non-batch-corrected read counts. Cells from the patient and his brother were analyzed. The Naive T, Memory T, and Effector T clusters were combined for T cell analysis. Differential expression analysis was conducted between “branches” to identify genes characteristic of each branch, in which a “branch” was defined as a node plus all subnodes belonging to that node. Gene-set enrichment analysis was conducted with the top 10,000 genes (selected based on the FDR-adjusted *P* values and ranked by their $\log_2$ fold-change values) against the Gene Ontology (GO) gene sets obtained from the MSigDB Collections (http://www.gsea-msigdb.org/gsea/msigdb/index.jsp) with the *fgsea* package in R. Significantly enriched GO terms (with FDR-adjusted *P* values below 0.05) were further inspected manually.

Sorting of primary leukocytes

Frozen PBMCs were rapidly thawed at 37°C and gently resuspended by serial additions of Lymphocyte medium to a final volume of 10 mL. Cells were centrifuged at 300 x *g* for 6 minutes and resuspended in 1 mL of Lymphocyte medium and 10 U/mL DNase I

(New England Biolab, Cat: M0303). PBMCs (3.0×10^6 cells) were stained by incubation with the following panel at 4°C for 20 minutes: FcR blocking reagent (Miltenyi Biotec, 1:50), anti-αβTCR-PE/Cy7 (BioLegend, Clone: IP26, Cat: 306720, 1:100), anti-CD3-BV421 (BioLegend, Clone: UCHT1, Cat: 300434, 1:100), anti-CD4-redFluor 710 (Tonbo Biosciences, Clone: OKT4, Cat: 80–0048, 1:100), anti-CD8-PerCP/Cy5.5 (BioLegend, Clone: RPA-T8, Cat: 301032, 1:100), anti-CD14-APC/Cy7 (BioLegend, Clone: HCD14, Cat: 325620, 1:100), anti-CD16-APC (Tonbo Biosciences, Clone: 3G8, Cat: 20–0166, 1:100), anti-CD19-Super Bright 645 (eBioscience, Clone: SJ25C1, Cat: 64–0198-42, 1:100), and anti-CD56-Alexa Fluor 488 (BD Biosciences, Clone: B159, Cat: 557699, 1:100) antibodies. Cells were then spiked with 7-AAD (Tonbo Biosciences, 1:200) and incubated at 4°C for 10 minutes. Cells were washed once, resuspended in 200 μL of FACS buffer, and filtered in Cell Strainer tubes (Corning, Cat: 352235). Cells were sorted with a BD FACS Aria (BD Biosciences).

Analysis of autoimmunity-ssociated genes by RT-qPCR

We validated the genes identified as differentially expressed in the scRNASeq experiment, using the patient's $CD4^+$ αβ T cells sorted from freshly thawed PBMCs cryopreserved at a different time from those used for scRNASeq (*i.e.,* biological replicates). $CD4^+$ αβ T cells ($\alpha\beta TCR^+CD3^+CD4^+CD8^-CD19^-$) from two healthy controls, two $FAS^{-/-}$ patients, one patient with a *STAT3* GOF mutation, and the PD-1 patient were directly sorted in the RLT buffer of the RNeasy Plus Micro Kit (Qiagen, Cat: 74034), with an RLT buffer-to-sorting buffer (PBS) ratio of 3:1. RNA was extracted, and reverse transcription was performed with SuperScript IV (Invitrogen, Cat: 18090050). The expression levels of *BCL6, HDAC9, IFIT1, IFIT3, OASL,* and *RSAD2* were assessed with FAM-MGB *Taq*Man probes purchased from Thermo Fisher Scientific (Hs00153368_m1, Hs01081558_m1, Hs00356631_g1, Hs01922752_s1, Hs00984387_m1, and Hs00369813_m1, respectively). The VIC-TAMRA probe for *GUSB* (Applied Biosystems) was used as an endogenous control. Real-time qPCR was performed as described above.

RNA sequencing (RNASeq)

Double-negative (DN) αβ T cells ($\alpha\beta TCR^+CD3^+CD4^-CD8^-CD19^-$) and monocytes ($CD3^-CD14^{+/dim}CD19^-CD56^-$) from three and five healthy controls, respectively, and from two $FAS^{-/-}$ patients, one patient with a *STAT3* GOF mutation, and the PD-1 patient were directly sorted in TRIzol LS (Invitrogen, Cat: 10296010), with a Trizol LS-to-sorting buffer (PBS) ratio of 3:1. Phase separation was induced with chloroform, and RNA was extracted from the aqueous phase with the miRNeasy Micro Kit (Qiagen, Cat: 217084) on a QIAcube Connect (Qiagen). After RiboGreen quantification and quality control on an Agilent BioAnalyzer, 1–2 ng of total RNA with RNA integrity numbers of 3 to 10 was subjected to amplification with the SMART-Seq v4 Ultra Low Input RNA Kit (Clontech, Cat: 63488), and 12–16 cycles of amplification. We then used 5–10 ng of amplified cDNA to prepare libraries with the KAPA Hyper Prep Kit (Kapa Biosystems KK8504), with eight additional PCR cycles. Samples were barcoded and analyzed on a HiSeq 4000 in paired-end 2×100 bp mode, with the HiSeq 3000/4000 SBS Kit (Illumina). A mean of 26 million paired reads were generated per sample. The FASTQ files were first inspected with *fastqc* to ensure that the raw data were of high quality. The FASTQ reads of each sample were

then aligned to the GENCODE human reference genome GRCh38.p13 with *STAR* aligner ver. 2.7, and the alignment quality of each BAM file was evaluated with *RSeQC*. Reads were quantified with *featureCounts* ver. 1.6, to generate gene-level feature counts from the read alignment. Differential expression (DE) was analyzed with the *DESeq2* package[69] in R. Genes with summed read counts across samples of less than 10 were excluded from the analysis. Principal component analysis (PCA) was performed on the count matrix after variance-stabilizing transformation (VST). Commonly upregulated genes in the PD-1 patient and the patient with a *STAT3* GOF mutation (with $\log_2$ fold-change of at least 2 relative to controls) were subjected to gene set overrepresentation testing for GO terms with the *clusterProfiler* package[73] in R. Results were filtered with the FDR-adjusted *P* value and q value cutoffs of 0.1 and 0.2, respectively, and were further inspected manually. Heatmaps were generated from Z-score-transformed normalized counts, for which normalization was achieved by adding a pseudocount of 1 and then calculating the $\log_2$ value, with the *ComplexHeatmap* package in R. Gene set enrichment analysis (GSEA) was conducted with the genes ranked by their $\log_2$ fold-change values, with the *fgsea* package in R. Gene sets corresponding to the GO terms were retrieved from the MSigDB Collections (http://www.gsea-msigdb.org/gsea/msigdb/index.jsp). The patients with PD-1 deficiency and STAT3 GOF mutation were grouped together and compared to either i) the three controls or ii) the two FAS-deficient patients. The two FAS-deficient patients were also compared to controls (iii). GO terms commonly enriched or depleted (with FDR-adjusted *P* values below 0.05) in i) and ii) but not in iii) were further inspected manually.

Statistical analysis

All statistical analyses were performed in R v4.0 (http://www.R-project.org/)[74]. The statistical significance of quantitative differences between groups was assessed in two-tailed non-paired Wilcoxon's rank-sum tests unless otherwise stated. FDR adjustment was performed by the Benjamini and Hochberg method[75]. *P* values below 0.05 were considered statistically significant.

Extended Data

a

	$pncA_{nt169}$	$oxyR_{nt285}$	$narG_{nt-215}$
M. tuberculosis	C	G	T
M. bovis	G	A	C
Reference (PMID)	8640557	8818900	12843072
Results (# of tissue extractions sequenced in denominator)	C: 2/2 G: 0/2	G: 4/4 A: 0/4	T: 2/2 C: 0/2

b

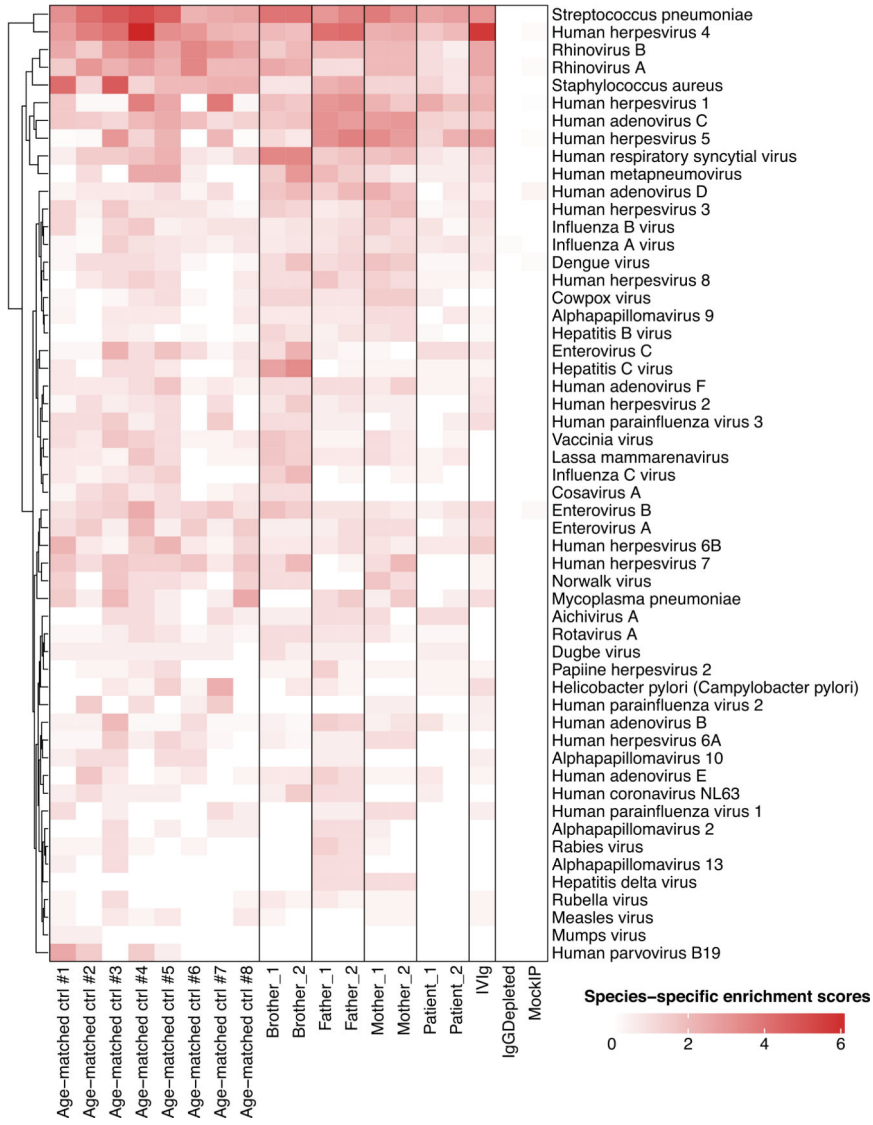

Extended Data Fig. 1. A pediatric case of severe tuberculosis and autoimmunity.

(a) Species-specific PCR for mycobacteria. Three conserved single-nucleotide polymorphisms (SNPs) for differentiating between *M. tuberculosis* and *M. bovis* (including the *M. bovis* BCG substrain) were sequenced from the DNA samples extracted from the paraffin-embedded biopsy material. (b) VirScan. Serum samples were collected from the patient, his brother, father, and mother, at two time points (at initial presentation and during follow-up). Serum samples from eight healthy age-matched (pediatric) controls

were also included. An intravenous immunoglobulin (IVIg) product was also included as a positive control, whereas IgG-depleted serum and mock immunoprecipitation (IP) samples were included as negative controls. Species-specific enrichment scores were calculated as previously described[56]. (c) Clinical course. The time points of blood sample collection for this study are also shown. (d) A chest CT scan taken after the patient developed dyspnea, showing bilateral ground-glass opacities. (e-g) T cell receptor (TCR) repertoire analysis. Genomic DNA extracted from whole blood was used to amplify TCR-β rearranged genomic regions. Total reads for productive clonotypes were used for the analysis. (e) Complementarity-determining region 3 (CDR3) sequence length. (f) GRAVY hydrophobicity score. The overlayed boxplot shows median (the horizontal bar), 25% and 75% quantiles (the lower and upper hinge), with the whiskers show the interquartile range multiplied by 1.5. (g) *TRBV*-to-*TRBJ* pairing circos plots. The Shannon entropy index of diversity [H] and Simpson index of clonality [1-D] are also shown.

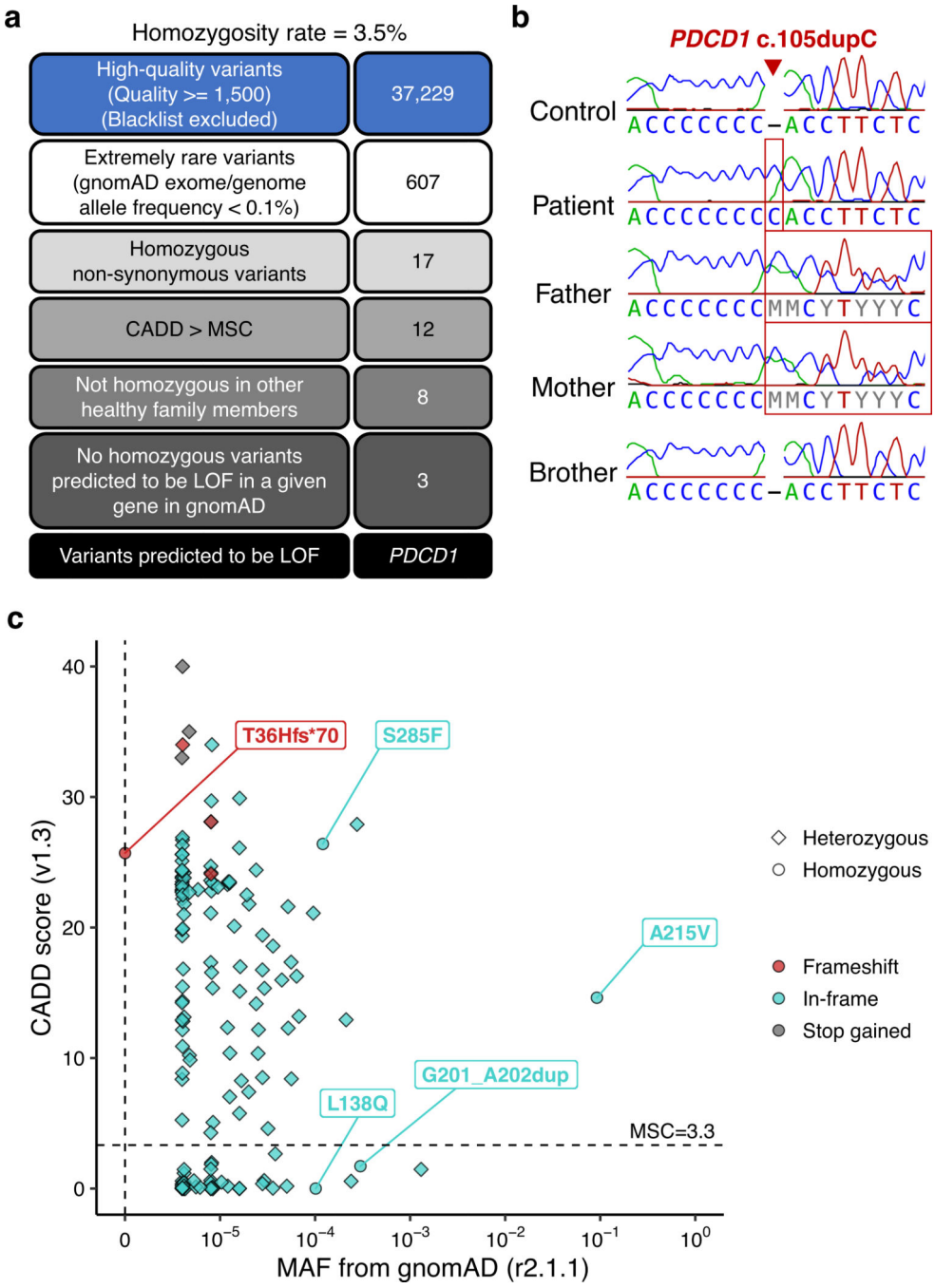

Extended Data Fig. 2. Autosomal recessive complete PD-1 deficiency.

(a) Whole-exome sequencing (WES). We reasoned that only an extremely uncommon homozygous variant (including copy number variants) would be able to account for the unusually severe immunological abnormalities of the patient (*i.e.*, severe TB and lethal autoimmunity) at the age of 10 years. The 17 extremely rare non-synonymous (missense, in-frame, frameshift, stop-gained, and essential splicing site) variants were further filtered based on their allele frequencies and CADD scores. Variants also found in the homozygous state in other healthy family members were discarded. Besides,

variants were discarded if other homozygous variants predicted to be loss-of-function (pLOF) of the same gene were found in the gnomAD database. After these filtrations, three candidate variants were retained (summarized in Supplementary Table 4), none of which were variants of genes known to underlie inborn errors of immunity (IEIs). Only one variant, *PDCD1* c.105dupC, was predicted to be LOF, due to a premature stop codon generated by the frameshift. CADD, combined annotation-dependent depletion score (v1.3); MSC, mutation significance cutoff[19]. (b) Sanger sequencing chromatograms of the *PDCD1* region harboring the c.105dupC mutation. (c) Population genetics of *PDCD1*. Minor allele frequency (MAF) and combined annotation-dependent depletion score (CADD) for non-synonymous *PDCD1* variants reported in the gnomAD database are shown. Only homozygous variants are labeled. The horizontal dotted line indicates the mutation significance cutoff (MSC). The patient's mutation (T36Hfs*70) has a CADD score of 25.7. (d and e) Studies of homozygous *PDCD1* alleles frequently observed in the general population. Four homozygous *PDCD1* alleles found in gnomAD were studied by overexpressing the corresponding cDNA in HEK293T cells. (d) Surface PD-1 expression, as determined by flow cytometry. Representative data from three independent experiments are shown. (e) Surface retention of recombinant PD-L1-Fc and PD-L2-Fc, as determined by flow cytometry. Representative data from three independent experiments are shown. (f) T:B cell coculture assay. HuT78 T cells stably transduced with EV, WT PD-1, or mutant (T36Hfs*70) PD-1 were cocultured for 6 hours with Raji B cells stably transduced with EV, PD-L1, or PD-L2 with or without blinatumomab (anti-CD3-CD19 bispecific engager), and IFN-γ and TNF production was measured by flow cytometry. Technical triplicates are shown. (g) *PDCD1* mRNA levels, as determined by RT-qPCR relative to controls, in EBV-B cells from two controls, the father, and the patient (results of two experiments combined) and PHA blasts from seven controls, the brother, the parents, and the patient (technical duplicates prepared only for the patient's cells). *GUSB* was used as an endogenous control. (h) Degranulation assay. HVS-T cells from two controls and the patient were incubated for five hours with Dynabeads conjugated with anti-CD3, anti-CD28, and either mouse IgG1 (clone: PD1.D3) or IgG2b (clone: 9X21) anti-PD-1 monoclonal antibodies (mAbs) or their corresponding isotype controls, and the levels of surface-translocated CD107a were determined by flow cytometry. Technical duplicates were prepared for samples incubated with anti-PD-1 mAbs. Representative data from two independent experiments are shown. (i) TCR signaling assay. PHA blasts from two controls and the patient were incubated for 24 hours with Dynabeads conjugated with anti-CD3 and anti-CD28 mAbs and recombinant human IgG1 Fc, PD-L1-Fc, or PD-L2-Fc protein. The levels of phospho-ERK1/2 were determined by flow cytometry. Technical duplicates were prepared for samples incubated with PD-L1-Fc or PD-L2-Fc. Representative data from two independent experiments are shown. Bars represent the mean and SEM.

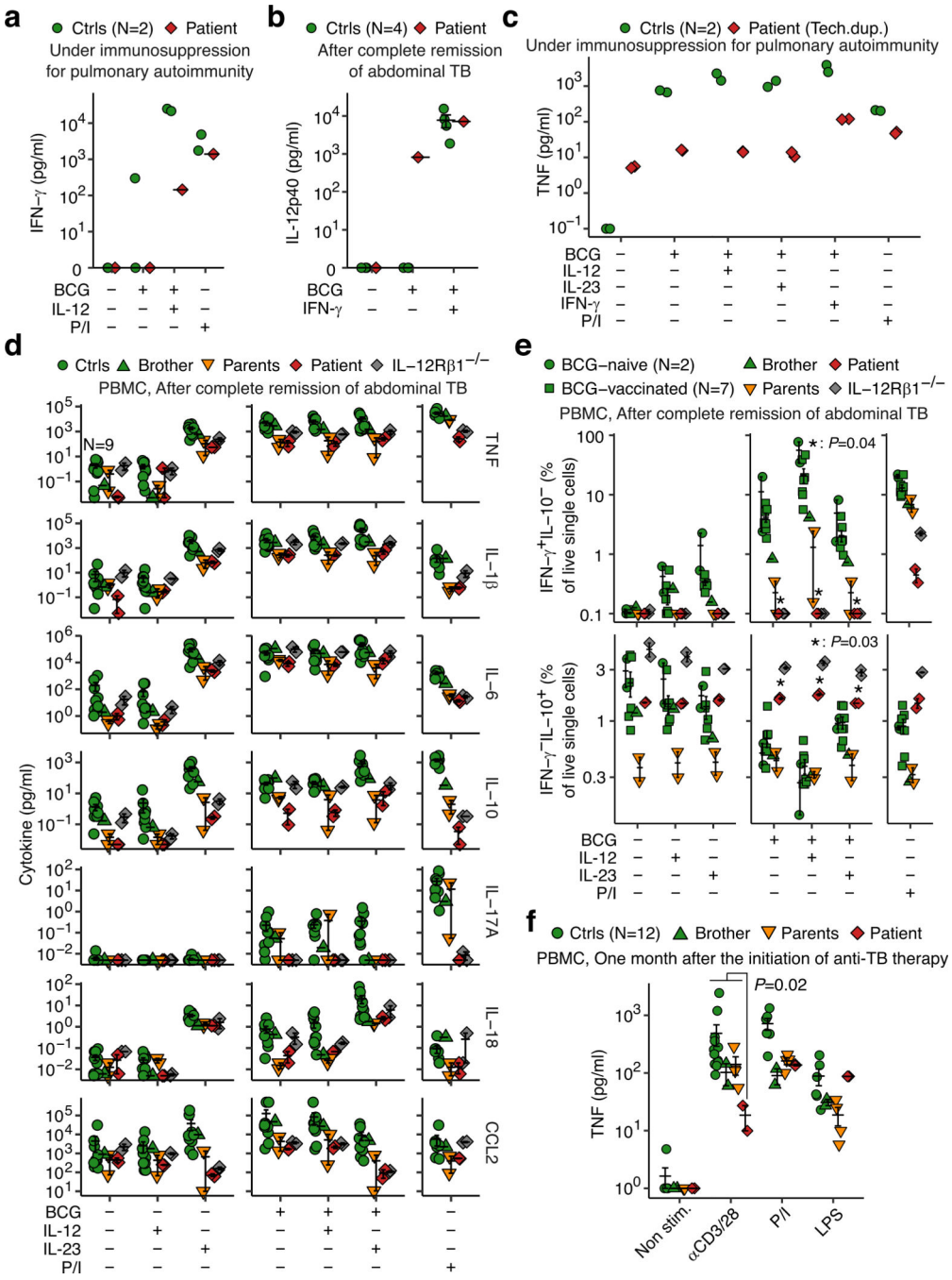

Extended Data Fig. 3. Impaired IFN-γ and TNF production by PD-1-deficient leukocytes in response to mycobacterial and T-cell stimuli.

(a-c) Secreted cytokine levels in a whole-blood BCG assay. (a) Secreted IFN-γ levels, as determined by ELISA after BCG stimulation of the whole-blood sample drawn from the patient two weeks before his death, while on immunosuppression therapy, including abatacept, for aggressive pulmonary autoimmunity. Samples from one control and the father (grouped as controls) were tested simultaneously. (b) Secreted IL-12p40 levels, as determined by ELISA after BCG stimulation of the whole blood sample of the patient drawn after complete remission of abdominal TB. Samples from one control, the brother,

and the parents (grouped as controls) were tested simultaneously. (c) Secreted TNF levels, as determined with a LEGENDplex assay after BCG stimulation of the whole-blood sample from the patient drawn two weeks before his death, while on immunosuppression therapy. (d and e) PBMC BCG assay. The patient's PBMCs were obtained after complete remission of abdominal TB. Freshly thawed PBMCs from controls (N=9, two BCG-naïve and seven BCG-vaccinated), the brother, the parents, and the patient, and one IL-12Rβ1$^{-/-}$ patient were dispended into a U-bottomed 96-well plate at a density of 2×10^5 cells/well and were stimulated. After 40 hours, a cytokine secretion inhibitor was added to the culture. After an additional eight hours of incubation, the supernatant and the cells were collected. (d) Secreted cytokine levels, as determined with a LEGENDplex assay. (e) Frequency of total IFN-γ^+IL-10$^-$ and IFN-γ^-IL-10$^+$ cells, as determined by flow cytometry. (f) PBMC stimulation assay. The patient's cells were obtained one month after the initiation of anti-TB treatment. Secreted TNF levels were determined with a LEGENDplex assay after 24 hours of stimulation. Technical duplicates were prepared for the patient and his healthy brother and parents. Bars represent the mean and SEM. Statistical significance was determined via two-tailed non-paired Wilcoxon's rank-sum tests with FDR adjustment for (e) the patient vs. local controls plus his brother and (f) the patient vs. local plus all family controls. P/I, PMA/ionomycin.

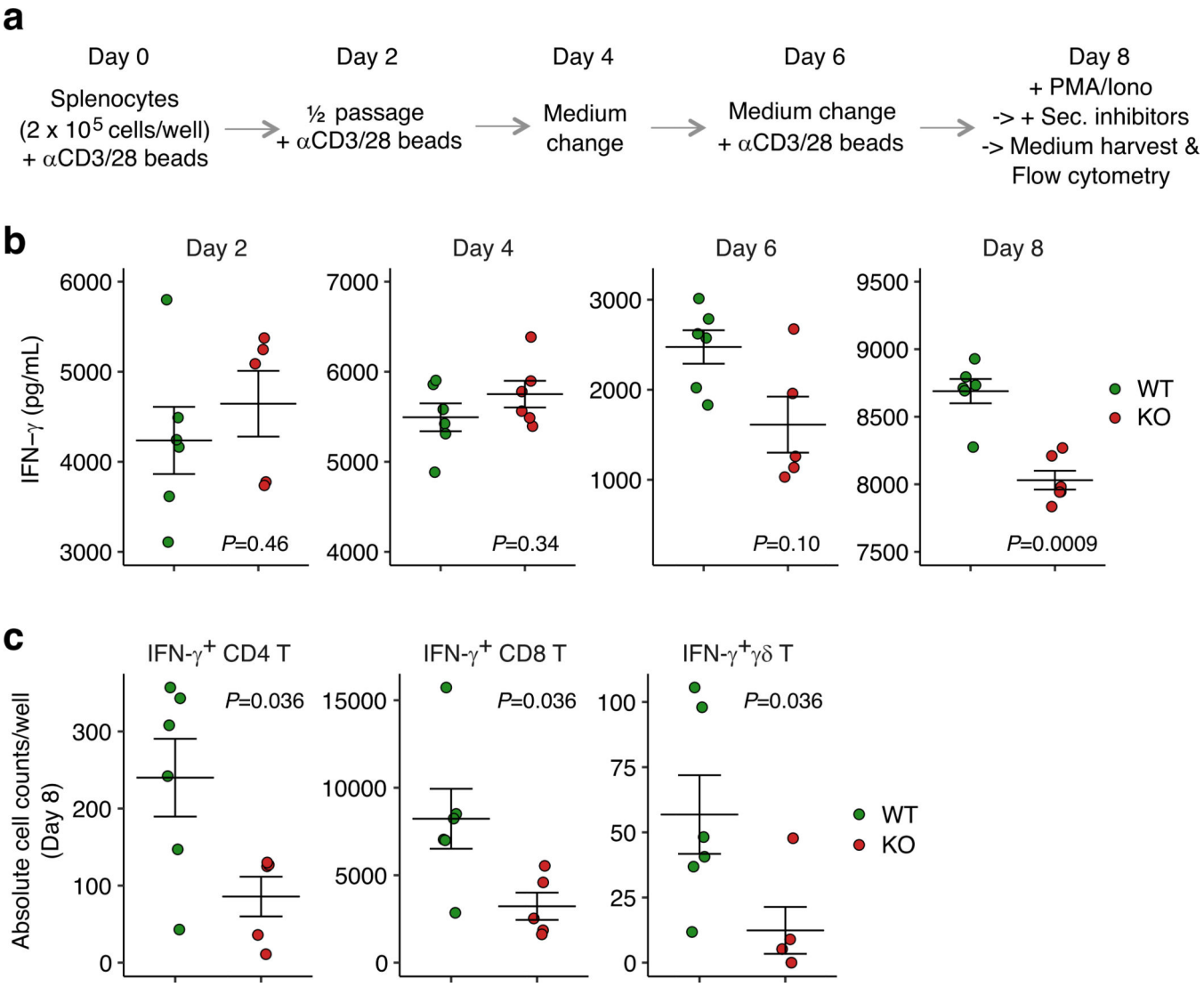

Extended Data Fig. 4. Impaired IFN-γ production by splenocytes from PD-1-deficient mice repetitively stimulated *in vitro*.

(a) Experimental design. Splenocytes were isolated from six PD-1-deficient mice and six age-matched wild-type (WT) controls and continuously cultured. (b) Secreted IFN-γ levels, as determined by ELISA. For WT mice, N=6 for all time points. For PD-1-deficient mice, N=6 for days 4 and 8, and N=5 for days 2 and 6. (c) Absolute counts of IFN-γ-producing cells on day 8, as determined by flow cytometry. N=6 and 5 for WT and PD-1-deficient mice, respectively. Bars represent the mean and SEM. Statistical significance was determined with a two-tailed Student's *t*-test with FDR adjustment.

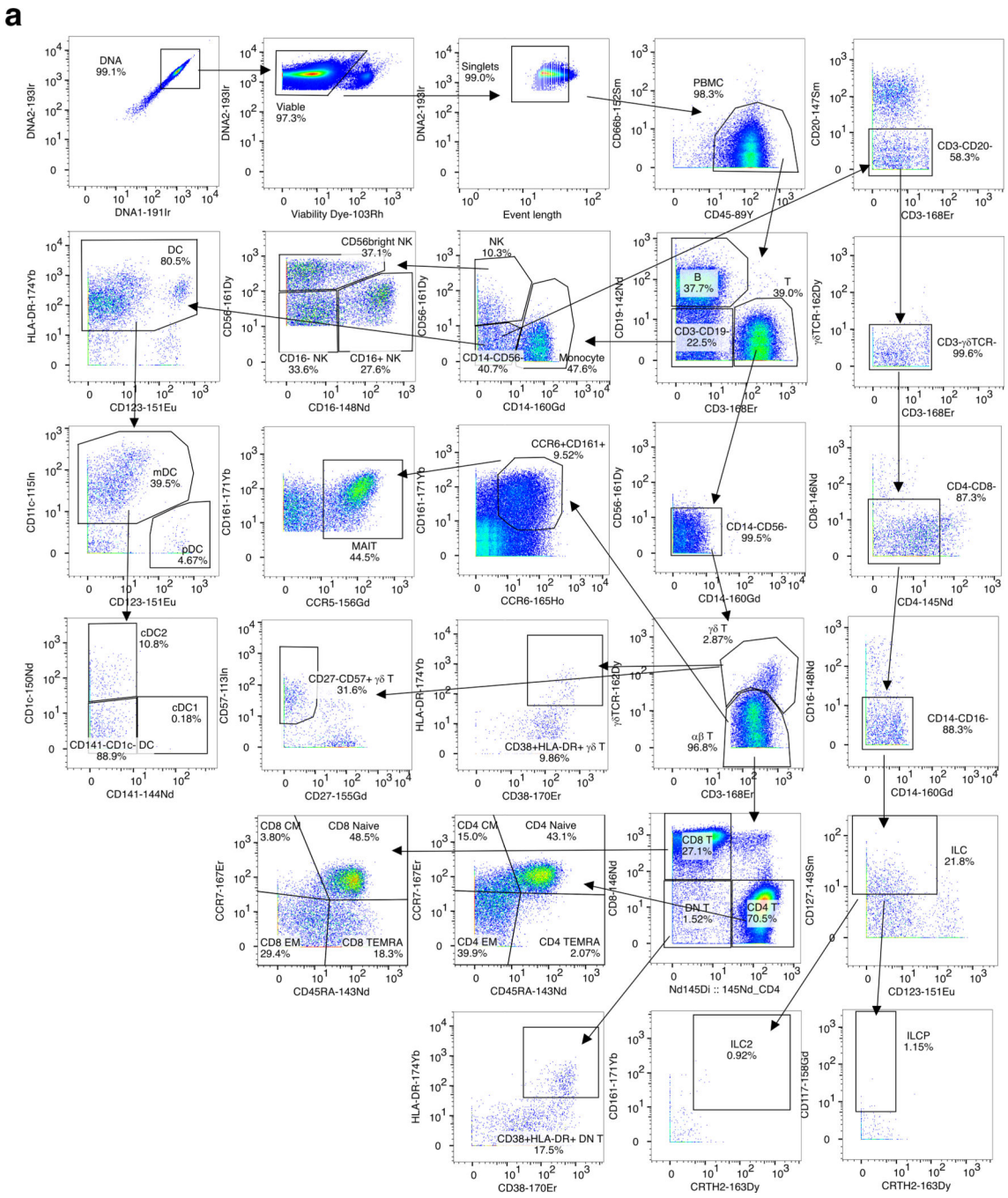

Extended Data Fig. 5. Depletion and dysfunctional immunophenotypes of multiple IFN-γ-producing T and NK lymphocyte subsets in inherited PD-1 deficiency.

(a-o) Mass cytometry (cytometry by time-of-flight, CyTOF). PBMCs from healthy controls, the patient, his brother, and his parents were analyzed by CyTOF with general surface immunophenotyping (CyTOF-G) and T cell-focused (CyTOF-T) panels. The patient's cells were obtained one month after initiating treatment for TB. (a and b) Gating strategies for (a) CyTOF-G and (b) CyTOF-T. (c) Major cell subsets. (d) Dendritic cell subsets. (e) $CD56^{bright}$ NK cells. (f) Innate lymphoid cell subsets. (g) $CD4^+$ αβ T cell subsets. (h) $CD8^+$ αβ T cell subsets. (i) γδ T cells. (j) γδ T cell subsets. (k) $CD4^+$ T helper subsets. (l) $PD\text{-}1^+$

follicular helper T (Tfh) cells. (m) CD28-TIGIT+ $CD4^+$ αβ T cells. (n) CD28-TIGIT+ γδ T cells. (o) Scaled median expression levels of costimulatory and coinhibitory receptors across T and NK cell subsets. In (c, e, and g-j), CyTOF-G and CyTOF-T data are compiled as technical duplicates. In (d and f), CyTOF-G data were analyzed. In (k-o), CyTOF-T data were analyzed. (p-r) Flow cytometry. (p and q) Innate-like T lymphocytes. In (p), PBMCs from healthy controls, the patient and his father were analyzed. The patient's cells were obtained two weeks before his death. Technical duplicates were prepared. In (q), PBMCs from healthy controls, the patient, his brother, and both of his parents were analyzed. The patient's cells were obtained one month after initiating TB treatment. (r) Regulatory T cells (Tregs). PBMCs from healthy controls, the patient and his brother were analyzed. The patient's cells were obtained one month after initiating TB treatment. Bars represent the mean and SEM. Statistical significances were determined via two-tailed non-paired Wilcoxon's rank-sum tests with FDR adjustment.

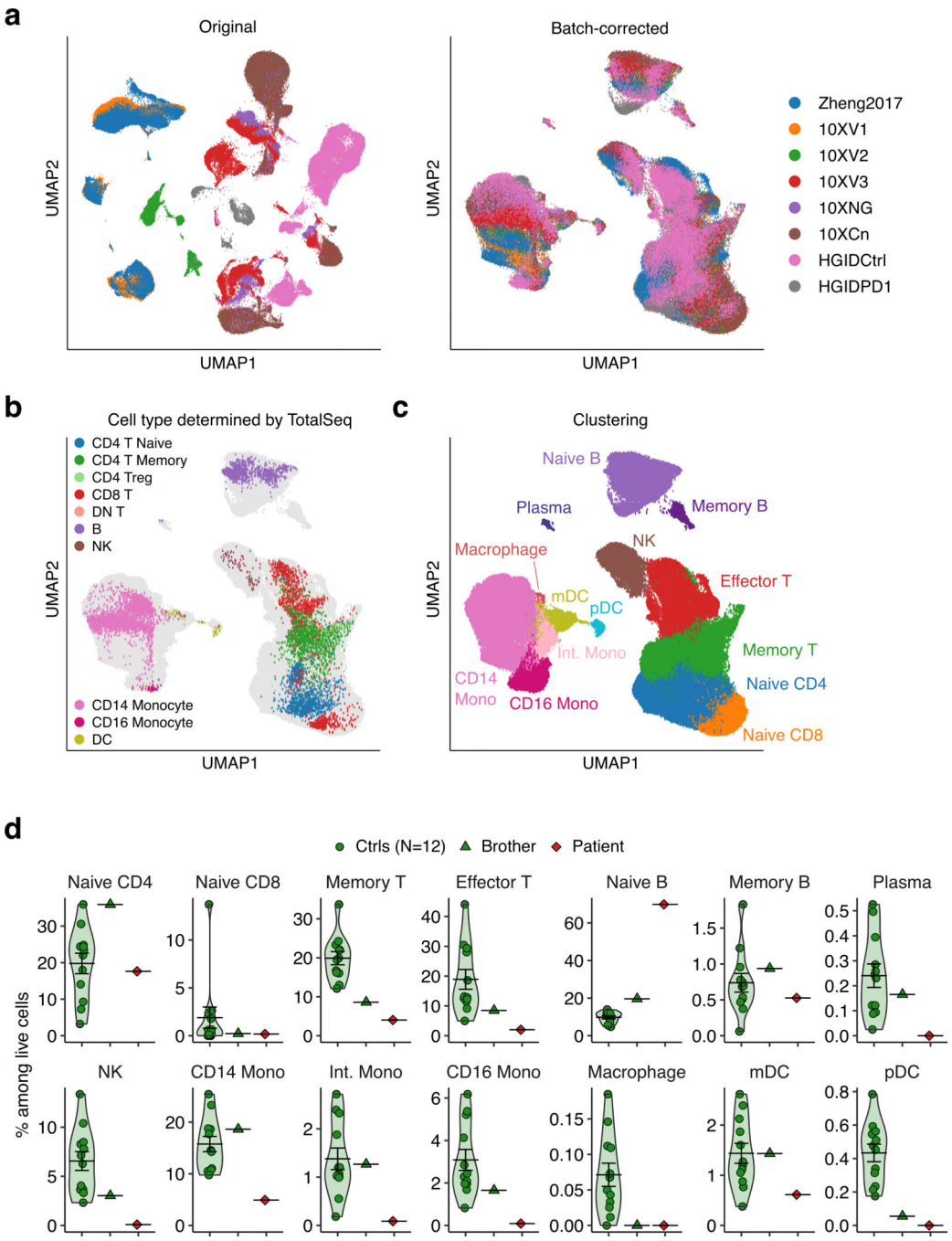

Extended Data Fig. 6. Aberrant expression of type-I IFN-stimulated genes and type-I IFN-encoding genes in inherited PD-1 deficiency.

(a-g) Single-cell RNA sequencing. PBMCs from the patient and his healthy brother were analyzed on the 10X droplet-based single-cell RNA sequencing (scRNASeq) platform. Four in-house control datasets and ten publicly available PBMC datasets downloaded from the 10X website (https://support.10xgenomics.com/single-cell-gene-expression/datasets) were also integrated into the analysis. Among the ten publicly available datasets, two 10X TotalSeq datasets were used for annotating clusters. (a) Batch correction with log-normalized count data with *Batchelor*[66]. Data were visualized with UMAP. 10X

datasets are color-coded by batch [Chromium Connect (Cn), Next GEM (NG), V3, V2, and V1, and the data reported by Zheng et al.[65]]. Here, the patient and his brother are grouped as HGIDPD1. (b) Cell types defined based on surface marker expression levels in the two TotalSeq datasets. $CD14^+$ monocyte, $CD3^-CD14^+CD16^-CD19^-CD56^-$; $CD16^+$ monocyte, $CD3^-CD14^-CD16^+CD19^-CD56^-$; DC, $CD3^-CD14^-CD16^-CD19^-CD56^-$ $HLA\text{-}DR^+$; B, $CD3^-CD14^-CD16^-CD19^+CD56^-$, NK, $CD3^-CD14^-CD16^-CD19^-CD56^+$. T cells ($CD3^+CD14^-CD16^-CD19^-CD56^-$) were further gated into: $CD8^+$ T, $CD4^-CD8^+$; DN T, $CD4^-CD8^-$; $CD4^+$ Treg, $CD4^+CD25^+CD127^{lo}$. Non-Treg cells were further gated into: $CD4^+$ naïve T, $CCR7^+CD45RO\text{-}CD45RA^+$; $CD4^+$ memory T, $CD45RO^+CD45RA^-$. (c) Clustering. The batch-corrected log-normalized count data were dimension-reduced with UMAP, and the top 50 components were used to construct a shared nearest-neighbor graph. The graph was then divided into clusters with the Louvain algorithm. TotalSeq-based cell types and the expression patterns of marker genes were inspected manually for annotating the clusters. Clusters representing platelets, basophils, and dying cells with high mitochondrial transcript contents were excluded from the visualization. (d) Differential abundance (DA) analysis of manually annotated clusters. Two TotalSeq datasets and the corresponding non-TotalSeq datasets were considered technical duplicates and were aggregated before DA analysis. Bars represent the mean and SEM. (e) Per-cluster differential expression (DE) analysis between groups through a “pseudobulk” approach[67]. The goal of this analysis was to identify genes differentially upregulated in the patient’s cells relative to cells from the public, historical, and familial controls. Two TotalSeq datasets and the corresponding non-TotalSeq datasets were considered technical duplicates and were aggregated before DE analysis. The pDC cluster was excluded from the analysis because of the small number of cells obtained from the patient. The Naïve B, Memory B, and Plasma clusters were merged as B, and the CD14 Mono, Int. Mono, and CD16 Mono clusters were merged as Monocyte. We adopted a conservative approach detecting only the genes displaying the most robust differential expression in the patient’s cells. Three DE testing strategies, with two pseudobulk approaches, were applied. First, mimicking total read counts in conventional RNA sequencing experiments, summed non-normalized read counts were analyzed with *DESeq2*[69] and *edgeR*[70]. Second, read counts normalized by per-cell library size were averaged, essentially reflecting the mean read counts per single cell, and were then further divided by the mean expression levels of multiple housekeeping genes for normalization. The normalized read counts were then analyzed with *NOISeq*[71]. Here, we focus on upregulated genes, defined according to the following criteria: (i) statistical significance relative to controls (10X and in-house controls combined), (ii) $\log_2$ fold-change > 1 relative to controls, and (iii) $\log_2$ fold-change > 1 relative to the brother. For *DESeq2* and *edgeR*, false discovery rate-adjusted P values < 0.05 were considered significant. For *NOISeq*, a probability > 0.9 was considered significant. Only genes identified as differentially expressed by all three strategies were retained. The heatmap was generated from the $\log_2$ fold-change values derived from housekeeping-gene-normalized expression levels. Red, genes with GO terms associated with type I IFN signaling or antiviral immunity. Purple, genes induced by LPS in human monocytes, as previously reported[76]. (f) Single-cell clade analysis. scRNASeq data for T cells from the patient and his brother were jointly analyzed with TooManyCells[72]. The trajectories from the root node to Branches #1 and #2 are depicted with arrows, where a branch is defined as a node plus all subnodes belonging

to that node. (g) DE analysis between branches of cells. DE genes were detected with the *differential* mode implemented in TooManyCells. A volcano plot is shown for genes differentially expressed between Branches #1 and #2.

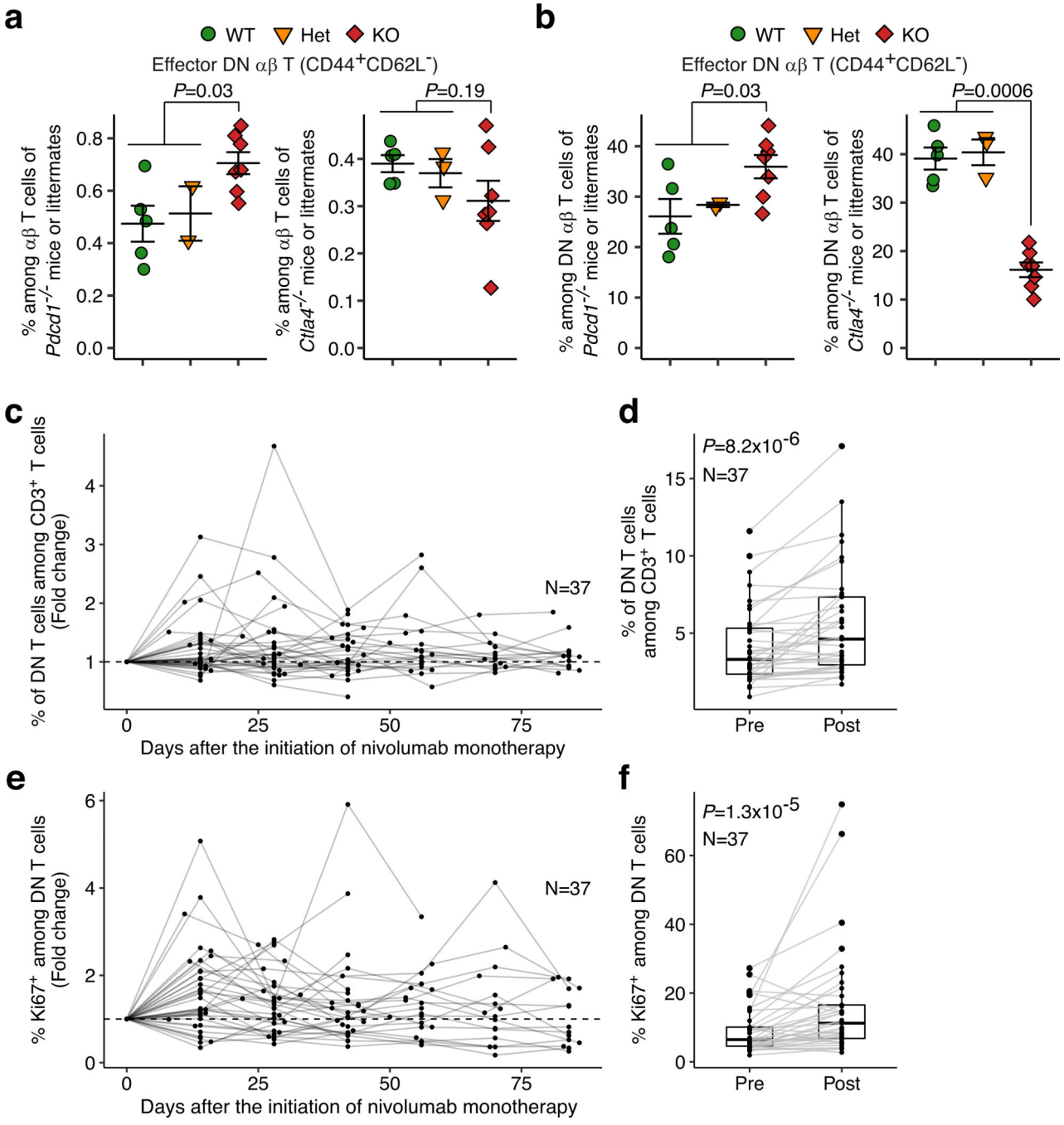

Extended Data Fig. 7. Expansion, activation, and proliferation of CD4$^-$CD8$^-$ double-negative (DN) T cells in inherited and acquired PD-1 deficiency.

(a and b) Effector DN αβ T cells. Previously published CyTOF data for peripheral lymph node-derived CD19$^-$CD3ε$^+$ T cells from adult PD-1-deficient and CTLA-4-deficient mice were downloaded from the FlowRepository (accessions FR-FCM-ZYFS and FR-FCM-

ZYFQ, respectively)[38]. The control wild-type (WT) and heterozygous (Het) mice are the littermates of knockout (KO) mice. PD-1-deficient, N=5, 2, and 7 for WT, Het, and KO, respectively. CTLA-4-deficient mice, N=5, 3, and 7 for WT, Het, and KO, respectively. Bars represent the mean and SEM. Statistical significances were determined via two-tailed non-paired Wilcoxon's rank-sum tests with FDR adjustment. (c-f) Expansion and proliferation of DN T cells in patients on PD-1 blockade. A cohort of patients with advanced bladder cancer or melanoma treated with nivolumab monotherapy (*N*=37) were immunophenotyped by flow cytometry. (c and d) Total DN T cells. (e and f) $Ki67^+$ DN T cells. In (d and f), values before immunotherapy (Pre) and the highest values within 30 days after the initiation of immunotherapy (Post) were compared through two-tailed paired Wilcoxon's rank-sum tests with FDR adjustment. The overlayed boxplot shows median (the horizontal bar), 25% and 75% quantiles (the lower and upper hinge), with the whiskers show the interquartile range multiplied by 1.5.

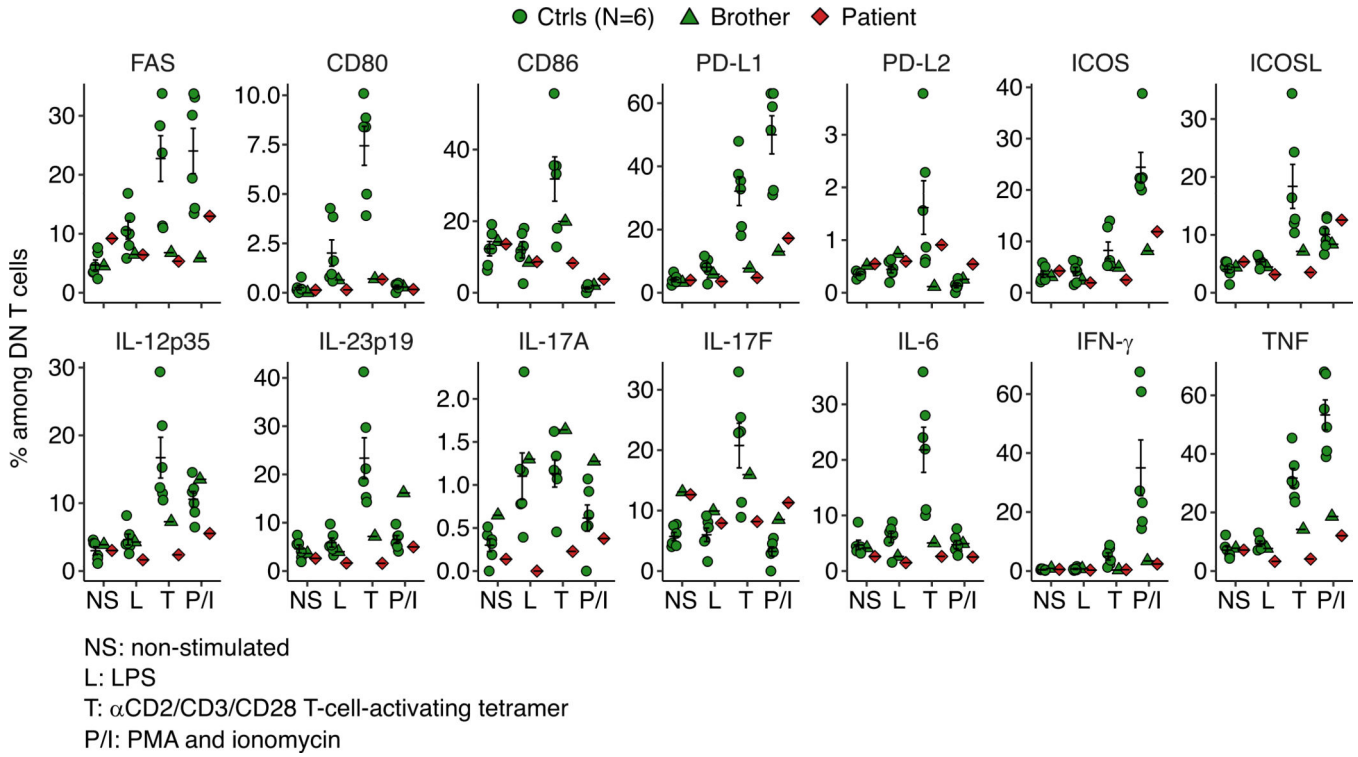

Extended Data Fig. 8. Cellular responses of PD-1-deficient $CD4^-CD8^-$ double-negative (DN) T cells.

PBMCs from the patient (obtained one month after anti-TB treatment) and his healthy brother were stimulated for 24 hours with indicated stimuli, and DN T cells were analyzed by flow cytometry. Bars represent the mean and SEM.

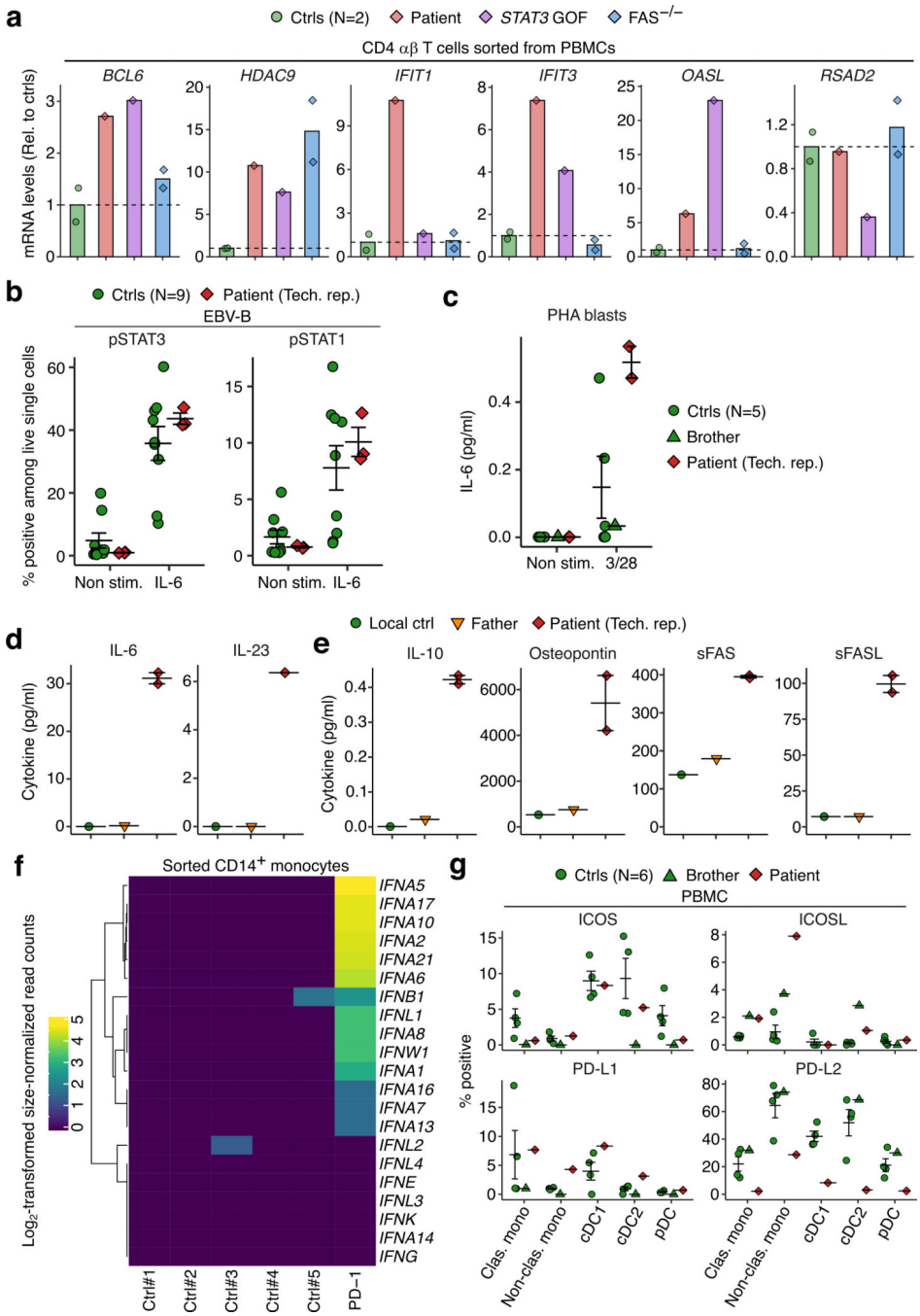

Extended Data Fig. 9. Inherited PD-1 deficiency phenocopies STAT3 gain-of-function through excessive production of STAT3-activating cytokines by dysregulated T lymphocytes and myeloid cells.

(a) Autoimmunity-associated gene expression levels in sorted CD4$^+$ αβ T cells, as determined by RT-qPCR. To identify phenotypic similarities between the PD-1-deficient patient and other patients with monogenic forms of lymphoproliferative autoimmunity, PBMCs from the patient (obtained two weeks before his death), one patient with a heterozygous *STAT3* gain-of-function (GOF) mutation, and two patients with FAS deficiency [*i.e.*, autoimmune lymphoproliferative syndrome (ALPS)] were studied. Selected

autoimmunity-associated genes significantly upregulated in the patient's effector T cells relative to his healthy brother's effector T cells, as determined by the pseudobulk differential expression analysis of scRNASeq data, were tested by RT-qPCR with the patient's PBMCs obtained at a different time point (*i.e.*, biological replicates). In addition, the gene expression levels were compared between cells with PD-1 deficiency, *STAT3* GOF, and FAS deficiency to identify phenotypic similarities. (b) Induction of STAT3 and STAT1 phosphorylation, as determined by flow cytometry. EBV-B cells were either left unstimulated or were stimulated with IL-6 (100 ng/mL) for 30 minutes. Technical triplicates were prepared only for the patient. (c) Levels of IL-6 secreted by expanded PHA blasts, as determined in a LEGENDPlex assay. PHA blasts were either left unstimulated or were stimulated with anti-CD3/CD28 antibody-conjugated beads for 24 hours. Technical duplicates were prepared only for the patient. (d and e) Cytokine levels in the bloodstream. Heparinized plasma samples from the patient, his father, and one local control were subjected to a custom LEGENDplex assay. (d) STAT3-activating cytokines. (e) Serological markers of FAS deficiency. sFAS, soluble FAS; sFASL, soluble FAS ligand. (f) Aberrant expression of type I and type III IFN-encoding genes in the non-stimulated monocytes ($CD3^{-}CD19^{-}CD56^{-}CD14^{+/dim}$) sorted from PBMCs from the patient (obtained two weeks before his death), as determined by RNA sequencing. Log_2-transformed size-factor-normalized read counts are shown. (g) Immunophenotyping of myeloid cell subsets. PBMCs from the patient (obtained one month after anti-TB treatment) and his healthy brother were analyzed by flow cytometry. Bars represent the mean and SEM.

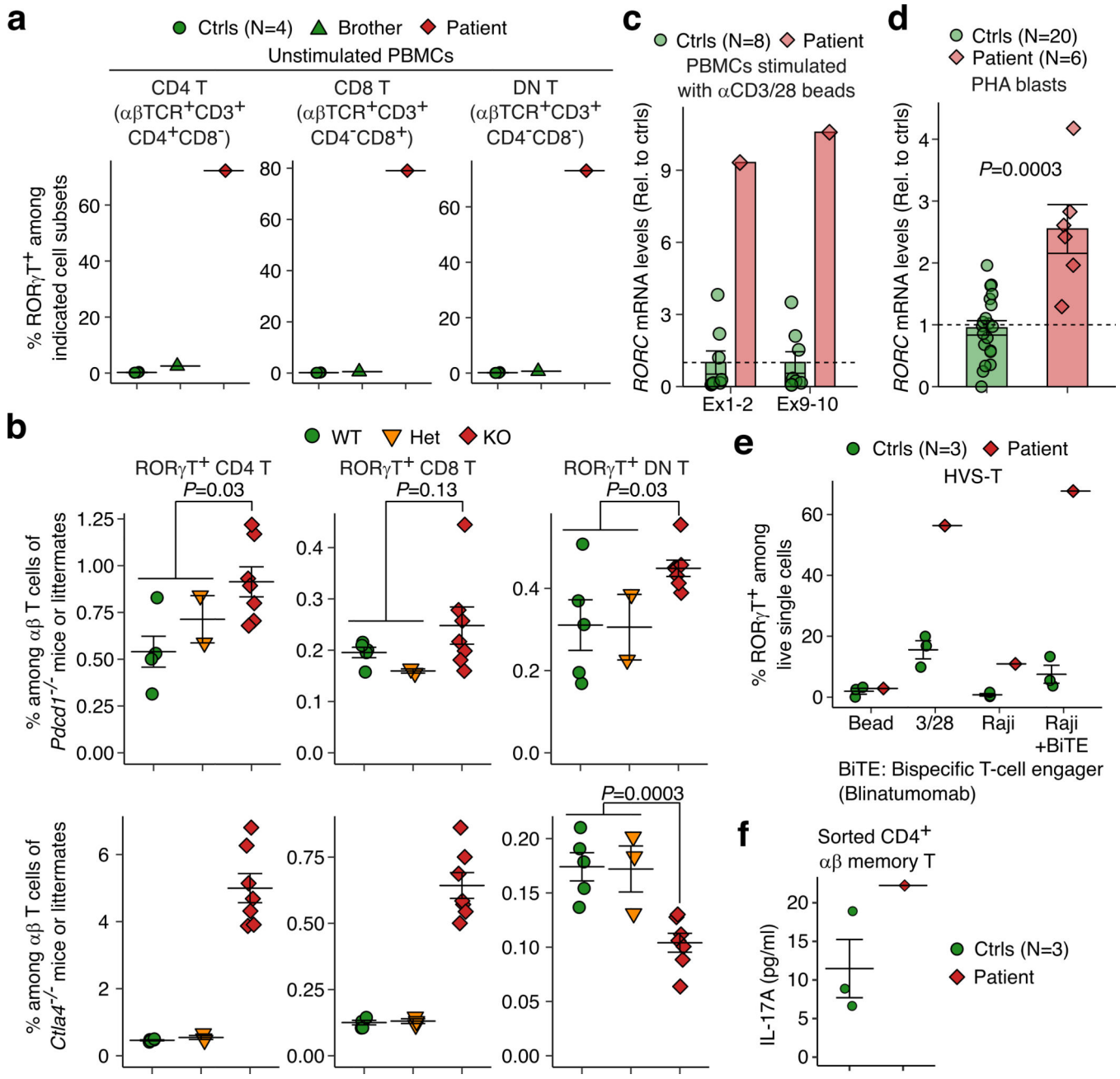

Extended Data Fig. 10. Activation-induced upregulation of RORγT in PD-1-deficient T lymphocytes.

(a, c, and f) PBMCs from the patient (obtained one month after the initiation of anti-TB treatment) were studied. (a) RORγT expression in αβ T cell subsets, as determined by flow cytometry. (b) Expansion of RORγT-expressing DN αβ T cells in PD-1-deficient, but not in CTLA-4-deficient, mice. Previously published CyTOF data for peripheral lymph node-derived $CD19^{-}CD3\varepsilon^{+}$ T cells from adult PD-1-deficient and CTLA-4-deficient mice were downloaded from the FlowRepository (accessions FR-FCM-ZYFS and FR-FCM-ZYFQ, respectively)[38]. The control wild-type (WT) and heterozygous (Het) mice are the littermates of knockout (KO) mice. PD-1-deficient mice, N=5, 2, and 7 for WT, Het, and KO,

respectively. CTLA-4-deficient mice, N=5, 3, and 7 for WT, Het, and KO, respectively. (c) *RORC* mRNA levels in PBMCs stimulated with anti-CD3/CD28 antibody-conjugated Dynabeads for 24 hours, as determined by RT-qPCR with two different TaqMan probes. *GUSB* was used as an endogenous control. (d) RORC mRNA levels in PHA-activated T cell blasts, as determined by RT-qPCR. Results from three consecutive experiments with technical duplicates are compiled. (e) Induction of RORγT in HVS-T cells upon activation. HVS-T cells were incubated for 24 hours with mock Dynabeads, Dynabeads coated with anti-CD3 and anti-CD28 antibodies, Raji cells, or Raji cells plus blinatumomab (anti-CD3-CD19 bispecific engager). RORγT expression was measured by flow cytometry. (f) IL-17A production. $CD4^+$ αβ memory T cells were sorted from cryopreserved PBMCs and activated with beads conjugated with anti-CD2/CD3/CD28 antibodies. Supernatants were harvested on day 5, and the levels of secreted cytokines were determined in a cytometric bead array. Bars represent the mean and SEM. Statistical significances were determined via two-tailed non-paired Wilcoxon's rank-sum tests with FDR adjustment.

Supplementary Material

Refer to Web version on PubMed Central for supplementary material.

Authors

Masato Ogishi[1,2,@], Rui Yang[1], Caner Aytekin[3], David Langlais[4,5,6], Mathieu Bourgey[4], Taushif Khan[7], Fatima Al Ali[7], Mahbuba Rahman[7], Ottavia M. Delmonte[8], Maya Chrabieh[9,10], Peng Zhang[1], Conor Gruber[11,12,13,14], Simon J. Pelham[1], András N. Spaan[1], Jérémie Rosain[9,10], Wei-Te Lei[1], Scott Drutman[1], Matthew D. Hellmann[15], Margaret K. Callahan[15,16], Matthew Adamow[17,18], Phillip Wong[17], Jedd D. Wolchok[15,16,18,19], Geetha Rao[20], Cindy S. Ma[20,21], Yuka Nakajima[22], Tomonori Yaguchi[22], Kenji Chamoto[22], Samuel C. Williams[23,24], Jean-Francois Emile[25], Flore Rozenberg[26], Michael S. Glickman[27], Franck Rapaport[1], Gaspard Kerner[9,10], Garrett Allington[28,29,30], Ilhan Tezcan[31], Deniz Cagdas[31], Ferda O. Hosnut[32], Figen Dogu[33], Aydan Ikinciogullari[33], V. Koneti Rao[34], Leena Kainulainen[35], Vivien Béziat[1,9,10], Jacinta Bustamante[1,9,10,36], Silvia Vilarinho[28,29,30], Richard P. Lifton[28,37], Bertrand Boisson[1,9,10], Laurent Abel[1,9,10], Dusan Bogunovic[11,12,13,14], Nico Marr[7,38], Luigi D. Notarangelo[8], Stuart G. Tangye[20,21], Tasuku Honjo[22], Philippe Gros[5,39], Stéphanie Boisson-Dupuis[1,9,10,@,#], Jean-Laurent Casanova[1,9,10,40,@,#]

Affiliations

[1.]St. Giles Laboratory of Human Genetics of Infectious Diseases, Rockefeller Branch, Rockefeller University, New York, NY, USA.

[2.]The David Rockefeller Graduate Program, Rockefeller University, New York, NY, USA.

[3.]Department of Pediatric Immunology, Dr. Sami Ulus Maternity and Children's Health and Diseases Training and Research Hospital, Ankara, Turkey.

[4.]McGill University Genome Center, Montreal, QC, Canada.

[5.]McGill Research Centre on Complex Traits, Montreal, QC, Canada.

[6.]Department of Human Genetics, McGill University, Montreal, QC, Canada.

[7.]Department of Immunology, Research Branch, Sidra Medicine, Doha, Qatar.

[8.]Immune Deficiency Genetics Section, Laboratory of Host Defenses, Division of Intramural Research, National Institute of Allergy and Infectious Diseases, National Institutes of Health, Bethesda, MD, USA.

[9.]Laboratory of Human Genetics of Infectious Diseases, Necker Branch, INSERM U1163, Paris, France.

[10.]University of Paris, Imagine Institute, Paris, France.

[11.]Department of Microbiology, Icahn School of Medicine at Mount Sinai, New York, NY, USA.

[12.]Department of Pediatrics, Icahn School of Medicine at Mount Sinai, New York, NY, USA.

[13.]The Mindich Child Health and Development Institute, Icahn School of Medicine at Mount Sinai, New York, NY, USA.

[14.]Precision Immunology Institute, Icahn School of Medicine at Mount Sinai, New York, NY, USA.

[15.]Department of Medicine, Sloan Kettering Institute, Memorial Sloan Kettering Cancer Center, New York, NY, USA.

[16.]Weill Cornell Medicine, New York, NY, USA.

[17.]Immune Monitoring Core Facility, Memorial Sloan Kettering Cancer Center, New York, NY, USA.

[18.]Parker Institute for Cancer Immunotherapy, San Francisco, CA, USA.

[19.]Human Oncology and Pathogenesis Program, Memorial Sloan Kettering Cancer Center, New York, NY, USA.

[20.]Garvan Institute of Medical Research, Darlinghurst, New South Wales, Australia.

[21.]St Vincent's Clinical School, Faculty of Medicine, UNSW Sydney, Darlinghurst, Australia.

[22.]Department of Immunology and Genomic Medicine, Center for Cancer Immunotherapy and Immunobiology, Kyoto University Graduate School of Medicine, Kyoto, Japan.

[23.]Laboratory of Investigative Dermatology, Rockefeller University, New York, NY, USA.

[24.]Weill Cornell/Rockefeller/Sloan Kettering Tri-Institutional MD-PhD Program.

[25.]Department of Pathology, Assistance Publique-Hôpitaux de Paris, Ambroise Paré Hospital, Boulogne-Billancourt, France.

[26]Department of Virology, Cochin Hospital, University of Paris, Paris, France.

[27]Immunology Program, Sloan Kettering Institute, New York, NY, USA.

[28]Department of Genetics, Yale University School of Medicine, New Haven, CT, USA.

[29]Section of Digestive Diseases, Departments of Internal Medicine, Yale University School of Medicine, New Haven, CT, USA.

[30]Department of Pathology, Yale University School of Medicine, New Haven, CT, USA.

[31]Department of Pediatric Immunology, Hacettepe University Medical Faculty, Ankara, Turkey.

[32]Department of Pediatric Gastroenterology, Dr. Sami Ulus Maternity and Children's Health and Diseases Training and Research Hospital, Ankara, Turkey.

[33]Department of Pediatric Immunology and Allergy, Ankara University School of Medicine, Ankara, Turkey.

[34]Laboratory of Clinical Immunology and Microbiology, Division of Intramural Research, National Institute of Allergy and Infectious Diseases, National Institutes of Health, Bethesda, MD, USA.

[35]Department of Pediatrics and Department of Medicine, Turku University Hospital, Turku, Finland.

[36]Study Center of Immunodeficiencies, Necker Hospital for Sick Children, Paris, France.

[37]Laboratory of Human Genetics and Genomics, The Rockefeller University, New York, NY, USA.

[38]College of Health and Life Sciences, Hamad Bin Khalifa University, Doha, Qatar.

[39]Department of Biochemistry, McGill University, Montreal, QC, Canada.

[40]Howard Hughes Medical Institute, New York, NY, USA.

Acknowledgments

We would like to thank the patients, their relatives, and their physicians for participating in this study; Dominick Papandrea, Yelena Nemirovskaya, Mark Woollett, Lazaro Lorenzo-Diaz, and Cécile Patissier for administrative assistance; Tatiana Kochetkov and Ji Eun Han for technical assistance; the members of the laboratory for helpful discussions. We thank the Flow Cytometry Resource Center at the Rockefeller University and the Empire State Stem Cell Fund for providing support through NYSDOH Contract #C023046. We thank the Human Immune Monitoring Core at the Icahn School of Medicine at Mount Sinai for technical assistance with mass cytometry. We thank the National Institutes of Health (NIH) Tetramer Core Facility (NTCF) for providing the MR1 tetramer, which was developed jointly with Dr. James McCluskey, Dr. Jamie Rossjohn, and Dr. David Fairlie. We thank Cycle for Survival, the Integrated Genomics Operation Core of the Memorial Sloan Kettering Cancer Center, funded by the NIH/National Cancer Institute (NCI) Cancer Center Support Grant (CCSG, P30 CA008748), the Marie-Josée and Henry R. Kravis Center for Molecular Oncology, the Ludwig Center for Cancer Immunotherapy, and the Parker Institute for Cancer Immunotherapy, for technical assistance with RNA sequencing.

The study was supported in part by grants from the St. Giles Foundation, The Rockefeller University, *Institut National de la Santé et de la Recherche Médicale* (INSERM), University of Paris, Sidra Medicine, the National

Institute of Allergy and Infectious Diseases (R37AI095983 to J.-L.C., U19AI142737 to S.B.-D., and U19AI111143 and to M.S.G), the National Institute of Diabetes and Digestive and Kidney Diseases (K08 DK113109 to S.V.), the National Center for Research Resources, the National Center for Advancing Sciences of the National Institutes of Health (UL1TR001866), NIH/NCI Cancer Center Support Grant (CCSG, P30 CA008748), NIH/NCI R01 CA056821, the Swim Across America, the Ludwig Institute for Cancer Research, the Ludwig Center for Cancer Immunotherapy, the Cancer Research Institute, the Parker Institute for Cancer Immunotherapy, the French National Research Agency (ANR) under the “Investments for the Future” program (ANR-10-IAHU-01), the Integrative Biology of Emerging Infectious Diseases Laboratory of Excellence (ANR-10-LABX-62-IBEID), GENMSMD (ANR-16-CE17.0005–01, to J.B.), the French Foundation for Medical Research (FRM) (EQU201903007798), and the SCOR Corporate Foundation for Science.

M.O. was supported by the David Rockefeller Graduate Program, the Funai Foundation for Information Technology (FFIT), the Honjo International Scholarship Foundation (HISF), the New York Hideyo Noguchi Memorial Society (HNMS), and the Cooperative Center on Human Immunology (CCHI) at The Rockefeller University. R.Y. was supported by the Immune Deficiency Foundation and the Stony Wold-Herbert Fund. A.N.S. was supported by the European Commission (EC, Horizon 2020 Marie Skłodowska-Curie Individual Fellowship #789645), the Dutch Research Council (NWO, Rubicon Grant #019.171LW.015), and the European Molecular Biology Organization (EMBO, Long-Term Fellowship #ALTF 84–2017, non-stipendiary). J.R. was supported by the INSERM PhD program (*poste d’accueil* INSERM). S.C.W. was supported by a Medical Scientist Training Program grant from the National Institute of General Medical Sciences of the National Institutes of Health to the Weill Cornell/Rockefeller/Sloan Kettering Tri-Institutional MD-PhD Program (T32GM007739). C.S.M is supported by an Early-Mid Career Research Fellowship from the Department of Health of the New South Wales Government of Australia. S.G.T is supported by an NHMRC Leadership 3 Investigator Grant (1176665) and NHMRC program grant (1113904).

References

1. Picchi H. et al.Infectious complications associated with the use of immune checkpoint inhibitors in oncology: reactivation of tuberculosis after anti PD-1 treatment. Clin. Microbiol. Infect. 24, 216–218 (2018). [PubMed: 29269089]
2. Postow MA, Sidlow R. & Hellmann MD Immune-Related Adverse Events Associated with Immune Checkpoint Blockade. N. Engl. J. Med. 378, 158–168 (2018). [PubMed: 29320654]
3. Altare F. et al.Interleukin-12 Receptor β1 Deficiency in a Patient with Abdominal Tuberculosis. J. Infect. Dis. 184, 231–236 (2001). [PubMed: 11424023]
4. Kreins AYet al.Human TYK2 deficiency: Mycobacterial and viral infections without hyper-IgE syndrome. J. Exp. Med. 212, 1641–62 (2015). [PubMed: 26304966]
5. Boisson-Dupuis S. et al.Tuberculosis and impaired IL-23-dependent IFN-γ immunity in humans homozygous for a common TYK2 missense variant. Sci. Immunol. 3, (2018).
6. Boisson-Dupuis S. The monogenic basis of human tuberculosis. Hum. Genet. 139, 1001–1009 (2020). [PubMed: 32055999]
7. Flanagan SEet al.Activating germline mutations in STAT3 cause early-onset multi-organ autoimmune disease. Nat. Genet. 46, 812–814 (2014). [PubMed: 25038750]
8. Nabhani S. et al.STAT3 gain-of-function mutations associated with autoimmune lymphoproliferative syndrome like disease deregulate lymphocyte apoptosis and can be targeted by BH3 mimetic compounds. Clin. Immunol. 181, 32–42 (2017). [PubMed: 28579554]
9. Milner JDet al.Early-onset lymphoproliferation and autoimmunity caused by germline STAT3 gain-of-function mutations. Blood125, 591–9 (2015). [PubMed: 25359994]
10. Haapaniemi EMet al.Autoimmunity, hypogammaglobulinemia, lymphoproliferation, and mycobacterial disease in patients with activating mutations in STAT3. Blood125, 639–648 (2015). [PubMed: 25349174]
11. Houben RMGJ & Dodd PJ The Global Burden of Latent Tuberculosis Infection: A Re-estimation Using Mathematical Modelling. PLoS Med. 13, 1–13 (2016).
12. Vynnycky E. & Fine PEM Lifetime Risks, Incubation Period, and Serial Interval of Tuberculosis. Am. J. Epidemiol. 152, 247–263 (2000). [PubMed: 10933272]
13. Kerner G. et al.Homozygosity for TYK2 P1104A underlies tuberculosis in about 1% of patients in a cohort of European ancestry. Proc. Natl. Acad. Sci. U. S. A. 116, 201903561 (2019).
14. Kerner G. et al.Human ancient DNA analyses reveal the high burden of tuberculosis in Europeans over the last 2,000 years. Am. J. Hum. Genet. 108, 517–524 (2021). [PubMed: 33667394]

15. Toubiana J. et al.Heterozygous STAT1 gain-of-function mutations underlie an unexpectedly broad clinical phenotype. Blood127, 3154–3164 (2016). [PubMed: 27114460]
16. Gonzalez-mancera MS, Johnson B. & Mirsaeidi M. STAT3 gain-of-function mutation in a patient with pulmonary Mycobacterium abscessus infection. Respir. Med. Case Reports 101125 (2020). doi:10.1016/j.rmcr.2020.101125
17. Kalluri R, Gattone VH, Noelken ME & Hudson BG The α3 chain of type IV collagen induces autoimmune Goodpasture syndrome. Proc. Natl. Acad. Sci. U. S. A. 91, 6201–6205 (1994). [PubMed: 8016138]
18. Rentzsch P, Witten D, Cooper GM, Shendure J. & Kircher M. CADD: predicting the deleteriousness of variants throughout the human genome. Nucleic Acids Res. 47, D886–D894 (2019). [PubMed: 30371827]
19. Itan Y. et al.The mutation significance cutoff: gene-level thresholds for variant predictions. Nat. Methods13, 109–110 (2016). [PubMed: 26820543]
20. Rapaport F. et al.Negative selection on human genes underlying inborn errors depends on disease outcome and both the mode and mechanism of inheritance. Proc. Natl. Acad. Sci. 118, (2021).
21. Ishida Y, Agata Y, Shibahara K. & Honjo T. Induced expression of PD-1, a novel member of the immunoglobulin gene superfamily, upon programmed cell death. EMBO J. 11, 3887–95 (1992). [PubMed: 1396582]
22. Wang J. et al.PD-1 deficiency results in the development of fatal myocarditis in MRL mice. Int. Immunol. 22, 443–452 (2010). [PubMed: 20410257]
23. Nishino M, Sholl LM, Hatabu H, Ramaiya NH & Hodi FS Anti–PD-1–Related Pneumonitis during Cancer Immunotherapy. N. Engl. J. Med. 373, 288–290 (2015). [PubMed: 26176400]
24. Zhang B, Chikuma S, Hori S, Fagarasan S. & Honjo T. Nonoverlapping roles of PD-1 and FoxP3 in maintaining immune tolerance in a novel autoimmune pancreatitis mouse model. Proc. Natl. Acad. Sci. U. S. A. 113, 8490–5 (2016). [PubMed: 27410049]
25. Lázár-Molnár E. et al.Programmed death-1 (PD-1)-deficient mice are extraordinarily sensitive to tuberculosis. Proc. Natl. Acad. Sci. 107, 13402–13407 (2010). [PubMed: 20624978]
26. Barber DLet al.Tuberculosis following PD-1 blockade for cancer immunotherapy. Sci. Transl. Med. 11, (2019).
27. Wang L, Das H, Kamath A. & Bukowski JF Human Vγ2Vδ2 T Cells Produce IFN-γ and TNF-α with an On/Off/On Cycling Pattern in Response to Live Bacterial Products. J. Immunol. 167, 6195–6201 (2001). [PubMed: 11714780]
28. Le Bourhis L. et al.Antimicrobial activity of mucosal-associated invariant T cells. Nat. Immunol. 11, 701–708 (2010). [PubMed: 20581831]
29. Gold MC, Napier RJ & Lewinsohn DM MR1-restricted mucosal associated invariant T (MAIT) cells in the immune response to Mycobacterium tuberculosis. Immunol. Rev. 264, 154–166 (2015). [PubMed: 25703558]
30. Cooper MAet al.Human natural killer cells: a unique innate immunoregulatory role for the CD56(bright) subset. Blood97, 3146–3151 (2001). [PubMed: 11342442]
31. Ndhlovu ZMet al.Magnitude and Kinetics of CD8+ T Cell Activation during Hyperacute HIV Infection Impact Viral Set Point. Immunity43, 591–604 (2015). [PubMed: 26362266]
32. Li M. et al.T-cell immunoglobulin and ITIM domain (TIGIT) receptor/poliovirus receptor (PVR) ligand engagement suppresses interferon-γ production of natural killer cells via β-arrestin 2-mediated negative signaling. J. Biol. Chem. 289, 17647–17657 (2014). [PubMed: 24817116]
33. Jacquelot N. et al.Sustained Type I interferon signaling as a mechanism of resistance to PD-1 blockade. Cell Res. 29, 846–861 (2019). [PubMed: 31481761]
34. Nguyen KBet al.Interferon α/β-mediated inhibition and promotion of interferon γ: STAT1 resolves a paradox. Nat. Immunol. 1, 70–76 (2000). [PubMed: 10881178]
35. Moreira-Teixeira L. et al.Type I IFN exacerbates disease in tuberculosis-susceptible mice by inducing neutrophil-mediated lung inflammation and NETosis. Nat. Commun. 11, 5566 (2020). [PubMed: 33149141]
36. Cantaert T, Baeten D, Tak PP & van Baarsen LGM Type I IFN and TNFα cross-regulation in immune-mediated inflammatory disease: basic concepts and clinical relevance. Arthritis Res. Ther. 12, 219 (2010). [PubMed: 21062511]

37. Magerus-Chatinet A. et al.FAS-L, IL-10, and double-negative CD4−CD8− TCR α/β+ T cells are reliable markers of autoimmune lymphoproliferative syndrome (ALPS) associated with FAS loss of function. Blood113, 3027–3030 (2009). [PubMed: 19176318]
38. Wei SCet al.Negative Co-stimulation Constrains T Cell Differentiation by Imposing Boundaries on Possible Cell States. Immunity50, 1084–1098.e10 (2019). [PubMed: 30926234]
39. Ma CSet al.Deficiency of Th17 cells in hyper IgE syndrome due to mutations in STAT3. J. Exp. Med. 205, 1551–7 (2008). [PubMed: 18591410]
40. Okada S. et al.Impairment of immunity to Candida and Mycobacterium in humans with bi-allelic RORC mutations. Science (80-.). 349, 606–613 (2015).
41. Casanova J-L, Conley ME, Seligman SJ, Abel L. & Notarangelo LD Guidelines for genetic studies in single patients: lessons from primary immunodeficiencies. The Journal of experimental medicine 211, 2137–2149 (2014). [PubMed: 25311508]
42. Fabre A. et al.Clinical Aspects of STAT3 Gain-of-Function Germline Mutations: A Systematic Review. J. Allergy Clin. Immunol. Pract. 7, 1958–1969.e9 (2019). [PubMed: 30825606]
43. Forbes LRet al.Jakinibs for the treatment of immune dysregulation in patients with gain-of-function signal transducer and activator of transcription 1 (STAT1) or STAT3 mutations. J. Allergy Clin. Immunol. 142, 1665–1669 (2018). [PubMed: 30092289]
44. Li H. & Tsokos GC Double-negative T cells in autoimmune diseases. Curr. Opin. Rheumatol. 33, 163–172 (2021). [PubMed: 33394752]
45. Crispín JCet al.Expanded Double Negative T Cells in Patients with Systemic Lupus Erythematosus Produce IL-17 and Infiltrate the Kidneys. J. Immunol. 181, 8761–8766 (2008). [PubMed: 19050297]
46. Prokunina L. et al.A regulatory polymorphism in PDCD1 is associated with susceptibility to systemic lupus erythematosus in humans. Nat. Genet. 32, 666–669 (2002). [PubMed: 12402038]
47. Stroud CRet al.Tocilizumab for the management of immune mediated adverse events secondary to PD-1 blockade. J. Oncol. Pharm. Pract. Off. Publ. Int. Soc. Oncol. Pharm. Pract. 25, 551–557 (2019).
48. Martins F. et al.New therapeutic perspectives to manage refractory immune checkpoint-related toxicities. Lancet. Oncol. 20, e54–e64 (2019). [PubMed: 30614479]
49. Kauffman KDet al.PD-1 blockade exacerbates Mycobacterium tuberculosis infection in rhesus macaques. Sci. Immunol. 6, eabf3861 (2021).
50. Tousif S. et al.T Cells from Programmed Death-1 Deficient Mice Respond Poorly to Mycobacterium tuberculosis Infection. PLoS One6, e19864 (2011). [PubMed: 21589883]
51. Nathan CF, Murray HW, Wiebe ME & Rubin BY Identification of interferon-gamma as the lymphokine that activates human macrophage oxidative metabolism and antimicrobial activity. J. Exp. Med. 158, 670–689 (1983). [PubMed: 6411853]
52. Jouanguy E. et al.Partial interferon-gamma receptor 1 deficiency in a child with tuberculoid bacillus Calmette-Guérin infection and a sibling with clinical tuberculosis. J. Clin. Invest. 100, 2658–2664 (1997). [PubMed: 9389728]
53. Flynn JLet al.Tumor necrosis factor-alpha is required in the protective immune response against Mycobacterium tuberculosis in mice. Immunity2, 561–572 (1995). [PubMed: 7540941]
54. Harris J. & Keane J. How tumour necrosis factor blockers interfere with tuberculosis immunity. Clin. Exp. Immunol. 161, 1–9 (2010). [PubMed: 20491796]

References (Method)

55. Xu GJet al.Comprehensive serological profiling of human populations using a synthetic human virome. Science (80-.). 348, aaa0698--aaa0698 (2015).
56. Kerner G. et al.Inherited human IFN-γ deficiency underlies mycobacterial disease. J. Clin. Invest. 130, 3158–3171 (2020). [PubMed: 32163377]
57. Mina MJet al.Measles virus infection diminishes preexisting antibodies that offer protection from other pathogens. Science (80-.). 366, 599–606 (2019).

58. Mohan D. et al.PhIP-Seq characterization of serum antibodies using oligonucleotide-encoded peptidomes. Nat. Protoc. 13, 1958–1978 (2018). [PubMed: 30190553]
59. Belkadi A. et al.Whole-exome sequencing to analyze population structure, parental inbreeding, and familial linkage. Proc. Natl. Acad. Sci. U. S. A. 113, 6713–8 (2016). [PubMed: 27247391]
60. Maffucci P. et al.Blacklisting variants common in private cohorts but not in public databases optimizes human exome analysis. Proc. Natl. Acad. Sci. 116, 950–959 (2019). [PubMed: 30591557]
61. Gentili M. et al.Transmission of innate immune signaling by packaging of cGAMP in viral particles. Science349, 1232–1236 (2015). [PubMed: 26229115]
62. Patsoukis N. et al.Selective effects of PD-1 on Akt and Ras pathways regulate molecular components of the cell cycle and inhibit T cell proliferation. Sci. Signal. 5, ra46 (2012).
63. Yang R. et al.Human T-bet Governs Innate and Innate-like Adaptive IFN-γ Immunity against Mycobacteria. Cell183, 1826–1847.e31 (2020). [PubMed: 33296702]
64. Ma CSet al.Unique and shared signaling pathways cooperate to regulate the differentiation of human CD4+ T cells into distinct effector subsets. J. Exp. Med. 213, 1589–1608 (2016). [PubMed: 27401342]
65. Zheng GXYet al.Massively parallel digital transcriptional profiling of single cells. Nat. Commun. 8, (2017).
66. Haghverdi L, Lun ATL, Morgan MD & Marioni JC Batch effects in single-cell RNA-sequencing data are corrected by matching mutual nearest neighbors. Nat. Biotechnol. 36, 421–427 (2018). [PubMed: 29608177]
67. Crowell HLet al.muscat detects subpopulation-specific state transitions from multi-sample multi-condition single-cell transcriptomics data. Nat. Commun. 11, 6077 (2020). [PubMed: 33257685]
68. Eisenberg E. & Levanon EY Human housekeeping genes, revisited. Trends Genet. 29, 569–574 (2013). [PubMed: 23810203]
69. Love MI, Huber W. & Anders S. Moderated estimation of fold change and dispersion for RNA-seq data with DESeq2. Genome Biol. 15, 1–21 (2014).
70. Robinson MD, McCarthy DJ & Smyth GK edgeR: A Bioconductor package for differential expression analysis of digital gene expression data. Bioinformatics 26, 139–140 (2009). [PubMed: 19910308]
71. Tarazona S, Garcia-Alcalde F, Dopazo J, Ferrer A. & Conesa A. Differential expression in RNA-seq: A matter of depth. Genome Res. 21, 2213–2223 (2011). [PubMed: 21903743]
72. Schwartz GWet al.TooManyCells identifies and visualizes relationships of single-cell clades. Nat. Methods17, 405–413 (2020). [PubMed: 32123397]
73. Yu G, Wang L-G, Han Y. & He Q-Y clusterProfiler: an R package for comparing biological themes among gene clusters. OMICS 16, 284–287 (2012). [PubMed: 22455463]
74. R Core Team. R: A Language and Environment for Statistical Computing. (2018).
75. Benjamini Y. & Hochberg Y. Controlling the False Discovery Rate: A Practical and Powerful Approach to Multiple Testing. J. R. Stat. Soc. Ser. B 57, 289–300 (1995).

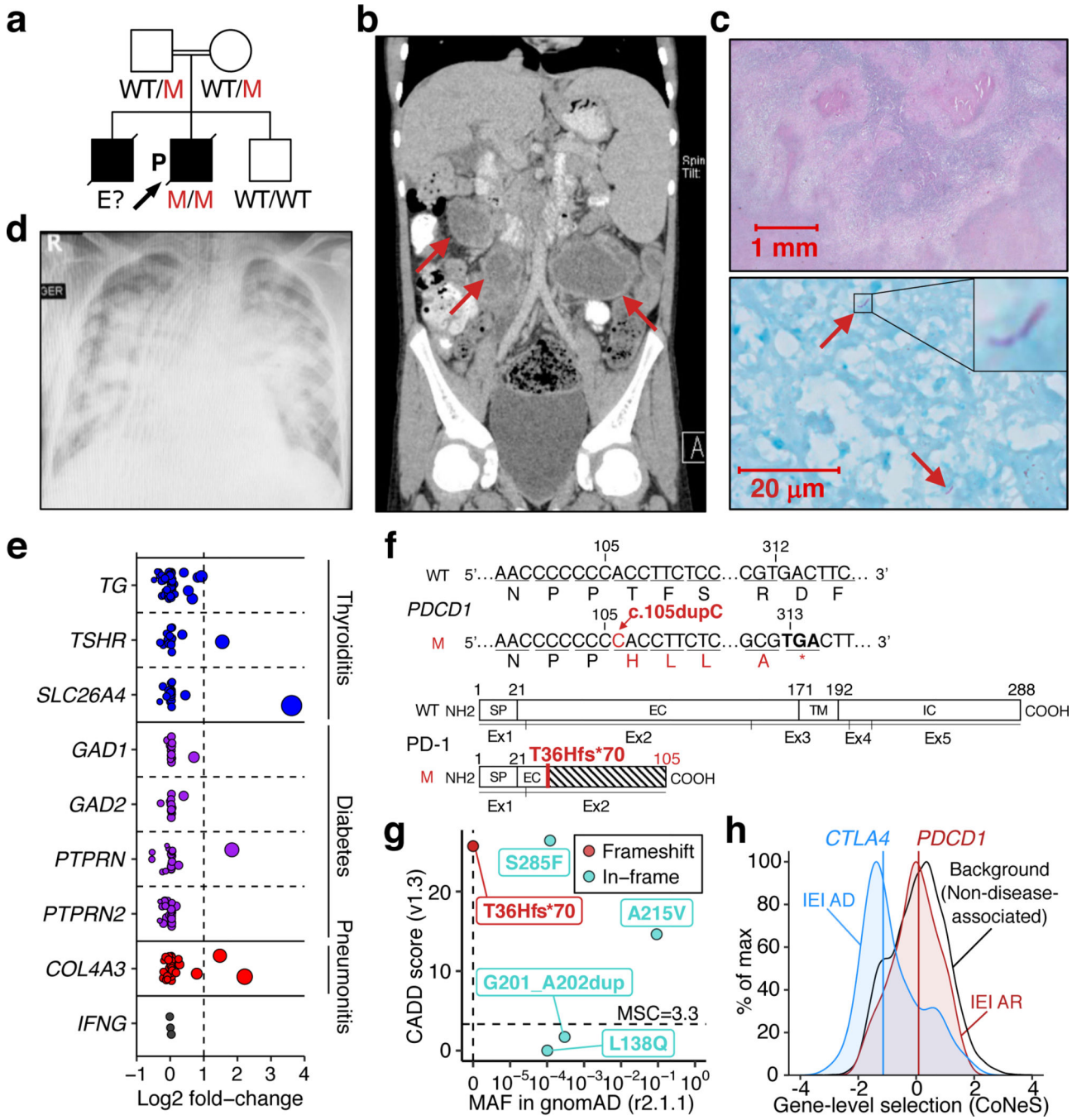

Figure 1.

A child with autosomal recessive inherited PD-1 deficiency suffering from tuberculosis and autoimmunity. (a) Pedigree of the family. Black and barred symbols indicate affected and deceased individuals, respectively. Genotypes for *PDCD1* are also shown. WT: wild-type. M: c.105dupC. E?: unknown. (b) Contrasted computed tomography (CT) scan at the initial presentation, showing three cystic lesions (arrows) in the abdomen. Therapeutic drainage was performed. (c) Pathological examination of the biopsy material from the abdominal lymph nodes. Upper panel: hematoxylin and eosin staining (×12) showing granulomas

centered by caseous necrosis. Lower panel: Ziehl-Neelsen stain (×1000) showing acid-fast bacilli (arrows). (d) Chest X-ray on admission to the pediatric intensive care unit, showing bilateral diffuse infiltrates in the lungs. (e) Serum autoreactivity profiling. Fold-changes of reactivity to selected autoantigens associated with autoimmune thyroiditis (blue), diabetes (purple), and pneumonitis (red) for the patient's sample (obtained at initial presentation) relative to other healthy family members and negative controls are shown. *IFNG* is also shown as a negative example. Dot size represents the peptide enrichment score. (f) Nucleotide-level and protein-level representations of the patient's mutation. WT: wild-type, M: c.105dupC (T36Hfs*70). SP: signal peptide. EC: extracellular domain. TM: transmembrane domain. IC: intracellular domain. The shaded bar represents new amino acids due to the frameshift. Exons and their boundaries are also shown. (g) Population genetics of *PDCD1*. Minor allele frequency (MAF) and combined annotation-dependent depletion (CADD) scores are shown for all homozygous non-synonymous *PDCD1* variants reported in the gnomAD database. The patient's mutation has a CADD score[18] of 25.7, well above the mutation significance cutoff (MSC)[19] of 3.3 (horizontal dotted line). (h) Gene-level negative selection. *PDCD1* is not under negative selection, similar to other genes for which mutations underlie AR IEIs, whereas *CTLA4* is under strong negative selection, as determined by CoNeS[20].

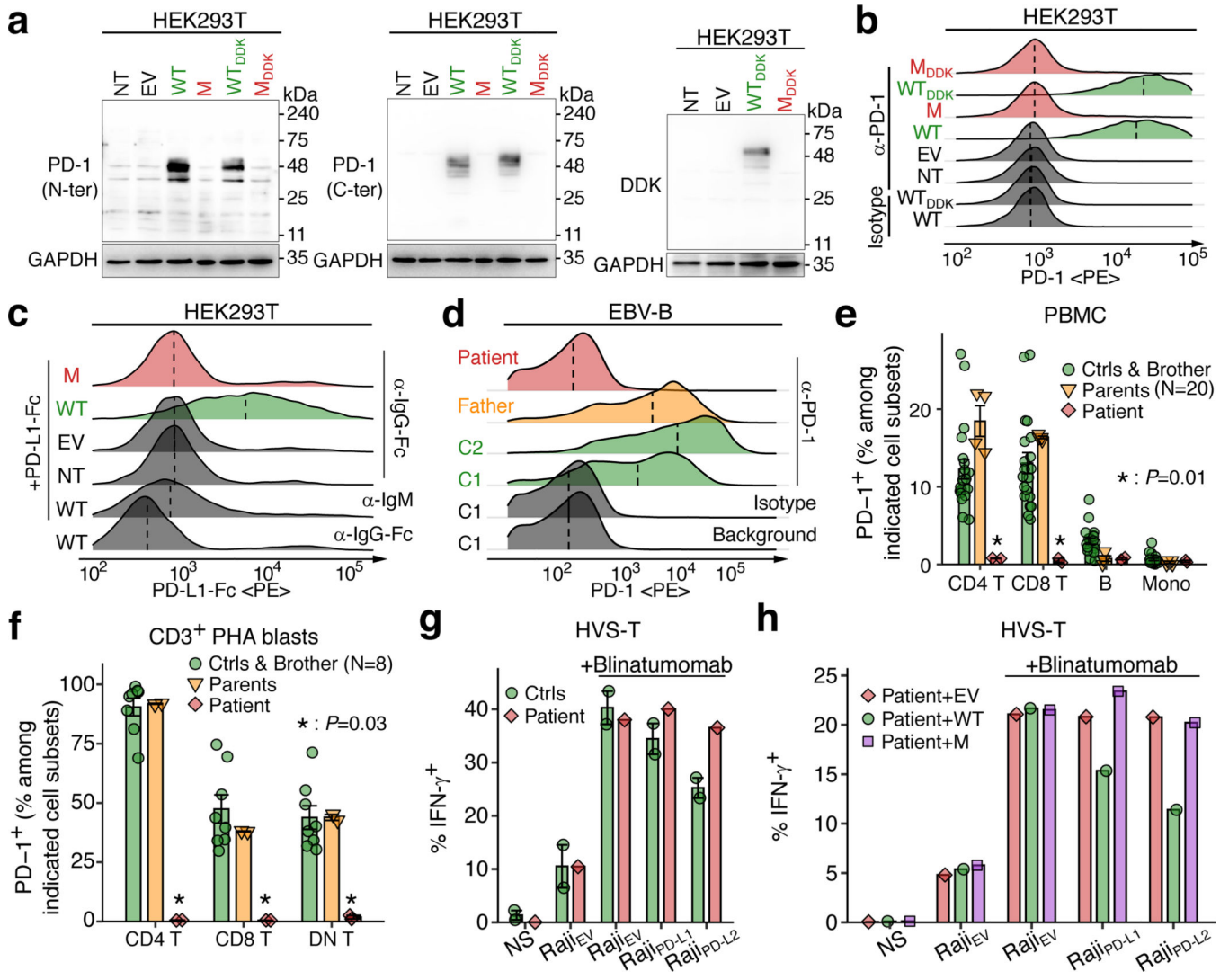

Figure 2.

Analysis of the expression and function of PD-1 in an overexpression system and in the patient's cells. (a-c) Studies of the patient's *PDCD1* allele in an overexpression system. HEK293T cells were transfected with an empty vector (EV) plasmid or with plasmids harboring cDNA corresponding to the wild-type (WT) or mutant (c.105dupC, M) *PDCD1* allele, with or without a C-terminal DDK tag. (a) Western blot of total protein extract with a monoclonal antibody (mAb) against the PD-1 N-terminal epitope, a polyclonal antibody against the PD-1 C-terminal epitope, and an anti-DDK mAb. GAPDH was used as a loading control. (b) Surface PD-1 expression as determined by flow cytometry with PE-conjugated anti-PD-1 mAb. (c) Surface retention of recombinant PD-L1-Fc as determined by flow cytometry. Cells were stained with anti-IgG Fc-biotin mAb followed by streptavidin-PE. (d-h) Studies of the patient's cells. (d-f) Surface PD-1 expression in (d) EBV-B cell lines, (e) PBMCs (technical duplicates), and (f) PHA blasts (technical duplicates prepared only for the patient's cells) from the patient, his healthy brother and parents, and healthy controls. (g and h) T:B cell coculture assay. (g) HVS-T cells from two controls and the

patient and (h) the patient's HVS-T cells stably transduced with EV, WT PD-1, or mutant (T36Hfs*70, M) PD-1 were cocultured for 24 hours with Raji cells stably transduced with EV, PD-L1, or PD-L2 with or without blinatumomab (anti-CD3-CD19 bispecific engager), and IFN-γ production was measured by flow cytometry. Representative data from three independent experiments are shown. In (b-d), dashed lines indicate the median. In (e and f), bars represent the mean and SEM. Statistical significances were determined by comparing the patient and controls (including the brother and parents) via two-tailed non-paired Wilcoxon's rank-sum tests with false-discovery rate (FDR) adjustment.

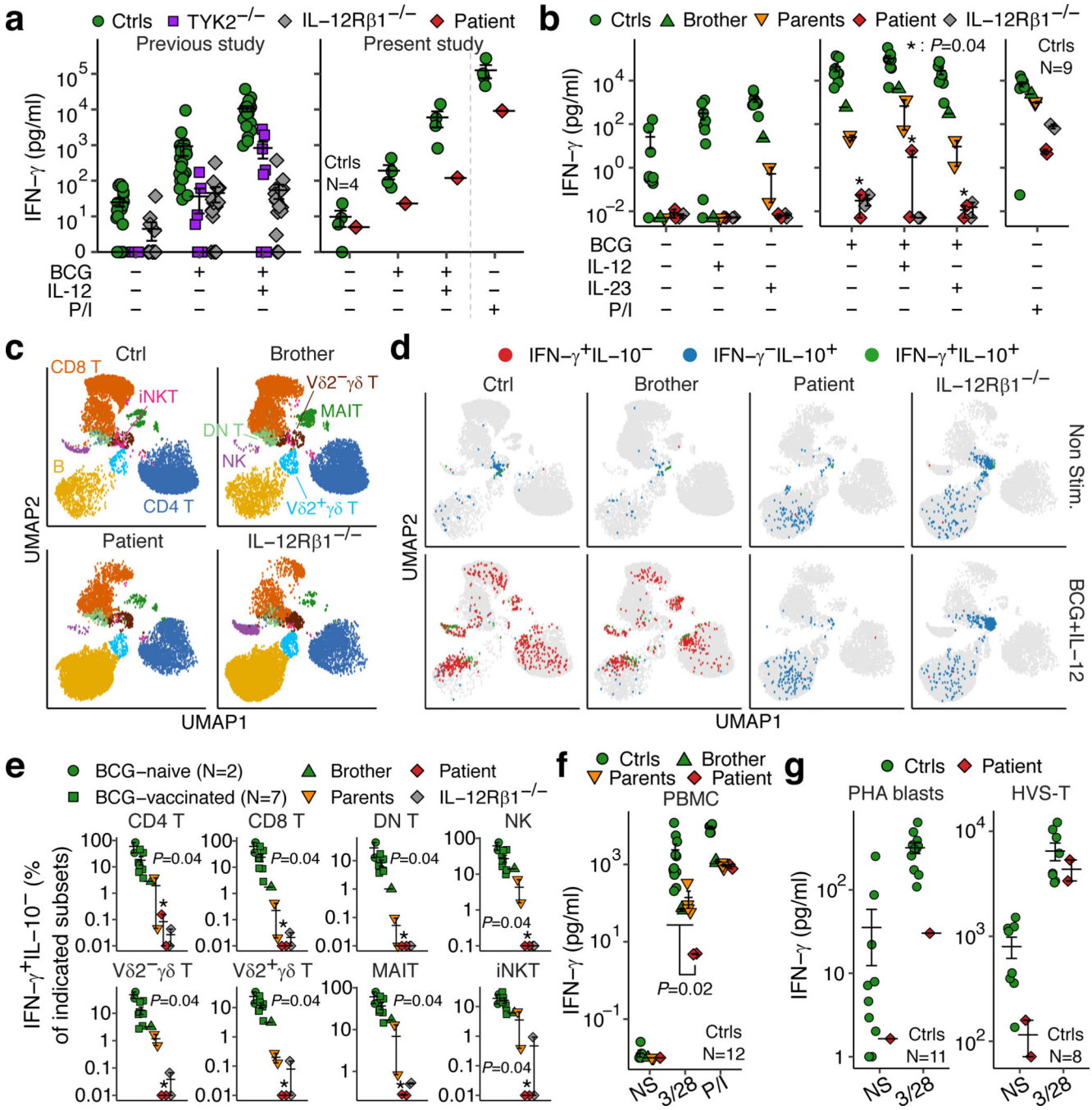

Figure 3.

Impaired IFN-γ production by PD-1-deficient leukocytes in response to mycobacterial or T-cell stimuli. (a-e) BCG stimulation assay. The patient's cells were obtained after the complete remission of TB. (a) Whole-blood BCG assay. After 48 hours of stimulation with BCG, secreted IFN-γ levels were determined by ELISA. Here, healthy family members (brother and parents) and one local control are grouped together as controls. Previously published data are also shown for comparison[5]. (b-e) PBMC BCG assay. Freshly thawed PBMCs from controls (*N*=9, two BCG-naïve and seven BCG-vaccinated), the patient's

brother and parents, and the PD-1-deficient patient, together with one IL-12Rβ1$^{-/-}$ patient, were stimulated for 40 hours with various combinations of IL-12, IL-23, and BCG, and then incubated with a cytokine secretion inhibitor for another eight hours. Technical duplicates were prepared only for the PD-1-deficient patient and the IL-12Rβ1$^{-/-}$ patient. (b) Secreted IFN-γ levels, as determined with a LEGENDplex assay. (c-e) Cellular responses to BCG challenge as deconvoluted by flow cytometry. (c and d) UMAP visualization of (c) non-stimulated cell subsets and (d) cytokine production patterns without stimulation or with stimulation with BCG plus IL-12. Data from technical duplicates were combined. (e) The proportion of IFN-γ^{+}IL-10^{-} cells among the indicated cell subsets after stimulation with BCG plus IL-12. (f) PBMC activation assay. The patient's cells were obtained one month after the initiation of anti-TB treatment. Secreted IFN-γ levels after 24 hours of stimulation were determined with a LEGENDplex assay. Technical duplicates were prepared for the patient and his healthy brother and parents. (g) T cell activation assay. Secreted IFN-γ levels after 24 hours of stimulation were determined by ELISA. Two experiments were compiled for HVS-T cells. NS, non-stimulated; 3/28, Dynabeads coated with anti-CD3 and anti-CD28 antibodies; P/I, PMA/ionomycin. Bars represent the mean and SEM. Statistical significances were determined via two-tailed non-paired Wilcoxon's rank-sum tests with FDR adjustment (b and e) for the patient vs. local controls plus his brother, and (f) for the patient vs. local plus all family controls.

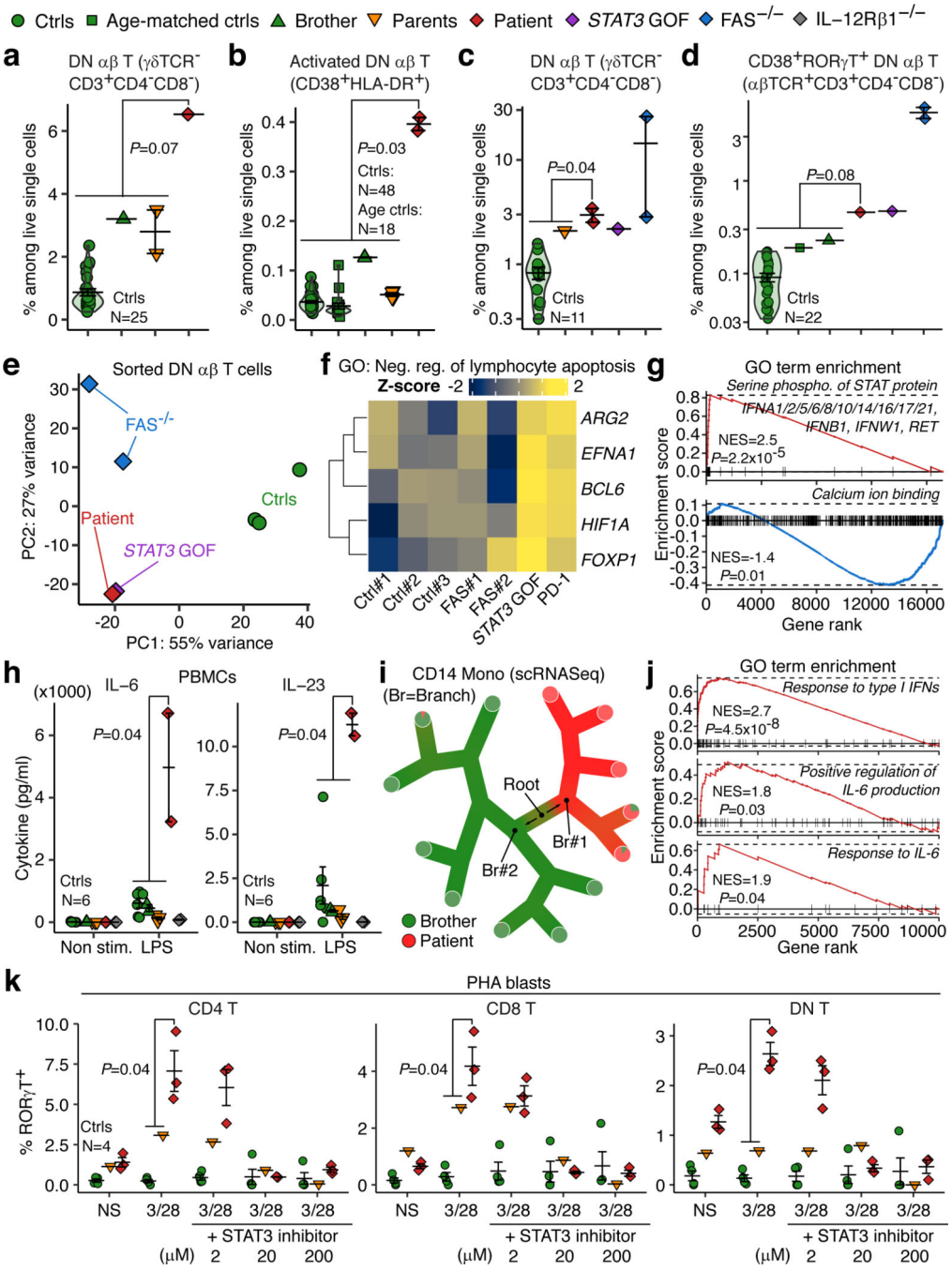

Figure 4.

Inherited PD-1 deficiency phenocopies STAT3 gain-of-function and triggers lymphoproliferative autoimmunity through excessive production of STAT3-activating cytokines and STAT3-dependent RORγT expression. The patient's PBMCs were obtained (a, b, d, and h-j) one month after anti-TB treatment and (c and e-g) two weeks before his death. (a-d) $CD4^-CD8^-$ double-negative (DN) αβ T cells and their subsets by (a, c, and d) flow cytometry and (b) CyTOF. In (b), experiments with general (CyTOF-G) and T cell-focused (CyTOF-T) panels were compiled as technical duplicates. (e-g) RNA sequencing

of sorted DN αβ T cells. (e) Principal component analysis. (f) Gene set overrepresentation analysis. Genes upregulated (log_2 fold-change of at least 2) in both the PD-1-deficient patient and the *STAT3* GOF patient relative to controls were tested for Gene Ontology (GO) term overrepresentation. The heatmap illustrates Z-score-transformed normalized counts for genes related to the negative regulation of lymphocyte apoptosis. (g) Gene set enrichment analysis. The following groups were compared: i) PD-1/STAT3 vs. controls, ii) PD-1/STAT3 vs. FAS, and iii) FAS vs. controls. Two representative GO terms identified in i) and ii) but not iii) are shown. Inset: leading-edge genes, the normalized enrichment score (NES), and the FDR-adjusted *P* value. (h) Secreted IL-6 and IL-23 levels, as determined with a LEGENDplex assay. PBMCs were stimulated with lipopolysaccharide (LPS) for 24 hours. Technical duplicates were prepared only for the patient, his relatives, and the IL-12Rβ1$^{-/-}$ patient. (i) Single-cell clade analysis of CD14 monocytes from the patient and his healthy brother via TooManyCells[72]. (j) Gene set enrichment analysis of the top 10,000 differentially expressed genes in Branch #1 vs. Branch #2 in (i). Three representative enriched GO terms are shown. (k) STAT3 inhibition assay. Expanded PHA blasts were activated by incubation with anti-CD3/CD28 antibody-conjugated beads with or without a STAT3 inhibitor for 6 hours. RORγT expression levels were determined by flow cytometry. Technical triplicates were prepared only for the patient. In (a-d, h, and k), bars represent the mean and SEM. In (a-d, h, and k), statistical significances were determined via two-tailed non-paired Wilcoxon's rank-sum tests with FDR adjustment.